# Chlorophyll fluorescence retrieval method and its application on detecting the early water stress

Zhuoya Ni

# UNIVERSITÉ DE STRASBOURG

*ÉCOLE DOCTORALE Mathématiques, Sciences de l'Information et de l'Ingénieur*

**UdS – INSA - ENGEES**

# THÈSE présentée par :

**Zhuoya NI**

soutenue le **30 Mai 2016**

pour obtenir le grade de : **Docteur de l'université de Strasbourg**

Discipline/ Spécialité : Electronique / Télédétection

# Méthode pour l'estimation de la fluorescence de la chlorophylle et son application pour la détection précoce du stress hydrique

**THÈSE dirigée par :**

| | |
|---|---|
| **Mme Françoise Nerry** | Directrice de Recherches CNRS |
| **M. Rui Sun** | Professeur, Beijing Normal University |

**RAPPORTEURS :**

| | |
|---|---|
| **M.José Sobrino** | Professeur, University of Valencia |
| **M. Pengxin Wang** | Professeur, China Agricultural University |

---

**AUTRES MEMBRES DU JURY :**

| | |
|---|---|
| **M. Zhao-Liang Li** | Directeur de Recherches CNRS |
| **M. Xiaoguang Jiang** | Professeur, University of Chinese Academy of Sciences |

# Achnowledgements

The process of earning a doctorate and writing a dissertation is long and arduous—and it is certainly not done without the help and support of the kind people around me, to only some of whom it is possible to give particular mention here.

First and foremost, I would like to thank my husband Huo Hongyuan for his support and great patience at all times. My parents, brother and sister have given me their support throughout, as always, for which my mere expression of thanks likewise does not suffice. Without their constant support, encouragement, and understanding, it would not have been possible for me to achieve my educational goals.

I would certainly be remiss to not mention and sincerely thank Dr. Françoise NERRY, professor, mentor, and dissertation advisor extraordinaire. Without her help, advice, expertise, and encouragement, this research and dissertation would not have happened. The good advice, support and friendship of my second supervisor, Prof. Zhao-Liang Li and his wife Ms. Minjie Zhao, have been invaluable on both an academic and a personal level, for which I am extremely grateful.

I would like to thank my principal supervisor in Beijing Normal University, Prof. Xiaowen Li, although he died in last year. His help, support and patience, were influential and essential during my doctorate research time range, not to mention his invaluable advice and unsurpassed knowledge of quantitative Remote Sensing. Many thanks to my second supervisors Prof. Rui Sun and associate Prof. Zhigang Liu for their invaluable advice throughout the dissertation-writing process. I would also like to thank the other members of my dissertation committee: Prof. J. Sobrino, Prof. Pengxin Wang, and Prof. Xiaoguang Jiang. Their insight and feedback are influential.

I would also like to thank my many friends and colleagues in the ICUBE Lab of Strasbourg University and Beijing Normal University where it has been my pleasure and honor to work for the last 4 years. The help of both academic and life of Dr. Yuan Liu, Dr. Pei Leng, Dr. Xiwei Fan, Dr. Enyu Zhao, Dr. Xinke Zhong, Dr. Gula Tang, Scientist Bohui Tang, and Dr. Laure Roupioz is very important during my study in University of Strasbourg and the

dissertation-writing process. Many thanks for the support and help of Dr. Shu Wang, Dr. Linna Wu, Dr. Yuebin Wang, Dr. Hu Zhang, Dr. Peiqi Yang, Qingshan Wang, Shan Xu, Xijia Zhou, Weiwei Zhang and Dr. Lei Zhang during my study in Beijing Normal University.

I would also like to acknowledge the financial support of the China Scholarship Council (CSC) during my study in University of Strasbourg in France, the academic and technical support of the ICUBE Lab of Strasbourg University and the Beijing Normal University.

*This dissertation is dedicated to all my family.*

Beijing, April 29, 2016

Zhuoya NI

# Contents

# List of figures

# List of Tables

# Résumé

La végétation concerne une grande variété de plantes qui se développent sur la surface terrestre, jouant un rôle important dans le système de la terre, et c'est également une ressource renouvelable très importante dans la surface terrestre. La végétation est la plus active et la plus représentative pour les indicateurs du changement global, influençant le bilan énergétique du système de la terre-atmosphère, jouant un rôle important dans le climat, les cycles hydrologiques et biochimiques, et est un indicateur sensible des impacts climatiques et des sciences humaines sur l'environnement. La végétation libère de l'oxygène par la photosynthèse, qui établit un environnement confortable pour la survie humaine. En outre, la végétation a de grands impacts sur le changement climatique. Par conséquent, la végétation peut être appelée le thème des écosystèmes de la terre, qui joue un rôle important dans le cycle global de la matière et de l'énergie. Cependant, avec la pression du changement climatique global, la demande énergétique et la croissance démographique, il y a un risque croissant, à l'échelle globale ou régionale sur l'approvisionnement de la production agricole. Il est important pour la sécurité de la nourriture et le développement d'humain de prendre en compte la situation de la production alimentaire globale en temps réel. Il est avéré que la fluorescence de chlorophylle de végétation est un moyen efficace, non destructif et direct de surveillance des changements de l'état physiologique de végétation. La fluorescence chlorophyllienne, la photosynthèse et la dissipation thermique sont les trois manières de dissiper l'énergie absorbée par la végétation. Ces trois manières se concurrencent les unes avec les autres. La réduction d'énergie pour la photosynthèse mènera à l'augmentation d'énergie pour l'émission de fluorescence de chlorophylle, et vice versa. Par conséquent, l'émission de fluorescence de chlorophylle peut être employée comme indicateur dans la mesure de la photosynthèse. Des changements du système de végétation peuvent être surveillés par le changement de fluorescence de la chlorophylle du fait de la relation étroite entre la photosynthèse de la végétation et la fluorescence chlorophyllienne.

Dans cette dissertation, il y a six chapitres et chaque chapitre est présenté comme suit :

Le chapitre 1 est l'introduction. Nous présentons le fond de recherches, le progrès de recherches de la fluorescence de la chlorophylle, les objets de recherches et la structure de ce document.

La fluorescence induite par le soleil est considérée comme une manière directe et non destructive de surveiller l'état physiologique de végétation. La fluorescence, la photosynthèse et la chaleur absorbée sont trois manières de consommer l'énergie absorbée. Ces trois processus se concurrencent les uns avec les autres. Par conséquent, la mesure de la variation de la fluorescence de chlorophylle est une bonne manière de surveiller la végétation, et a l'avantage comparée aux méthodes traditionnelles. Dans ce document, nous effectuons une recherche sur les méthodes de détection de fluorescence de chlorophylle induite par le soleil à multi-échelle.

Vu l'importance de la surveillance de la végétation pour le bilan global écologique et l'efficacité de la surveillance de la fluorescence chlorophyllienne, dans cette thèse la fluorescence de chlorophylle à l'échelle de la feuille est choisie comme point de départ pour développer une recherche sur la dynamique de la fluorescence de chlorophylle et la température de feuille dans différents états de teneur en eau. La fluorescence de chlorophylle à l'échelle de la feuille peut être mesurée directement par un instrument de mesure de fluorescence, ou être extraite directement du spectre de réflexion des feuilles. Dans ce processus, la fluorescence de la chlorophylle peut être proche de la véritable fluorescence de chlorophylle due à moins d'impact d'autres facteurs influents. Sur cette base, prenant le maïs mis en pot comme sujet, la recherche des réponses de la fluorescence de chlorophylle au stress précoces en eau sont développées, et les résultats prouvent que la fluorescence de la chlorophylle et la température de feuille pourraient illustrer les changements dus au stress précoces en eau.

Pour élargir l'application de la fluorescence de la chlorophylle dans la surveillance de végétation, les changements de l'état physiologique de la végétation devraient être analysés par la fluorescence causée induite par le soleil pour la plate-forme satellite ou au sol. Le point clé de l'extraction de la fluorescence de la chlorophylle avec la technique de la télédétection est de séparer la fluorescence chlorophyllienne de l'énergie réfléchie. Les effets atmosphériques sont négligeables quand l'extraction de la fluorescence chlorophyllienne est proche du sol du fait de la distance limitée et dans ce cas l'algorithme d'extraction de fluorescence est relativement simple. Par contre, l'extraction de la fluorescence

chlorophyllienne à partir de satellites est beaucoup plus complexe en raison de l'absorption et la diffusion atmosphérique et donc des corrections atmosphériques sont nécessaires pour obtenir la vraie fluorescence chlorophyllienne. Nous récapitulons toutes les méthodes d'extraction de la fluorescence de chlorophylle près au sol et constatons que l'algorithme basé sur r l'extraction de la réflectivité est dans certains cas la seule méthode. Ceci montre également la nécessité de développer un algorithme quantitatif basé sur la réflectivité. Dans cette étude, un nouvel algorithme quantitatif d'extraction basé sur l'index de réflectivité est développé au sol et comparée à d'autres algorithmes classiques pour montrer la faisabilité de cette méthode quantitative d'extraction. En outre, pour l'extraction de la fluorescence chlorophyllienne à partir de satellites, nous explorons les impacts de l'absorption atmosphérique et de la dispersion sur l'extraction de la fluorescence pour préparer le développement de l'algorithme d'extraction de la fluorescence de chlorophylle à partir de satellites.

Le chapitre 2 présente la théorie et les méthodes de détermination de la fluorescence chlorophyllienne. Dans cette thèse, nous présentons entièrement la génération de la fluorescence chlorophyllienne, les méthodes de mesure et les méthodes de détermination du SIF au sol ou à partir de mesures aéroportées/satellitaires.

Quand la molécule de chlorophylle absorbe la lumière rouge (centrée à 670 nm), elle passe au premier état singulet excité; quand la molécule de chlorophylle absorbe la lumière bleue, elle passe au deuxième état singulet excité. Les molécules de chlorophylle dans le premier état excité font un travail chimique pour consommer l'énergie et revenir à l'état initial. La fluorescence, la phosphorescence et l'émission de chaleur sont aussi des conséquences de l'émission d'énergie des différents stades vers l'état initial.

Des mesures de fluorescence de chlorophylle actives peuvent être faites de deux façons: 1) le fluorimètre à impulsion modulée. Le fluorimètre à impulsion modulée utilise une électronique sophistiquée pour séparer la fluorescence de chlorophylle de la lumière ambiante. Le système réalise cela grâce à l'utilisation d'une lumière d'excitation à pulsations rapides pour provoquer une émission de fluorescence pulsée correspondante. Le fluorimètre utilise une photodiode fortement sensible pour détecter et enregistrer le signal de fluorescence pulsé et ignorer n'importe quel signal non-pulsé. 2) les fluorimètres à excitation continue. Le fluorimètre à excitation continue est conçue pour mesurer l'induction Kautsky ou l'induction de Fluorescence de la Chlorophylle Rapide.

La fluorescence de la chlorophylle passive exploite toujours la technologie de télédétection pour extraire la fluorescence de la chlorophylle induite par le Soleil de l'énergie réfléchie par la végétation. Le signal reçu au capteur inclut le signal réfléchi et la fluorescence de chlorophylle excitée par la végétation. La contribution de fluorescence de chlorophylle à la radiance reçue au capteur est très faible (seulement 1-5 % de la radiance réfléchie). Donc, les méthodes de détermination de la fluorescence de chlorophylle causée par le Soleil exploitent des stratégies différentes pour extraire la fluorescence.

Les méthodes utilisées en général pour estimer la fluorescence de la chlorophylle au sol sont divisées en deux catégories: 1) les approches basées sur la radiance. Les approches à base de radiance exploitent 2 ou 3 bandes spectrales (dont au moins une proche de la raie de Fraunhofer) ou des bandes continues pour extraire la fluorescence quantitativement. Ces méthodes sont développées sur les données de hautes résolutions spectrales. Les méthodes basées sur la radiance incluent la profondeur de la raie de Fraunhofer (FLD), (3FLD) 3 bandes FLD, (cFLD) corrigé FLD (iFLD), amélioré FLD, (eFLD) FLD prolongé et la méthode d'ajustement spectrale (SFM) (Meroni et al. 2009). La fluorescence extraite des approches basées sur de radiance a une signification physique; 2) les approches à base de réflectance. Les méthodes à base de réflectance exploitent principalement 2 ou 3 bandes dans la gamme de 650-800 nm pour construire un index de réflectance lié avec la fluorescence. Ces méthodes évaluent seulement la fluorescence qualitativement et la fluorescence n'a aucune unité physique. Les méthodes à base de réflectance peuvent être divisées en trois catégories: rapport de réflectance, indice dérivé et indice de remplissage.

Quand nous détectons la fluorescence de chlorophylle sur la feuille ou canopée, le trajet de propagation de fluorescence de chlorophylle est court. On peut penser que la fluorescence de chlorophylle observée n'est pas affectée par l'atmosphère et que c'est la vraie fluorescence de chlorophylle. Si nous détectons la fluorescence de chlorophylle à partir de l'espace, la fluorescence de chlorophylle passe par l'atmosphère et est affectée par la dispersion atmosphérique et l'absorption. Comparé à la réflexion de la végétation, l'intensité du signal de fluorescence est faible. Si nous voulons extraire la fluorescence chlorophyllienne, il est important d'enlever l'effet d'atmosphère. La manière d’enlever les effets atmosphériques et améliorer l'exactitude de récupération SIF a attiré les attentions des chercheurs. Ces dernières années, beaucoup de méthodes ont été développées pour mesurer la fluorescence de chlorophylle à partir de l'espace. Basées sur les littératures passées, les méthodes d’extraction

de la SIF de l'espace exploitent toujours des caractéristiques d'absorption atmosphérique, principalement la bande d'absorption d'oxygène ou les lignes de Fraunhofer.

Le chapitre 3 concerne la détection de fluorescence chlorophyllienne des feuilles sous différentes teneurs en eau (Ni et al. 2015a). La fluorescence chlorophyllienne est affectée par la structure du couvert végétal, la teneur en chlorophylle et l'illumination et ainsi de suite. A l'échelle de la feuille, la détection de fluorescence chlorophyllienne peut éviter de considérer les effets de la structure du couvert, et permet d'obtenir la fluorescence réelle. La mesure de la fluorescence de la chlorophylle comprend la mesure active et la passive mesure. Les mesures actives et passives sont utilisées pour mesurer la fluorescence de la chlorophylle, et la cohérence entre elles démontre la fiabilité des mesures (Zarco-Tejada et al., 2000c, 2009). La fluorescence chlorophyllienne peut refléter la variation de l'état physiologique de la végétation rapidement. Lorsque la plante est en état de stress, le tissu végétal peut augmenter la dissipation de la chaleur pour consommer de l'énergie supplémentaire, et dans le même temps diminuer le rendement de la fluorescence de la chlorophylle.

Dans ce chapitre, nous développons la recherche sur la détection de la fluorescence de la chlorophylle des feuilles, et étudions la cohérence entre la fluorescence active et passive pour les différentes teneurs en eau. De plus, nous observons la réponse de la fluorescence de la chlorophylle à la variation de la teneur en eau. Dans un premier temps, nous analysons la réponse de la fluorescence induite par le soleil et la température aux états différents de stress hydrique en utilisant le modèle de SCOPE. Ensuite, nous introduisons l'expérience de contrôle de l'eau du maïs en pot, analysons la relation entre la fluorescence active et la fluorescence passive, la température des feuilles et l'eau du sol contenu dans les pots de maïs. En dernier, nous analysons la cohérence entre la fluorescence active et passive, et la réponse différente de la fluorescence active et passive et des températures au stress hydrique précoce.

Grâce à l'étude de la fluorescence en chlorophylle des feuilles, on obtient plusieurs conclusions: 1) Le modèle SCOPE est utilisé pour simuler la variation quotidienne de fluorescence de la chlorophylle et de la température sous contrôle en eau. La comparaison avec des plantes en bonne santé montre que la fluorescence de la chlorophylle diminue sous la condition de contrainte en eau et la température augmente. La relation entre la fluorescence de la chlorophylle et de la température montre qu'il existe une bonne relation linéaire entre eux avant midi, et complexe l'après-midi; 2) Dans l'expérience du gradient d'arrosage, la fluorescence pour le maïs est faible sous stress hydrique. Quand le stress hydrique devient

plus sévère, la température augmente progressivement. La fluorescence active est intimement liée au niveau d'eau. Dans l'expérience d'arrosage, la différentes réponses de la fluorescence active et la température au changement teneur en eau illustrent que la fluorescence active est beaucoup plus sensible aux changements de teneur en eau que la température, et que la température peut refléter le stress hydrique précoce; 3) La fluorescence passive normalisée du maïs augmente tout d'abord, puis diminue, et est cohérent avec les résultats simulés par SCOPE. Les expériences contrôlées montrent que la fluorescence passive normalisée peut refléter le changement de teneur en eau, et que la plante peut retrouver un état sain quand le stress de la végétation diminue.

Le chapitre 4 présente la méthode de d'obtention du SIF dans des conditions proches du sol en utilisant l'indice de réflectance (Ni et al. 2015b). La fluorescence de la chlorophylle induite par le soleil (SIF) près du sol comprend les méthodes basées sur radiance et les méthodes basées sur la réflectance. La méthode basée sur la radiance permet de récupérer la fluorescence quantitativement, et la fluorescence récupérée a une signification physique avec l'unité de rayonnement. Ces méthodes exploitent le remplissage des SIF dans la ligne Fraunhofer pour extraire le SIF, et sont largement utilisés pour récupérer le SIF. Les méthodes basées sur la réflectance utilisent deux ou trois bandes pour construire l'indice de réflectance pour évaluer la SIF rapidement et simplement. Bien que les méthodes basées sur la réflectance évaluent seulement la SIF qualitativement, elles sont souvent les seules méthodes utilisables sous les certaines conditions, telles que la lumière artificielle ou quand la méthode basée sur la radiance est en défaut. Cela montre également qu'il est nécessaire de développer des méthodes basées sur la réflectance.

Dans le chapitre, une recherche est développée sur la base du modèle FluorMOD, et l'analyse de sensibilité du modèle FluorMOD est effectuée. Sur la base des résultats de l'analyse de sensibilité, nous sélectionnons les paramètres sensibles à utiliser pour générer les données simulées. Ensuite, nous construisons la relation quantitative entre la fluorescence et l'indice de réflectance en utilisant les données simulées, et comparons les résultats avec les méthodes traditionnelles, telles que FLD et 3FLD, pour valider nos méthodes.

De ce travail, nous obtenons deux conclusions principales : 1) On utilise le modèle FluorMOD et les indices de réflectance ( R685 / R850 , R740 / R630 ou R750 / R710), le rendement quantique de fluorescence, la température des feuilles et l'angle du zenithal solaire pour construire un modèle quantitatif pour estimer le rayonnement de fluorescence. En

comparant la méthode présentée dans ce document avec les méthodes FLD et 3FLD, il peut être montré que la méthode FluorMOD peut être appliquée pour extraire quantitativement la fluorescence ; 2 ) Les méthodes basées sur la réflectance avec d'autres paramètres permettent d'obtenir le SIF quantitativement, et apportent une nouvelle façon de détermination de la fluorescence et ouvre la voie aux combinaisons de la télédétection hyperspectrale et de la télédétection infrarouge thermique pour obtenir la fluorescence.

Le chapitre 5 porte sur les effets de l'absorption et la diffusion atmosphériques sur la récupération des SIF depuis l'espace (Ni et al. 2016). En observant le SIF mesuré près du sol, on peut considérer que le signal de SIF est la fluorescence réelle, car la fluorescence n'est pas affectée par l'absorption et la diffusion atmosphériques. Par conséquent, la détermination du SIF appliquée à la surveillance de la végétation à l'échelle de la feuille et près du sol est réussie. L'obtention du SIF à partir de données aéroportées/satellitaires fait face à des défis. L'intensité SIF est très faible par rapport à l'énergie réfléchie ne représentent 1-5% dans la région infrarouge. Ainsi, la récupération du SIF devra tenir compte des effets atmosphériques（Guanter et al., 2010; Frankenberg et al., 2011）. L'analyse des effets de l'atmosphère sur la récupération SIF est une façon d'appréhender l'idée des méthodes de récupération SIF. La détection SIF à partir de données aéroportées/satellitaires est une question de recherche importante, et est considéré comme la tâche essentielle de la mission FLEX. Jusqu'à présent, l'étude de la détection SIF a obtenu des résultats, et la littérature antérieure montre que la méthode de détermination du SIF peut être couronnée de succès quand elle est appliquée à GOSAT Tanso-FTS, GOME-2, SCIMACHY et OCO-2. Parce que la bande d'absorption de l'oxygène chevauche le pic du spectre de fluorescence, les bandes d'absorption de l'oxygène sont considérées comme les meilleures bandes pour récupérer le SIF (Damm et al., 2014). En combinant les informations atmosphériques, il est possible de séparer la fluorescence de l'énergie réfléchie.

Dans ce chapitre, nous utilisons les modèles SCOPE et MODTRAN pour générer le rayonnement simulé niveau capteur, y compris la contribution de la fluorescence. Selon différentes combinaisons de canopée (Cab, FQE et LAI), de conditions atmosphériques (VIS, contenu en eau) et des paramètres géométriques (SZA, hauteur du capteur et élévation), le rayonnement de TOA, y compris la contribution de la fluorescence, est simulé par l'équation de transfert du rayonnement. Sur la base des données simulées, nous sélectionnons quatre indicateurs en corrélation avec la fluorescence pour analyser les effets atmosphériques sur ces indicateurs. Parce que les bandes d'absorption d'oxygène sont les fenêtres idéales pour extraire

le SIF, nous portons plus d'attention à l'analyse des effets atmosphériques sur la profondeur d'absorption d'oxygène. Nous testons les sensibilités des cinq paramètres (SZA, hauteur du capteur, l'élévation, le VIS et la teneur en eau) sur la profondeur d'absorption d'oxygène et sur d'autres indicateurs relatifs à la fluorescence. De plus, nous analysons les effets atmosphériques sur trois méthodes d'extraction du SIF (méthodes de Damm, Braun et DOAS), et cela illustre la nécessité de la correction atmosphérique dans l'algorithme de récupération de SIF. Par ailleurs, l'expérience aéroportée est réalisée pour illustrer davantage que des paramètres atmosphériques précis peuvent améliorer la précision de la récupération de SIF. Les résultats de ce chapitre peuvent apporter un soutien théorique à la mise au point de méthodes de d'extraction du SIF.

Les principales conclusions de ce chapitre sont les suivantes: 1) L'analyse de sensibilité montre que le SZA, la hauteur du capteur et le VIS sont les paramètres importants et sensibles de ces quatre indicateurs. Nous nous sommes concentrés sur la sensibilité des paramètres atmosphériques sur la profondeur d'absorption d'oxygène. La profondeur augmente progressivement avec l'augmentation des SZA et la hauteur du capteur. En revanche, elle diminue avec l'augmentation de la VIS et l'élévation, et elle change peu avec la variation de la teneur en eau; 2) L'analyse des méthodes de Damm, Braun et DOAS montre que les paramètres atmosphériques précis peuvent améliorer la précision de la récupération de SIF. En outre, la méthode de Damm est sensible aux variations de hauteur et de SZA du capteur dans l'$O_2$-A et les bandes B-$O_2$. Pour la méthode DOAS, l'élévation et le VIS sont des paramètres sensibles dans les $O_2$-A et $O_2$-B bandes, respectivement; 3) Nous utilisons les méthodes Damm et 3FLD pour récupérer la fluorescence d'une image aéroportée AISA, et les résultats de ces deux méthodes ont une relation étroite avec les mesures sol du PAM-2500. La performance de la méthode Damm est meilleure que celle de la méthode 3FLD. L'analyse des cinq plantes, à savoir, Ailanthus, orme, pêcher de montagne, saules et de frêne, a révélé la présence de différences de fluorescence entre les différents types de végétation. Parmi ces cinq types de végétation, les valeurs de fluorescence des frênes et des ormes sont supérieures à celles des autres végétations. L'évolution de la variation de la fluorescence en utilisant la fluorescence active et passive est cohérentes.

Le chapitre 6 résume les conclusions et nous signalons les problèmes qui existent encore et donnons les perspectives de la télédétection du SIF.

Tout d'abord, nous étudions la détection de la fluorescence de la chlorophylle des feuilles à l'échelle sous contrôle d'arrosage. Pour la feuille, une expérience précise de la fluorescence de la chlorophylle est le mieux pour comprendre la cohérence de la fluorescence active et passive ainsi que la réponse de la fluorescence de la chlorophylle au stress hydrique. Le modèle SCOPE est utilisé pour simuler la fluorescence et la réponse en température au stress. Par ailleurs, l'expérience de l'eau de contrôle est effectuée sur le maïs. Une série de mesures diurnes, comme fluorescence de la chlorophylle des feuilles, le spectre de la feuille, la température et le rayonnement photosynthétiquement actif, sont menées pour le maïs au cours de l'expérience. La comparaison entre la fluorescence active et passive a montré la cohérence de la fluorescence active et passive dans le cadre du changement dynamique de la teneur en eau. Dans l'expérience de contrôle des eaux, nous étudions la fluorescence de la chlorophylle et la réponse de la température au changement teneur en eau. L'expérience montre que gradient de fluorescence de la chlorophylle peut refléter le changement de teneur en eau. L'expérience de remplissage montre que la fluorescence de la chlorophylle peut refléter le stress hydrique précoce. La fluorescence du maïs sous le déficit hydrique peut revenir à l'état initial dans des conditions de bon arrosage, mais la température ne récupère pas l'état initial dans ces conditions et révèle que le niveau de stress de température et de l'eau ont la relation complexe. L'étude de la détection de la réponse de fluorescence de la chlorophylle au déficit hydrique, l'analyse de réponse de la température à un déficit hydrique est ajoutée pour améliorer les résultats de détection.

Deuxièmement, nous développons la méthode de récupération de la fluorescence quantitative induite par le soleil à base de réflectance au niveau du sol. Sous la condition de lumière artificielle, la méthode basée sur les réflectances est la seule méthode pour détecter la fluorescence, mais ce genre de méthode ne peut pas extraire la fluorescence quantitativement. Dans cette thèse, sur la base des données simulées, nous avons construit la relation quantitative entre la fluorescence et l'indice de réflectance. Nous effectuons l'analyse de sensibilité avec le modèle FluorMOD pour générer les données simulées, et choisir l'indice de réflectance optimal, et construisons les relations quantitatives entre la fluorescence et l'indice de réflectance. Les méthodes développées ont de bons coefficients de corrélation avec la fluorescence. En outre, par comparaison avec les méthodes FLD et 3FLD, les méthodes présentées dans ce document donnent de meilleurs résultats, et peuvent être utilisées pour estimer la fluorescence. Cette méthodologie fournit de nouvelles perspectives pour la récupération quantitative de SIF à partir du spectre de réflectance

Troisièmement, nous étudions les effets de l'atmosphère sur l'estimation de fluorescence satellite solaire induite. La correction atmosphérique est l'étape nécessaire dans le procédé de d'extraction de la fluorescence induite par le soleil par satellite. Dans ce travail, radiance en haut de l'atmosphère (TOA) est générée par les modèles MODTRAN 4 et SCOPE. Sur la base des données simulées, l'analyse de sensibilité est effectuée pour évaluer la sensibilité des quatre indicateurs (depth_absorption_band, depth_nofs-depth_withfs, radiance et Fs / radiance) aux paramètres atmosphériques (angle soleil zénithal (SZA), hauteur du capteur, élévation, visibilité (VIS) et teneur en eau) dans les bandes d'absorption de l'oxygène. En outre, une comparaison de l'extraction de la fluorescence à l'aide de trois méthodes et la fluorescence SCOPE indique que la correction atmosphérique précise peut améliorer la précision sur la fluorescence. Pour valider la conclusion, nous extrayions la fluorescence de l'image hyperspectrale d'un capteur à bord d'un dirigeable en utilisant deux méthodes différentes, l'une prenant en compte la correction atmosphérique et l'autre non. Nous comparons la fluorescence de du dirigeable la fluorescence mesurer au sol et montrons la nécessité de la correction atmosphérique, ainsi que la cohérence entre la fluorescence active et passive.

Bien que l'étude de la détection de SIF multi-échelle a fait quelques réalisations et progrès dans cette thèse, il reste encore des problèmes à résoudre : 1) Dans le processus de la génération de données simulées, il serait intéressant d'examiner les différents types de LIDF pour couvrir les données complètes ; 2) Dans la méthode de d'estimation du SIF quantitatif en utilisant l'indice de réflectance , il reste encore une étape de validation en utilisant les données terrain; 3) Lorsque nous étudions les effets de l'absorption et la diffusion atmosphériques sur la récupération de SIF, nous devrions envisager d'autres paramètres et d'élargir la gamme des paramètres sélectionnés afin d'augmenter la couverture .

Cette thèse est dirigée par les superviseurs de l'Université de Strasbourg et de l'Université normale de Beijing, et est parrainé par le Programme national de recherche de base de la Chine (973 Programme), National Natural Science Foundation de Chine.

# 摘要

植被被定义为生长在地球表层的一切植物类型的总称。在整个地球系统中，植被扮演着十分重要的角色，也是地球表层内最重要的一种可再生资源。植被被认为是在全球变化中最具活跃性和最有价值的影响因子，对地气系统间的能量平衡有着重要影响，其在水文、生化循环和气候变化中起着十分重要的作用，是重要的衡量人文和气候因子对环境影响的敏感性指标。植被能够通过光合作用释放大量的氧气，构建了我们人类赖以生存的舒适环境，而且植被构成的有机物也是我们人类得以生存的粮食作物。此外，植被也影响着气候变化。因而植被常被看作为地球生态系统的主题，并在整个地球的物质和能量循环过程中起着重要的作用。然而，由于全球气候变化、人口激增以及能源需求剧增，给农业生产带来的压力愈来愈大，而全球或区域性的粮食供应短缺问题也时有发生。因而，实时准确地监测全球的粮食生产状况，对于粮食的安全和人类社会可持续发展具有重大意义。

植被叶绿素荧光从 80 年代不断被证明是监测植被生理状态变化的有效、无损和直接的探针。叶绿素荧光、光合作用和热耗散是植被吸收能量的三大耗散途径。三者之间相互竞争。用于光合作用的能量减少，则用于叶绿素荧光发射的能量增多，反之亦然。因此，发射叶绿素荧光的量可以作为衡量光合作用的指标。由于植被的光合作用和叶绿素之间的关系密切，监测叶绿素荧光的变化，在植被可见的变化症状出现前，通过叶绿素荧光的改变监测植被系统的变化。

本文主要分为六章，各章节介绍如下：

第一章为绪论。主要介绍了本论文的研究背景、研究意义、国内外研究现状、研究目标与内容以及本文的结构。

日光诱导叶绿素荧光是一种新的遥感监测手段，越来越多的用于监测植被生理状态的变化。叶绿素荧光、光合作用和热耗散作为植被吸收能量的三个主要耗散途径，三者之间相互竞争。通过估测叶绿素荧光，可以直接反映植被的光合作用变化。因此，利用叶绿素荧光监测植被变化及其相关生理变化相对于传统的植被监测方法更有优势。本文分别针对叶片、近地面、航空/航天等不同尺度日光诱导叶绿素荧光的探测问题展开了研究。

由于植被监测对全球生态平衡的重要性和叶绿素荧光的直接有效性，本文以叶片尺度的叶绿素荧光研究为切入点，开展了叶绿素荧光和叶片温度在不同水分状态下的变化。叶片叶绿素荧光可以通过荧光测量仪直接测得，或者直接从叶片反射光谱中提取。在叶片叶绿素荧光获得的过程中，所受到的影响因素较少，且得到的叶绿素荧光可近似认为是真实的叶绿素荧光。在此基础上展开的叶绿素荧光对早期水分胁迫的响应，以盆栽玉米为例，说明了叶绿素荧光和叶片温度能够反映盆栽玉米在早期水分胁迫时的变化。

为了扩大叶绿素荧光在植被监测中的应用，需要通过近地面或者卫星上日光诱导叶绿素荧光来分析植被的生理状态变化。通过遥感方式估测叶绿素荧光的关键是如何把叶绿素荧光从反射的能量中分离出来。在提取近地面叶绿素荧光时，收集信号的传感器距离地面较近，大气的影响可忽略不计，荧光提取算法相对简单，但是在星载叶绿素荧光的提取算法中，大气吸收和散射作用的影响较大，因而需要进行相应的大气校正，才能得到真实的叶绿素荧光。因此，我们总结了近地面叶绿素荧光提取的提取算法，基于反射率的荧光提取算法在某些时候是唯一可以的提取算法，也表明了发展基于反射率的荧光提取算法的必要性。在本文，我们发展了基于反射率指数的近地面叶绿素荧光定量提取算法，并与其它的经典算法做比较，以此说明定量提取算法的可行性。此外，在星载叶绿素荧光的提取中，我们探讨了大气吸收和散射对荧光提取的影响，为以后的星载叶绿素荧光提取算法的发展做了铺垫。

第二章是叶绿素荧光的基础理论及其提取方法研究。在本章，系统全面的介绍了叶绿素荧光的产生、测量方法及其在近地面和卫星上的提取方法研究。

叶绿素分子吸收量子之后，自身的能量状态发生改变，从稳定态变为激发态，处于激发态的叶绿素分子需要转移能量返回稳定态。当叶绿素分子吸收红光（670nm）后，被激发到第一单线态；吸收蓝光之后，被激发到第二单线态。处于第一单线态的叶绿素分子，进行光化学反应消耗能量，返回基态。光化学反应是消耗能量返回基态的重要途径。处于第一单线态的电子，也可以通过发出热量从不稳定状态返回稳定常态。此外，第一单线态的电子，也可以发射一个更长的光子返回常态，在这个过程电子所发射的波长较长的光称为荧光。当光合作用中的光化学反应过程受阻时，发射的荧光则增多，荧光强度相应增大。叶绿素荧光和磷光是叶绿素分子受激发之后的产物，叶绿素分子受激发是光能转化成化学能的第一步，叶绿素分子受激发之后需要通过释放能量返回稳定态，而释放的能量则被传递给光反应中心中的叶绿素 a 分子，用于进行光反应。正因为叶绿素荧光和光合作用的密切关系，叶绿素荧光被认为是探测植被的直接有效无损的探针。叶绿素荧光也广泛用于植被监测。

目前常用的叶片水平的叶绿素荧光的探测手段有主动测量和被动测量。主动式叶绿素荧光的测量包括两种方法：脉冲调制式荧光仪测量和连续激发式（非调制式）荧光仪测量。被动式荧光主要是通过遥感方法探测荧光。1983 年，WALZ 公司首席科学家，德国乌兹堡大学教授 Ulrich Schreiber 博士利用调制技术和饱和脉冲技术，设计制造了全世界第一台脉冲振幅调制荧光仪 PAM，利用荧光仪可以测得植被的荧光动力学曲线。叶绿素荧光动力学技术能够测定植被叶片光合作用过程中光系统对光能的吸收、传递、耗散、分配等方面，与气体交换参数相对比，叶绿素荧光参数更能反映植被的内在性特点。叶绿素荧光动力学参数被广泛用于测量植被的叶绿素荧光。通过 PAM 所测得的叶绿素荧光，与其他地面实验参数（气孔导度、植被叶水势及叶片温度等）结合，用于诊断植被胁迫。非调制式荧光仪对植物叶片照射之后，快速记录叶片的瞬时荧光，也广泛用于植被监测。

被动式荧光测量是通过遥感方式估测日光诱导荧光。在太阳光照下，传感器收到的信号包括两部分：叶片反射的能量和叶片发射的荧光。荧光对卫星上接收的辐亮度的贡献较小，大约占反射的辐亮度的 1%-5%。因此，如何把荧光从叶片反射的信号中分离出来是荧光提取算法的关键。

近地面上定量提取日光诱导荧光的方法主要分成两大类：基于辐亮度的方法和基于反射反射率的方法。基于辐亮度的方法是基于夫朗禾费暗线的窄吸收特征和高光谱分辨数据，使用 2 或 3 个通道（至少一个通道位于夫朗禾费吸收线附近）或者连续的感兴趣波段定量提取荧光。使用离散通道的多光谱方法有 Fraunhofer Line Depth（FLD）、3 波段 FLD （3FLD）、校正 FLD （corrected FLD, cFLD）；高光谱方法有改进 FLD（improved FLD，iFLD）、扩展 FLD（extended FLD，eFLD）和波谱拟合法（spectral fitting method ，SFM）。Plascyk 和 Plascyk & Gabriel 提出了 FLD 算法。所有的辐亮度方法均是在 FLD 算法的基础上发展的。FLD 算法利用位于夫琅禾费暗线内部和外部的入射太阳辐照度和目标辐亮度估算荧光对夫朗合费井的填充程度。在算法中，需要知道吸收线内部（$\lambda_{in}$，$O_2$-B 687nm 和 $O_2$-A760nm）的入射太阳辐照度和目标辐亮度，吸收暗线附近波段（$\lambda_{out}$，686nm 和 758nm）的入射太阳辐照度和目标辐亮度。FLD 算法比较简单，仅需要知道两个通道的入射太阳辐照度和目标辐亮度。实际上，尽管这两个通道足够接近，但是反射率 r 和荧光 F 在这两个通道上不会保持不变。FLD 算法的前提条件是 r 和 F 在吸收暗线内外两个通道上保持不变。许多作者针对这个假设前提提出了质疑，因此在 FLD 的基础上发展了其他算法。

基于反射率方法主要利用650-800nm波谱范围的两个或者三个通道构建与荧光有关的光谱指数，计算出的荧光没有物理意义。此类方法可以分为反射率比值指数，导数

指数和填充指数。反射率比值指数没有利用夫琅禾费暗线，而是利用了2-3个通道，其中至少一个通道受到荧光影响或者位于荧光峰值附近，其余通道不受荧光影响。构建指数时，通道之间的归一化处理可消除反射率形状的影响。导数指数是对几个通道的反射率导数进行归一化提取荧光。与反射率相比，反射率导数更能探测出荧光的细微变化。填充指数是用R760.5-R759.9估测表观反射率凸起的峰值高度。荧光叠加在表观反射率上表现为表观反射率曲线在氧气吸收带处存在一个峰值。通过这凸起峰值高度的估测来定性的表示荧光的大小。反射率比值和导数比值法只是对荧光比较敏感的指数，并不能把荧光从反射率中分离出来，在实际运用中存在着许多问题。使用填充指数时，要注意在氧气吸收带处的荧光填充深度受太阳高度角等因素的影响，使用此方法对植被分析时尽量保持测量时间和位置相对一致。基于反射率方法不需要其他方法复杂的过程，但是估测的荧光没有物理意义，且有些指数受叶绿素含量影响较大。尽管有这些局限性，基于反射率的方法在有的时候是唯一的估测荧光的方法，比如使用人工光源或者所有的辐亮度方法均不行。

光照下的植被叶片发射叶绿素荧光，在叶片或者植被冠层观测叶绿素荧光，获取的叶绿素荧光没有受到大气的影响，可认为是叶片真实的叶绿素荧光；假如在低空或者卫星上观测，叶绿素荧光从植被叶片传递到传感器，需要经过大气的吸收和散射，最终传感器上并不能得到真实的叶绿素荧光。太阳辐射在传播过程中，先穿透大气到达地球表面，与地表地物相互作用之后，地表反射的太阳辐射或发射的电磁波信息再经过大气到达传感器。因此，传感器接收到的信号包含了许多信息，有太阳的几何位置信息、大气信息、地表信息和传感器自身因素引起的信息衰减和失真等。因此，在对传感器接收到的信号分析时，需要考虑各种因素对太阳辐射传输的影响。在卫星或者低空上提取叶绿素荧光，需要去除大气的影响，得到真实的叶绿素荧光。目前，基于航空或航天数据提取叶绿素荧光的思路主要有两个：一是基于大气吸收带（主要是氧气吸收带），二是基于太阳夫琅禾费暗线。这两个方法目前应用范围较广，在许多文献中均有体现。光波在大气中传播时，某些波长的波被大气中各种气体成分吸收而产生暗线或暗带，主要气体有氧气$O_2$、水蒸汽$H_2O$、二氧化碳$CO_2$及臭氧$O_3$等气体，其中$CO_2$和$O_3$气体含量比较少，一般不考虑。在$O_2$-A吸收带（758-778nm）中，需要考虑的气体类型单一，氧气所占的比例稳定，透过率的变化范围比较大，且$O_2$-A与叶绿素荧光的峰值（740nm）相近，因此，$O_2$-A吸收带是比较理想的叶绿素荧光探测窗口。在轨运行的具备$O_2$-A带探测能力的科学仪器有SeaWiFS，GOME，GOSAT，SCIAMACHY，POLDER，OCO和MERIS等。

第三章是不同水分状态下的叶片叶绿素荧光探测。叶绿素荧光受植被冠层结构、叶绿素含量及光照等影响。叶绿素荧光、光合作用和热耗散是叶片吸收的能量的三个

主要用途。通过对叶绿素荧光的观测，可以观察到植被生理变化情况。传统的遥感手段通过植被的反射、发射和散射的信息反演植被的生化参数，如叶绿素含量、叶面积指数等，通过对植被生化参数的监测间接判断植被的生理状况。叶绿素荧光与光合作用的密切关系，使其成为一种直接有效的植被遥感监测手段。在叶片尺度上探测叶绿素荧光时，可以避免考虑植被冠层结构等因素的影响，得到更加准确的植被叶绿素荧光。叶绿素荧光常见的探测方法包括主动探测和被动探测。主动荧光测量和被动荧光测量用于植被的监测中，通过对主被动荧光探测的一致性说明了测量结果的可靠性。叶绿素荧光与植被光合作用密切相关，能够快速反映植被的生理变化。当植被处于某种胁迫时，通过观测叶绿素荧光的响应判断植被生理状况的变化。当植被处于胁迫的初期或者中期阶段时，植被组织通过增加热耗散释放多余的能量，降低叶绿素荧光产量。

在本章节中，我们开展了叶片尺度的叶绿素荧光探测研究，探讨了水分状态动态变化过程中的主被动荧光测量的一致性，且观测了叶绿素荧光对水分状态变化的响应。如图 3-1 所示，首先利用 SCOPE 模型模拟不同胁迫状态下的荧光和温度的日变化，从理论上了解荧光和温度对水分胁迫的响应；其次通过对玉米叶片的主被动荧光观测，探索荧光对不同水分等级的响应，同时分析叶片温度对水分胁迫的响应。理论和实验结合分析了荧光和温度对水分状况的不同响应，说明了荧光和温度结合能更好地反映植物的水分状况和胁迫程度。

通过本章节叶片尺度的叶绿素荧光研究，我们说明了在水分状态变化的情况下，主被动荧光仍然保持一致，且能够反映其变化。此外通过分析温度对水分状态变化的响应，能够与荧光协同反映植被早期水分胁迫。在本章中，我们通过理论模拟和实验分析说明了主被动荧光对不同水分状态的响应，在且实验中说明了水分动态变化过程中的主被动荧光的一致性。

本章节的主要贡献如下：（1）使用了 SCOPE 模型模拟了不同胁迫程度下荧光和温度的日变化。与处于健康状态的植被叶绿素荧光相比，胁迫状态下的植被叶绿素荧光下降，温度上升。从叶绿素荧光和温度的关系可以，在中午前两者存在较好的线性关系，在中午后两者之间的关系变得较为复杂。（2）梯度浇水实验表明了在土壤含水量较低的情况下玉米主动荧光较低，叶片温度缓慢较高，且主动荧光相对与温度来说能够准确反映水分含量等级；补齐浇水实验通过主动荧光和温度对水分变化的不同响应说明了主动荧光对土壤水分的敏感性大于温度对土壤水分的敏感性，且主动荧光能够反映植被的早期水分胁迫。（3）玉米的归一化被动荧光的日变化呈现先升高后下降的趋势，与 SCOPE 模型的荧光日变化趋势一致。控水实验说明归一化被动荧光能够反

映不同水分状态的变化，且在植被早期水分胁迫解除时能够恢复到正常状态。（4）通过整个实验阶段的主被动荧光的比较，说明了在水分状态变化的情况下，主被动荧光仍然保持一致性。主被动荧光间的一致性充分表明了两者测量结果的可靠性，且叶片尺度上主动荧光可以作为被动荧光测量结果的验证方法。

第四章为基于反射率指数的近地面日光诱导叶绿素荧光提取。日光诱导荧光是监测植被生理状态变化和早期环境胁迫的有效指针。叶绿素荧光与植被光合作用、热耗散是叶片吸收能量的三大耗散途径。叶绿素荧光的波谱范围为 650-850nm，且在波谱范围内具有两个波峰。其中一个波峰位于 687nm 附近，另一个位于 740nm 附近。因此一些反射率指数用于探测叶绿素荧光，比如红/近红波谱比值。叶片尺度的叶绿素荧光研究使人们认识了叶绿素荧光，加深了对叶绿素荧光的理解，相反，人们对叶绿素荧光的深入了解也加速了叶绿素荧光遥感的发展，把叶绿素荧光的研究从叶片上扩展到近地表。荧光模型的出现帮助了人们更好了理解冠层叶绿素荧光与其他光合参数环境参数之间的关系。目前已有的荧光模型有 FluorMOD 模型和 SCOPE 模型。这两个模型均能够模拟植被的荧光变化。荧光强度随着植被的状态（种类、物候和活力等）和光合有效辐射而变化。在不同的光照条件下，近地面红外荧光的变化范围为 0.5-10.5 mW $m^{-2}$ $nm^{-1}$ $sr^{-1}$，近地面远红外荧光的变化范围为 0.5-12.0 mW $m^{-2}$ $nm^{-1}$ $sr^{-1}$。在此荧光变化的范围主要归结为光照条件的变化和测量的不确定性。

近地面日光诱导荧光的提取方法主要分为辐亮度方法和反射率方法。基于辐亮度的方法能够准确的估测日光诱导荧光的大小，所得的荧光具有物理意义，与辐亮度单位相同。此类方法利用日光诱导荧光在夫琅禾费暗线处的填充作用，准确的得到植被日光诱导荧光值，广泛用于植被的日光诱导荧光提取中。基于反射率的方法仅使用两个或者三个波段构建不同的指数，相对简单，能够快速简捷得到相对的日光诱导荧光大小。尽管基于反射率的方法只能定性地估测日光诱导荧光，但是在某些情况却是唯一估测叶绿素荧光的方法，比如在使用人工光源的环境下，基于辐亮度的叶绿素荧光估测方法失效。因此，这个事实也说明了发展基于反射率荧光提取算法的必要性。

在本章中，首先利用FluorMOD模型进行数据模拟，在模拟数据的基础上，构建我们所需要的模拟数据数据库。在敏感性分析的基础上选择出对L(F)761影响较大的参数；其次是选择最优的反射率指数，在模拟数据的基础上，建立761nm处日光诱导荧光与反射率指数和其它参数的定量关系。由于FluorMOD模型的模拟条件是自然光照射和无胁迫状态，因此本章节发展的基于反射率定量提取荧光算法适用于无胁迫、自然光照射下的植被。

本章节主要说明了使用反射率指数定量提取日光诱导荧光是可行的。传统的基于反射率提取荧光的方法只能够定性描述荧光的相对大小，在实际运用中受限。本文所提出的定量模型是基于反射率指数和其它植被生理参数构建，用于定量提取近地表的日光诱导荧光。由于本文所使用的模拟数据是由 FluorMOD 模拟生成，FluorMOD 主要用于模拟自然光照射下、无胁迫情况下的冠层反射率及荧光辐亮度，因此本章节的方法主要适用于无胁迫、生长正常的植被。

本章节的主要贡献如下：（1）在 FluorMOD 模型的基础上，我们利用反射率指数（R685/R850、R740/R630 和 R750/R710）、荧光量子产量 Fi、叶片温度 T 和太阳天顶角 θ 建立了定量模型，用于估测冠层叶绿素荧光。通过与已有的方法 FLD 和 3FLD 对比，相关性 $R^2$ 和均方差误差 RMSE 表明此方法能够用于定量提取叶绿素荧光。（2）通过本章节的分析，我们明确了使用反射率指数可以定量提取荧光，但是要辅助其它的参数。这种方法为日光诱导叶绿素荧光提取提供了一条新思路，也为利用高光谱遥感和热红外遥感提取叶绿素荧光做了铺垫。

第五章为大气吸收和散射对航空/航天日光诱导叶绿素荧光提取的影响。在观测近地表植日光诱导荧光信号时，不需要考虑大气吸收和散射对荧光信号的影响，因此在叶片和近地面上应用比较成功，本文也在第三章和第四章分别探讨了叶片尺度和近地面的日光诱导荧光探测。但是，从卫星上估测日光诱导荧光面临着挑战，因为日光诱导荧光与反射的能量相比，比例较小，在近红外区域，仅占反射能量的 1-5%，且近地表的荧光信号到达传感器时受到大气吸收和散射的影响。因此在卫星上探测日光诱导荧光信号时，必须要考虑大气吸收和散射对荧光信号的影响。分析大气对星载日光诱导荧光的提取的影响，有助于理解星载日光诱导荧光提取算法的构建思路。

从航天平台使用遥感技术探测叶绿素荧光是当前的一个重要研究课题，已经作为欧空局荧光探测计划 FLEX 的核心任务。目前为止，关于航天平台荧光探测的初步研究已经取得了一些成果，从已有的文献中可知，一些研究学者发展了航天平台的叶绿素荧光提取算法，并应用于 GOSAT TANSO-FTS、MetOp 卫星上的 GOME-2 传感器、Envisat 卫星的 SCIMACHY 传感器和 OCO-2 所获得的影像。由于氧气吸收波段与荧光波谱峰值有重叠，因此氧气吸收波段是比较认可的荧光提取波段。结合大气信息，准确地从反射的太阳辐亮度中分离出荧光辐亮度是可行的。

本章节的目的是探讨大气影响在氧气吸收带对日光诱导叶绿素荧光提取的影响。与夫琅禾费暗线相比，由于氧气吸收带波段比较宽和深，因此用的更广，但是氧气吸收带范围内的大气影响也会引起叶绿素荧光的提取偏差。在本章节中，我们利用 SCOPE 荧光模型和 MODTRAN 4 生成模拟星载辐亮度数据，并评价了日光诱导荧光提

取对大气参数（太阳高度角 SZA，卫星高度 Sensor height，高程 Elevation, 能见度 VIS 和水汽含量 Water content）的敏感性。此外，我们从航空高光谱成像仪 AISA 影像中利用两种荧光提取算法（考虑大气校正和不考虑大气校正）提取日光诱导荧光，并进行了分析，分析结果进一步说明了大气校正对星载日光诱导荧光提取的必要性。

在叶绿素荧光的提取中，大气的影响是不可忽略的。因此，在本章节中，通过对模拟数据和野外飞行高光谱数据的分析，说明了大气吸收和散射对日光诱导荧光提取的影响，同时说明了大气校正在星载日光诱导提取算法中的必要性。我们利用 MODTRAN 和 SCOPE 模型模拟得到了高光谱数据，研究了在氧气吸收带大气参数对叶绿素荧光的影响。在不同的植被参数（叶绿素含量 Cab、荧光量子产量 Fqe 和叶面积指数 LAI）、大气参数（能见度 VIS 和水汽含量 Water content）和成像几何参数（太阳天顶角 SZA、卫星高度 Sensor height 和高程 Elevation）组合下，通过辐射传输方程计算卫星辐亮度 TOA（包括荧光信息的贡献）。我们分析了五种参数（太阳天顶角 SZA、卫星高度 Sensor height、高程 Elevation、能见度 VIS 和水汽含量 Water content）对氧气吸收深度和其它几种与荧光相关指标的影响；接着我们又分析五种参数对 Damm 算法、Braun 算法和 DOAS 算法提取结果的影响；最后我们利用 3FLD-like 算法从 AISA 航空影像中提取叶绿素荧光，并与 3FLD 提取结果及 PAM-2500 测量结果对比分析。

本章节的主要贡献如下：（1）敏感性分析的结果表明太阳天顶角、卫星高度和能见度是比较重要和敏感的参数，且它们的变化对荧光相关指标影响较为显著。其中，我们重点关注了氧气吸收深度这个指标。随着太阳天顶角和卫星高度的增加，氧气吸收深度逐渐增大，相反，随着能见度和高程的增加，氧气吸收深度减小，且水汽含量的变化对氧气吸收度的变化影响较小。（2）对 Damm 算法、Braun 方法和 DOAS 算法的分析结果表明精度的大气校正能够提高荧光提取的精度。此外，Damm 算法在氧气吸收波段对太阳天顶角和卫星高度的变化敏感，而 DOAS 算法对高程和能见度的变化较为敏感。（3）我们使用 Damm 算法和 3FLD 算法分别从 AISA 航空影像中提取叶绿素荧光，与 PAM-2500 测量荧光具有较强的相关性，且 Damm 算法的提取效果要优于 3FLD 的提取结果。我们分析了五种地物的叶绿素荧光，结果表明不同种类的植被叶绿素荧光存在差异，且不同方法得到的不同地物叶绿素荧光趋势一致。

第六章为结论与展望。叶绿素荧光作为一种新颖的植被监测手段，其在全球碳循环、植被光合作用监测等方面发挥着巨大作用。通过对叶绿素荧光的基础理论了解，我们在本文开展了三项工作，从叶片上、近地面和航空/航天分别对日光诱导叶绿素荧

光进行了研究。在本章节，首先总结了本文所有工作中所得的研究结论，其次分析了本文工作中所存在的不足以及可以改进的地方进行了展望。

综合分析本文的研究成果，所得的结论如下：

（1）不同水分状态下的叶片上叶绿素荧光探测

通过 SCOPE 模型模拟分析不同水分条件下的日光诱导叶绿素荧光和温度的响应，植被处于胁迫状态下，荧光下降，温度上升，日光诱导叶绿素荧光和温度的日变化趋势为先升高再降低，且不同水分条件的日光诱导叶绿素荧光的差别在中午左右达到最大。以盆栽玉米为研究对象，在玉米抽穗期进行控制浇水处理。玉米抽穗期需要大量的水分供给，缺失水分将影响到玉米植株的成长。通过梯度浇水和补齐浇水两组控水实验，分析叶绿素荧光（主动荧光和被动荧光）、叶片温度和土壤含水量的变化。梯度浇水实验充分说明了叶片尺度的叶绿素荧光和温度均能反映植被对早期水分胁迫状态。从正常的浇水量到没有浇水来模拟水分变化。在土壤含水量较少的状态下，叶绿素荧光降低，叶片温度升高。补齐浇水之后，所有的盆栽玉米通过两次浇水均给予了同样的浇水量。在植被早期水分缺失时，植被自身组织并没有缺水而损害。及时的给与水分，能够及时缓解植被的水分胁迫，使植被恢复到一个健康状态。而叶绿素荧光随着水分胁迫的缓解也逐渐回升到充足浇水时的水平，温度并没有得到恢复，说明了叶片日光诱导叶绿素荧光相对温度对早期水分胁迫状态的变化更为敏感，两者结合有望进一步提高早期水分胁迫的遥感监测能力。通过两个控水实验中的主被动荧光对比，表明了在土壤水分动态变化过程中主被动荧光监测一致性，且说明了叶片上主动荧光可以验证被动荧光测量结果准确性，同时表明了被动荧光测量结果的可靠性。

（2）基于反射率指数方法的近地面日光诱导叶绿素荧光提取方法研究

首先，通过荧光模型 FluorMOD 模拟无胁迫情况的日光诱导荧光数据。在 FluorMOD 模型和已有的反射率指数的基础上，构建定量关系式。把此方法的提取结果与已有的 FLD 和 3FLD 算法对比，通过相关性 $R^2$ 和均方根误差 RMSE 说明此方法对于定量提取日光诱导荧光是可行的。在分析过程中，首先对 FluorMOD 进行了敏感性分析，结果得到 L(F)761（761nm 处荧光）对太阳高度角 θ、荧光量子产量 Fi、冠层温度 T、叶面积指数 LAI、叶倾角分布 LIDF 和叶绿素含量 chl-a+b 的变化较为敏感。叶倾角类型常见的为半球型，因此选定叶倾角分布为半球型，构建由 θ、Fi、T、LAI 和 L(F)761 数据库。在已有的反射率指数中，选择出了三个最优反射率指数：R685/R850、R740/R630 和 R750/R710。这三个指数对 LAI 和 Cab 的变化不敏感，仅受到 θ、Fi 和 T 的影响。我们构建了 L(F)761 与 θ、Fi、T 和反射率指数之间的定量关

系。以模拟数据为基础，分别与 FLD 和 3FLD 的提取结果对比分析，说明了此方法可以用于定量提取日光诱导荧光。传统的基于反射率指数的荧光提取算法只能定性衡量日光诱导叶绿素荧光的相对大小，不能够得到定量的荧光值。基于反射率的定量荧光提取算法为我们提取日光诱导荧光提供了一条新思路，也为利用高光谱遥感和热红外遥感提取日光诱导荧光做了铺垫。

（3）大气吸收和散射对航空/航天日光诱导叶绿素荧光提取的影响

航空/航天日光诱导叶绿素荧光探测研究是当前的研究热点。在此研究中，基于 MODTRAN 辐射传输模型和 SCOPE 荧光模型，在不同的植被参数（叶绿素含量 Cab、荧光量子产量 Fqe 和叶面积指数 LAI）、大气参数（能见度 VIS 和水汽含量 Water content）和成像几何参数（太阳天顶角 SZA、卫星高度 Sensor height 和高程 Elevation）组合下，利用辐射传输方程生成含有叶绿素荧光贡献的星载辐亮度数据。选定四种的与叶绿素荧光相关的指标参数：氧气吸收深度 depth_oxygen_band、氧气吸收深度差 depth_nofs-depth_withfs、氧气吸收带处辐亮度 radiance 和氧气吸收带处荧光与辐亮度之比 fs/radiance。通过对四种指标参数的敏感性分析可知，太阳高度角 θ 和卫星高度 sensor height 的变化对四个指标影响较大。在此基础上，我们重点分析了大气参数对氧气吸收带深度的影响。结果表明太阳高度角、卫星传感器高度及能见度的变化对 $O_2$-A 和 $O_2$-B 吸收带深度影响较大，且 $O_2$-A 吸收带深度对这些参数的变化更为敏感。在航空/航天叶绿素荧光提取方法中，可以分为两大类：基于氧气吸收带的提取算法和基于夫琅禾费暗线的提取算法。从中我们选了了三种日光诱导荧光提取算法 Damm 算法、DOAS 和 Braun 算法。三钟算法提取结果与 SCOPE 模拟荧光的相关性及均方根误差结果表明 Damm 算法的提取效果最好，其次为 DOAS 方法，而 Braun 方法则存在着较大的偏差。在使用时，优先考虑使用 Damm 算法和 DOAS 方法。Damm 算法、DOAS 和 Braun 三种方法表明详细的大气校正能够提高日光诱导叶绿素荧光的提取精度。我们以河北保定区域的航空高光谱数据为例，分别采用了不考虑大气校正的 3FLD 方法和考虑大气校正的 Damm 算法提取叶绿素荧光。在我们的研究区域，选定了五种参考地物，在航空数据获得的同时，在地面上使用 PAM2500 测定了稳态荧光。通过对比两类方法提取结果与 PAM2500 测量结果，Damm 算法提取结果与 PAM2500 测量结果相关性为 0.91，而 3FLD 方法提取结果与 PAM2500 测量结果为 0.65。我们可以清楚的发现 Damm 算法的提取结果精度要远高于 3FLD 的提取结果，这也进一步说明了准确详细的大气校正能够提高叶绿素荧光的提取精度。此外，我们也通过对比分析了五种不同地物的荧光变化走向，说明了主被动荧光测量的一致性。

尽管针对多尺度日光诱导荧光研究已取得了一些研究成果，但是在研究过程中仍然存在不足。有待在以后的研究中进一步完善。

1）在控水实验中，直接测量植被水势，则能使实验结果更有说服力。此外，在航空飞行实验中，可以设计不同飞行高度的实验，与近地面实验结合起来，进一步说明大气校正对日光诱导荧光提取的影响；2）在生成模拟数据时，考虑到结果的全面性，需要加入叶倾角分布类型的考虑；3）在基于反射率指数的近地面日光诱导叶绿素荧光提取方法研究中，尚有待利用野外数据对所构建的方法进行验证。4）在探索大气散射和大气吸收对星上日光诱导叶绿素荧光提取的影响时，应该扩大所选择的大气参数个数及所选择范围，增大所选择参数的覆盖面。在以后的研究中，可以增加叶绿素荧光提取算法的种类，全面地对叶绿素荧光提取方法进行总结，并分析不同提取算法对大气参数的敏感性。

日光诱导叶绿素荧光遥感作为一种直接、有效且无损的植被监测方法，受到越来越多人的关注。欧空局的荧光探测计划 FLEX，把利用叶绿素荧光探测植被光合作用作为最主要的任务。经过多次提议，终于于 2015 年 11 月选为欧空局第八次地球探测计划，计划在 2022 年发射荧光探测卫星。通过 FLEX 计划，人们能够得到更多的关于陆表植被的生产力和健康信息。FLEX 计划的实施也将为全球的粮食产量的提高做贡献，为人口持续增长提供了物质保障。荧光卫星的发射也将为叶绿素荧光研究提供更高质量的数据源，进一步推进开展叶绿素荧光遥感的应用。

# Chapter1. Introduction

## 1.1 Research background

The so-called vegetation is a variety of plant types in general which are growing on the Earth's surface, playing an important role in the Earth system, and it is also very important renewable resource within the Earth's surface. Vegetation is the most active and valuable factors and indictor of the global change, influencing the energy balance of the earth-atmosphere system, playing an important role in the climate, hydrological and biochemical cycles, is a sensitive indicator of climatic and humanities' impacts on the environment. Vegetation releases oxygen through photosynthesis, which builds a comfortable environment for human survival, and vegetation composition of organic food composed by vegetation is our human's agricultural crops to survive. In addition, vegetation has great impacts on climate change. Therefore, the vegetation can be called the theme of the Earth's ecosystems, which is playing an important role in the global cycle of matter and energy. However, with the pressure of global climate change, energy demand and population growth on agricultural production growing, global or regional food supply shortage risk is also increasing. It is important for food security and sustainable human development to accurately grasp of the situation of global food production in a real time.

Traditional methods based on remote sensing technology for vegetation monitoring includes visible optical remote sensing, thermal infrared remote sensing, and microwave remote sensing. Although these methods are more widely used and achieve good results, the indicators cannot be directly linked to the physiological state of the vegetation. Thus, on the basis of the results, these monitoring indicators only indirectly reflect vegetation changes. As far as a variety of external stress is concerned, vegetation will start the self-protection mechanism due to the self-regulating mechanism of vegetation. Therefore, there will be the presence of hysteresis phenomena during the observation which will lead to a huge error of monitoring results in some times.

Since 1980s, vegetation chlorophyll fluorescence has been proved to be an effective, non-destructive and direct probe in constantly monitoring the changes of the vegetation physiological state. Chlorophyll fluorescence, photosynthesis and heat dissipation are the three ways of dissipation of energy absorbed by vegetation (Figure 1-1). These three ways compete with each other. The energy reduction for photosynthesis will lead to the energy increase for chlorophyll fluorescence emission, and vice versa. Therefore, the chlorophyll fluorescence emission can be used as an indicator in measurement of photosynthesis. Changes

of vegetation system can be monitored through the chlorophyll fluorescence change due to the close relationship between vegetation photosynthesis and chlorophyll fluorescence. Joiner et al. (2011) found that the chlorophyll fluorescence could provide the information of vegetation changes in stress before the change of chlorophyll content.

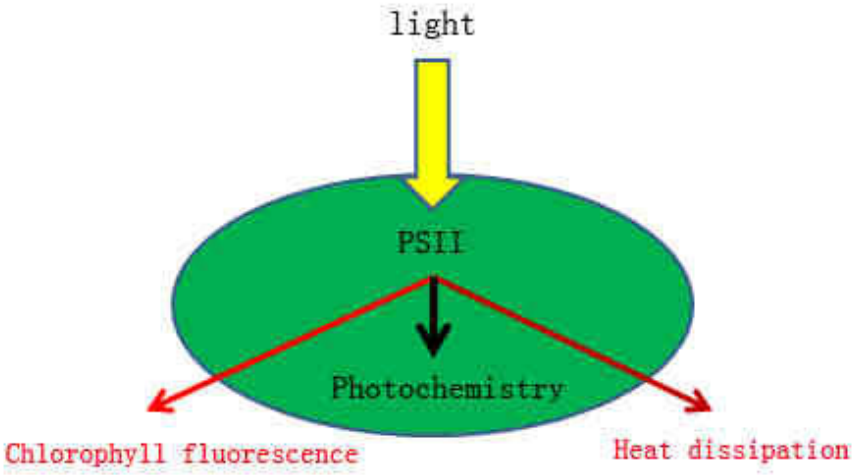


Figure 1-1The usage of the absorbed light

In recent years, remote sensing of chlorophyll fluorescence research has made significant progress: 1) Research about chlorophyll fluorescence extraction at different scales; 2) Research of detection on stress based on chlorophyll fluorescence, such as water stress, ozone stress and nitrogen stress, etc.; 3) Research of monitoring vegetation photosynthesis based on chlorophyll fluorescence, and estimating of global GPP.

With the EU plan of fluorescence detection being elected the eighth planet exploration mission, chlorophyll fluorescence remote sensing will play a more important role in the future's monitoring of vegetation. Considering the importance of vegetation monitoring to global ecological balance and directive effectiveness of vegetation monitoring to chlorophyll fluorescence, in this dissertation, chlorophyll fluorescence at leaf scale is chosen as the breakthrough point to develop a research over the dynamics of chlorophyll fluorescence and leaf temperature in different states of water content. Chlorophyll fluorescence at leaf scale can be measured directly by a fluorescence measuring instrument, or extracted directly from the reflection spectrum of the leaves. In the process of extracting chlorophyll fluorescence, the resulting chlorophyll fluorescence can be approximated to the true chlorophyll fluorescence due to less impact from other influential factors. On this basis, taking the potted corn as the subject, the research of responses of chlorophyll fluorescence to the early water stress are

developed, and the results show that the chlorophyll fluorescence and leaf temperature could illustrate the change of water stress of potted corn in early stage.

To widen the application of chlorophyll fluorescence in vegetation monitoring, the changes of the physiological state of the vegetation should be analyzed through the sunlight-induced chlorophyll fluorescence at the satellite platform or near the ground. The key point of extraction chlorophyll fluorescence with remote sensing technique is to separate the chlorophyll fluorescence from the reflected energy. The atmospheric effects are negligible when the extraction of chlorophyll fluorescence is near the ground due to the limited distance from the sensor to the ground, and the fluorescence extraction algorithm is relatively simple. However, extraction of chlorophyll fluorescence at satellite platform is much more complicate due to the atmospheric absorption and scattering influence, thus, corresponding atmospheric corrections are needed to get real chlorophyll fluorescence. Therefore, we summarize all the methods of extraction of chlorophyll fluorescence near the ground, and find that the reflectance-based extraction algorithm in some cases is the only method. This also shows the necessity of developing the reflectance-based quantitative extraction algorithm. In the study, a new quantitative extraction algorithm based on the reflectance index is developed near the ground, which is compared with other classical algorithms to show the feasibility and availability of this quantitative extraction method. In addition, in the process of extraction of chlorophyll fluorescence in the satellite platform, we explore the impacts of atmospheric absorption and scattering on the fluorescence extraction to prepare the groundwork for the development of extraction algorithm of chlorophyll fluorescence in the satellite platform.

## 1.2 The research progress

### 1.2.1 The leaf-scale chlorophyll fluorescence measurement

Under the solar illumination, chlorophyll molecules absorb the sun light, and transfer from the stable state to the excited state. Chlorophyll molecules in the excited state need dissipate the energy to return the stable state, and the released energy is used to do photosynthesis, heat dissipate and fluorescence. Now the leaf-scale chlorophyll fluorescence measurements have two ways: active measurement and passive measurement. The active measurement exploits the pulse modulated fluorimeter and (non-modulated) continuous excitation fluorimeter, while passive measurement uses the remote sensing technology to estimate the fluorescence.

Kautsky & Hirsch (1931) published a scientific paper about the variation process of chlorophyll fluorescence. In their experiment, they first treated the photosynthesis material as the dark adaption and then exposed the photosynthesis material to the sun light, and they observed that chlorophyll fluorescence quickly increased to the maximum value at first and then decreased gradually to the stable value. The curve of chlorophyll fluorescence along with the time decay is called chlorophyll fluorescence induction kinetics. Because this process was first found by Kautsky, this process was also called Kautsky curve or Kaustsky effect. In 1983, the professor Ulrich Schreiber, who was the WALZ company's chief scientist, and the professor in the Würzburg University, Germany, designed and manufactured the world's first pulse amplitude modulation fluorimeter PAM to measure chlorophyll fluorescence induction kinetics. Chlorophyll fluorescence kinetics technique can measure the energy absorption, transmission, dissipation and distribution of photosystem in the photosynthesis, and comparing with the gas exchange parameters, chlorophyll fluorescence parameters can better reflect the inherent characteristics of the vegetation. Chlorophyll fluorescence kinetics parameters are widely used to monitor the vegetation physiological state (Genty 1989； Schreiber 1994； White 1999； Zarco-Tejada et al., 2000b, 2011, 2013). The chlorophyll fluorescence parameters measured by PAM with other ground measurement parameters, such as stomatal conductance, leaf water potential and leaf temperature, are used to detect the vegetation stress (Guidi et al., 1997; Flexas et al., 2002). Non-modulated fluorimeter also widely used to record the instantaneous fluorescence (Mathur et al., 2009; Kalaji et al., 2014).

Passive fluorescence exploits the remote sensing technology to assess the SIF. Under the solar illumination, the received signal at sensor includes two parts: the reflected energy by the leaf and the fluorescence emitted by the leaf. How to distinguish the fluorescence from the leaf reflected signal is a difficult problem. In the fraunhofer lines, the fraunhofer well is partially filled owing to the contribution of the fluorescence. On the basis of this principle, the fluorescence radiometer is designed to obtain the fluorescence image directly (Carter et al., 1999; Flex et al., 2000). Besides, many fluorescence retrieval methods are developed by the researchers (Plascyk 1975； Maier et al., 2001,2003; Gómez-Chova et al., 2006; Guidi et al., 2006; Meroni et al., 2006; Zarco-Tejada et al., 2000b, 2000c; Dobrowski et al., 2005; Pérez-Priego et al., 2005).

### 1.2.2 The SIF retrieval methods near the ground

Remote sensing plays a unique and essential role in relating remote sensing data to the biochemistry at the earth's surface in a reliable and operational way. Recent studies have demonstrated the feasibility of the retrieval of solar-induced fluorescence (SIF) from hyperspectral images. SIF is considered to be an ideal, fast, non-invasive, and sensitive probe to detect the photosynthesis of vegetation (Liu & Cheng 2010; Liu et al., 2011, 2013a; Zhang et al., 2014) and provides a new way to monitor global vegetation and estimate global biomass (Krause & Weis 1984; Genty et al., 1989; Schreiber et al., 1994; Zarco-Tejada 2000a).

The methods for detecting SIF near the ground include radiance-based and reflectance-based methods (Meroni et al., 2009). Radiance-based methods are based on the fraunhofer Line Discriminator (FLD) principle. FLD, which was proposed by Plascyk (1975) and Plascyk & Gabriel (1975), uses sun irradiance and canopy radiance inside the fraunhofer line and outside the line to compute the SIF. The drawback of FLD is that the reflectance and fluorescence of the inside bands are assumed to be same as those of the outside bands. To overcome the drawback of FLD, a series of methods had been developed to modify this restriction, such as 3FLD (Maier et al., 2003), corrected FLD (cFLD) (Gómez-Chova et al., 2006; Moya et al., 2006), improved FLD (iFLD) (Alonso et al., 2007a, 2008), extended FLD (eFLD) (Mazzoni 2007), and spectral fitting methods (SFM) (Meroni & Busetto 2006). FLD-like methods are radiance-based methods that calculate SIF in radiance unit. Incoming sun irradiance is necessary in the FLD-like methods. It can be obtained experimentally using a reference standard panel near the ground; however, it is not feasible to use reference panels in airborne/space-borne remote sensing. Maier (2001) proposed a new method in which non-fluorescence objects are used to determine the radiance conditions on the ground and the influence of the atmosphere in airborne/space-borne measurements. However, this method still has one faulty: some non-fluorescence objects can show the fluorescence information under the large change in surface reflectance, and Yang & Liu (2013) further developed this method. Sobrino et al. (2011) used the Fluorescence Radiative Method (FRM) to estimate the fluorescence from the Airflex airborne data in the CEFLES2 campaign, and considered the effect of atmosphere. Liu et al. (2015) proposed a new spectral fitting method for full-spectrum solar-induced chlorophyll fluorescence retrieval based on principal components analysis. Zhao et al. (2015) estimated quantitatively fluorescence for crop leaves with Bayesian inversion.

Reflectance-based approaches do not exploit the fraunhofer lines but instead use a set of 2-3 spectral reflectance including at least one wavelength affected by the fluorescence (in the neighbourhood of the fluorescence emission maxima, about 685nm and 740nm) and one less or not affected (Meroni et al., 2009). Zarco-Tejada et al. (2000b) proposed the reflectance indices R750/R800, R685/R655, R690/R655 to estimate the leaf-scale fluorescence. Zarco-Tejada et al. (2000c) proposed the reflectance indices R680/R630, R685/R630, R686/R630 and R690/R630 to estimate the canopy fluorescence. Zarco-Tejada et al. (2003) proposed the derivative indices D705/D722 and D730/D706 to retrieve the fluorescence from the ASD reflectance spectrum. Dobrowski et al. (2005) exploited R690/R600 and R740/R800 to retrieve the fluorescence from the canopy reflectance spectrum. Pérez-Priego et al. (2005) used the filling index R760.59-R759.5 to retrieve the canopy fluorescence. Zarco-Tejada et al. (2000c) used the deviation indices D730/D706, DλP/D703 and the reflectance indices R6832/(R675×R691), R685/R655 to retrieve the fluorescence from the CASI imagery. Besides, Gamon et al. (1992) proposed the photochemical reflectance index (PRI= (R531-R570)/(R531+R570)), and used the PRI to detect the daily variation of the photosynthetic efficiency. PRI is widely used to detect the vegetation physiological state change. PRI is concerned with vegetation photosynthesis state directly, and can reflect the chlorophyll fluorescence non-chemical chlorophyll fluorescence quenching dynamic changes. Winkel et al. (2002), Meroni et al. (2008a, 2008b), Rahimzadeh-Bajgiran et al. (2012), Naumann et al. (2010), Panigada et al. (2014), Buddenbaum et al. (2015) analyzed the relationship between PRI and the fluorescence parameters.

### 1.2.3 The airborne/space-borne SIF retrieval methods

The intensity of SIF signals is small compared to reflected solar radiation (approximately 2-5% in the near infrared), decoupling the airborne/space-borne fluorescence radiation from the reflected radiation is challenging. Determining the airborne/space-borne fluorescence is affected by atmospheric effects. Thus, how to remove the atmospheric effects and to improve the accuracy of SIF retrieval has attracted researchers' attention.

In recent years, many methods have been developed to measure SIF from the space. Based on the past literatures, the SIF retrieving methods from the space always exploit atmospheric absorption features, primarily the oxygen absorption band or fraunhofer lines. The oxygen absorption band is relatively broad, deep and close to the two characteristic peaks of the fluorescence emission spectrum at 680 and 740 nm. It is thought to be the best candidate band

to retrieve SIF (Meroni et al., 2009), and the accuracy of the atmospheric correction can introduce high accuracy in SIF retrieval. Methods such as FLD, 3FLD, cFLD and SFM have been developed for use with space measurements combined with the atmospheric parameters computed by MODTRAN.

Guanter et al. (2007, 2010) estimated SIF based on oxygen absorption features using atmospheric correction based on the MODTRAN to avoid uncertainties caused by atmospheric absorption and scattering effects; they tested this method on Medium Resolution Imaging Spectrometer (MERIS) images and FLEX-like high-resolution data. Frankenberg et al. (2011) showed an efficient alternative fluorescence least-square retrieval method based on the O2-A band, decoupling fluorescence from scattering properties, and applied this method on GOSAT and OCO-2 images. Damm et al. (2011) used the FLD method combined with MODTRAN-4 simulated at-sensor radiances to derive canopy chlorophyll fluorescence, and then Damm et al. (2014) exploited a semi-empirical approach to estimate SIF using the 3FLD approach, focusing on atmospheric oxygen-absorption bands and using non-fluorescent surfaces to remove atmospheric effects. Joiner et al. (2013) used principal components to estimate the spectral structure of atmospheric absorption, and the atmospheric information was incorporated into a simplified radiative transfer model to estimate SIF. Raychaudhuri Braun (2014) compared the radiation ratio of the O2-A band for vegetated and non-vegetated regions in the same image to estimate SIF from Hyperion images. Liu et al. (2015) proposed a new PCA-based full-spectrum spectral fitting method (F-SFM) for the retrieval of SIF.

The Fraunhofer lines can also be used to disentangle fluorescence emissions from scattering effects. Joiner et al. (2011, 2012) used the filling in of the potassium K I solar fraunhofer line near 770 nm and the Ca II line at 866 nm to derive chlorophyll fluorescence from GOSAT images and SCIAMACHY. Guanter et al. (2012, 2013) used a linear forward model derived by a singular vector decomposition technique in the narrow window containing only Fraunhofer lines to inverse SIF from GOSAT images. Köhler et al. (2015a) provided a linear method for the retrieval of SIF from GOME-2 and SCIAMACHY data, and then Köhler et al. (2015b) proposed a simplified physically based fluorescence-retrieval method in a spectral range of 755-759 nm from GOSAT data.

### 1.2.4 The SIF models

In 2002, The FluorMOD model was developed by the European Space Agency (ESA) to advance the science of vegetation fluorescence simulation through the development and integration of leaf and canopy fluorescence models based on physical methods (Miller et al., 2005). The model has two modules: FluorMODleaf (Pedrós et al., 2010), developed based on PROSPECT to simulate the fluorescence at the leaf, and FluorSAIL (Verhoef 2004), developed from SAIL and used to simulate natural solar-induced fluorescence on the canopy level. FluorMOD is used to simulate the fluorescence radiance of the plant on the canopy under non-stress, favourable environmental and natural illumination conditions (Zarco-Tejada et al., 2004, 2006, 2012, 2013; Middleton et al., 2008; Liu et al., 2014; Ni et al., 2015b).

FluorMOD model is designed to solve the problem of coupling the leaf fluorescence model with the canopy fluorescence model under the ideal conditions. In fact, the fluorescence intensity is affected by the sun position, the structure, and the biochemical parameters and so on. Considering these defects, The SCOPE (Soil Canopy Observation, Photochemistry and Energy fluxes) model was developed by the ITC institute (International institute for geo-information science and earth observation) in the Netherlands. It is a vertical (1-D) integrated radiative transfer and energy balance model (Van der Tol et al., 2009). The objective of the SCOPE is to link top of canopy (TOC) observations of radiance with land surface processes. It contains the radiation transfer and energy balance module and can simulate spectra from 0.4 to 50 μm, including the visible, near- and short-wave infrared and thermal domains, with resolutions of 1, 1, 100 and 1000 nm, respectively (Zhang et al., 2014). Radiance modules include the thermal and the optical part, with a module dedicated to chlorophyll fluorescence. Land surface processes include photosynthesis, net radiation, sensible and latent heat flux and soil heat flux. This model is a 1-D model, and it means that horizontal variations in surface characteristics are ignored. The simulated results using the SCOPE model are much more close to the actual fluorescence, thus, the SCOPE model is widely used to simulate the response of the fluorescence to the different physiological state, estimate the plant GPP, and analyze the evapotranspiration change (Timmermans 2011; Lee et al., 2013; Zhang et al., 2014; Zhao et al., 2014; Verrelst et al., 2015, 2016; Ni et al., 2015a; Lee et al., 2015; Zarco-Tejada et al., 2016).

### 1.2.5 The progress of the SIF experiments

Chlorophyll fluorescence is one of the most effective and non-destructive tools for monitoring vegetation photosynthetic efficiency. To better monitor the global vegetation using chlorophyll fluorescence, fluorescence explorer (FLEX) project was chosen as the eighth earth explorer project. It aims to quantitative assess the vegetation photosynthesis activity, and obtain the vegetation fluorescence image, and better understand the vegetation healthy state. The airborne/space-borne SIF provide a direct and important way to estimate the vegetation GPP and monitor the vegetation stress.

#### 1.2.5.1 SIFLEX-2002 (Solar Induced Fluorescence campaign)

In 2002, a research of solar induced fluorenscence experiment (SIFLEXE) was carried out in Sodankylä in north Scotland. The purpose of this experiment is to collect the data through flux tower to demonstrate whether the sunlight induced fluorescence can be used to monitor and map the photosynthetic activities of coniferous forests or not, and to further promote the measurement accuracy of emission and absorption of carbohydrates at the aerospace platform, as well as to better understand the earth's warming process.

In the experiment, the main research work was to use the sensor made by laboratoire pour I'Utilisation du rayonnement electromagnetiqué (LURE) to measure the canopy fluorescence of pine at three levels including needle level, shoot level, and crown level. However, to better understand the manifestation of satellite canopy fluorescence signal, the researchers built a 20-meter-high flux tower before the experiment, and the flux tower provided a canopy vision for vegetation monitoring. A variety of combined sensors were boarded on the flux tower. The information of coniferous forest such as spectral signatures, thermal infrared signals and the respective atmospheric radiation, meteorological data were measured by the combined sensors to understand the relationship between the fluorescence signal and the light scattering.

SIFLEX experiment was successful, which not only shows the feasibility of measuring fluorescence (even under difficult conditions), but also provided a new idea for us in the future experiments(http://www.esa.int/Our_Activities/Observing_the_Earth/The_Living_Planet_Programme/Earth_Explorers/SIFLEX_Measuring_fluorescence_under_the_midnight_Sun; Moreno et al., 2002; Drusch 2008). After this successful experiment, the AirFlex was boarded on the aerospace platform to develop a series of experiments. AirFLEX, with six spectral

channels, was mainly used to monitor the oxygen absorption band (687 nm and 760 nm). AirFLEX was mainly used to two experiments including SEN2FLEX (Sentinel-2 and FLEX Experiment) and CEFLES2 (CarboEUROPE，FLEX and Sentinel-2).

1.2.5.2 SEN2FLEX experiment

From May to June in 2005, the SEN2FLEX experiment was carried out in the town of Barrax in Albacete of Spain. There are three purpose of the experiment: a) to collect the high spectral dataset and extract the fluorescence through AIRFLEX sensor and the CASI-3 sensor boarded on the airplane, to provide the feasibility of observation of fluorescence with aerospace remote sensing; b) to prepare for the Sentinel mission, ESA undertook the development of Sentinel-2 satellite in the global monitoring for environment and security program (GMES), the Sentinel-2 was a polar-orbiting satellite and capable of monitoring longtime series of variation of the surface using the imaging spectrometer boarded on the satellite; c) under the frame of EC Water Framework Directive (WFD) EO project, to launch a series of activities of water conservation and management

(http://www.esa.int/Our_Activities/Observing_the_Earth/ESA_campaign_leads_the_way_for_future_monitoring_of_the_Earth_s_vegetation).

1.2.5.3 CEFLES2 experiment

In April，June and September 2007, CEFLES2 experiments were carried out in the south of the Aquitaine region of France. In this experiment, multi-types of vegetation in different stages of growth were chosen as the subjects, of which the structural parameters (leaf area index LAI, canopy height or canopy cover fraction), biochemical parameters (chlorophyll content, water content and dry matter content), physiological parameters (PAM fluorescence, gas exchange parameters) and field spectral measurements were measured through synergic survey combining aviation platform and ground platform. The main object of study was winter wheat and maize as well as some other types of vegetation including canola flower, grass and pine trees in April, corn, potato, sunflower and pine trees in June, beans, kiwi, grapes and oak in September. On the leaf scale, the efficiency of photosynthesis and the diurnal variation of chlorophyll fluorescence were measured. On the canopy scale, we collected two types of data including sunlight induced fluorescence and laser-induced fluorescence, and find that results from two different technologies are consistent with each other in the detection of stress. At the regional scale, the fluorescence images were extracted

from HYPER aerial imagery, the dynamics of fluorescence of different objects and the respective change of NDVI and incident photosynthetically active radiation (PPFD) were analyzed. This experiment illustrated the obvious relationship in different scale between the carbon absorption and fluorescence, but it also showed the potential advantages of determining the energy conversion and energy utilization using fluorescence (Rascher et al., 2009).

#### 1.2.5.4 The SIF research process in china

Fluorescence Remote Sensing in China is still in its infancy. Recently, there's no large research projects being carried out, but in some institutes, the researchers have begun to study remote sensing fluorescence from different perspectives, such as Institute of Remote Sensing and Digital Earth of Chinese Academy of Sciences, Beijing Normal University and Beijing Institute of Agriculture and Forestry Science Academy and other units.

Researchers from Institute of Remote Sensing and Digital Earth of Chinese Academy of Sciences carried out several experiments, extracted chlorophyll fluorescence using the fraunhofer dark lines and principal component analysis methods (Liu et al., 2005; Liu & Liu 2015), analyzed the effects of the band selection on chlorophyll fluorescence extraction methods (Liu & Liu 2014), and detected vegetation photosynthesis (Liu et al., 2006, 2013b), solar energy utilization (Liu & Cheng 2010; Liu et al., 2013a), C3 and C4 vegetation types (Liu & Cheng 2011) based on chlorophyll fluorescence.

The research term from the School of Geography, Beijing Normal University, develop the research of the multi-scale SIF detection, compare the different SIF retrieval methods, improve the 3FLD and iFLD method, analyze the response of chlorophyll fluorescence to water stress (Ni et al., 2015a), nitrogen stress, develop the SIF retrieval method near the ground (Ni et al., 2015b), and analyze the atmospheric effects on the SIF retrieval methods (Ni et al., 2016).

### 1.2.6 The applications of chlorophyll fluorescence

Under the solar illumination, the energy absorbed by the leaf is used in three processes, photochemistry, heat dissipation and chlorophyll fluorescence (Lichtenthaler & Miehe 1997; Porcar-Castell et al., 2014). These three processes compete with each other, and variations in one process can affect the other. Chlorophyll fluorescence is directly related to plant

photosynthesis and the physiological state of vegetation. Thus, chlorophyll fluorescence has been used as a powerful, non-destructive and reliable tool in plant physiology for understanding the primary events of photosynthesis and the effects of stress on photochemistry (Méthy et al., 1994; Schreiber et al., 1994; Razavi et al., 2008; Zarco-Tejada et al., 2012).

Many studies have shown that both chlorophyll fluorescence and photochemistry for plants decrease due to deactivation of antennae to prevent damage by harmful radicals that are formed under stress condition, while heat dissipation increases aiming to dissipate the extra energy and protect the plant from destroy (Maxwell &Johnson 2000; Zarco-Tejada et al., 2003, 2009, 2012; Dobrowski et al., 2005; Pérez-Priego et al., 2005; Campbell et al., 2007; Chaerle et al., 2007; Van der Tol et al., 2009;). Therefore, many researchers have focused on chlorophyll fluorescence and have exploited it to monitor water stress, ozone stress, nitrogen stress, pest stress and estimate the GPP.

#### 1.2.6.1 The response of chlorophyll fluorescence to water stress

Vegetation water stress is a significant issue which affects plant growth and production. Accurately monitoring drought has always been a focus of research and has attracting the attention of many researchers (Peters et al. 2002; Wang & Qu 2009). Many studies have shown that vegetation water stress can be measured using optical and thermal infrared remote sensing, as well as passive and active microwave remote sensing techniques (Fuchs & Tanner 1966; Jackson et al., 1981; Paloscia & Pampaloni 1984; Hunt & Rock 1989; Gao 1996; Walker 1999; Peters et al., 2002; Sandholt et al., 2002; Wang & Qu 2009; Vereecken et al., 2012). These techniques exploit surface reflection, surface temperature, brightness, temperature and the backscatter coefficient separately to estimate soil moisture near the surface. Though these methods are widely used, they have several limitations. For example, they lack a direct relationship with the plant physiological state and estimate the plant drought based on the surface information. Thermal infrared remote sensing is a wide and effective method for detecting vegetation stress, and using the canopy temperature to track water stress is considered to be reliable for monitoring plant water status (Jackson et al., 1981). However, retrieving canopy component temperatures involves thermal infrared remote sensing problems, such as how to remove the effects of soil background (Bellvert et al., 2014), and the relationships between leaf temperature and water level are not clear (Zarco-Tejada et al., 2012).

To actively measure chlorophyll fluorescence, several chlorophyll fluorescence parameters, including the steady-state chlorophyll fluorescence (Ft), Fm/Fo, photochemical quenching coefficient (PQ) and non-photochemical quenching coefficient (NPQ), are measured using a chlorophyll fluorometer (PAM). These parameters and leaf gas-exchange parameters (CO2 assimilation rate, transpiration rate, leaf temperature and related parameters) are widely used to study the effects of water stress on the in vivo chlorophyll fluorescence in leaves (Rosema et al., 1998; Flexas et al., 2000, 2002; Zarco-Tejada et al., 2002; Marcassa et al., 2006; Meroni et al., 2009).

Active measurements can estimate the fluorescence effectively at the leaf. In addition, hyperspectral remote sensing can provide new methods for detecting sun-induced chlorophyll fluorescence and has made remarkable progress in recent years. It is possible to detect vegetation stress using hyperspectral remote sensing from the large scale. Dobrowski et al. (2005) used the simple chlorophyll fluorescence index DCI=D705/D722 to track the variation of chlorophyll fluorescence resulted from the water stress. Pérez-Priego et al. (2005) used the filling methods to retrieve the chlorophyll fluorescence and detect the water stress. Campbell et al. (2007) used the deviation index (D715/D705) to monitor the water stress. Zarco-Tejada et al. (2009, 2012, 2013) used the thermal and hyperspectral images obtained from an unmanned aerial vehicle (UAV), and field measurement (including the leaf water potential measurement, stomatal conductance measurement, and leaf chlorophyll fluorescence measurement) were used to assess the vegetation water stress. Burling et al. (2013) thought that BFRR (Blue-to-far-red fluorescence ratios) is a good fluorescence index and increased with the water stress deepening. Lee et al. (2013) used the fluorescence retrieved from the Greenhouse Gases Observing Satellite GOSAT, canopy water content and MODIS EVI data to analyze the water stress in Amazonia at a global scale. Panigada et al. (2014) used the fluorescence and PRI to monitor the plant water stress. Wang et al. (2015) used the SIF, the drought index and GPP to monitor and assess the drought phenomenon in 2012.

Besides, the laser-induced fluorescence is also used in the water stress detection. Marcassa et al. (2006) used the fluorescence ratio (F685/F735, F452/F685 and F452/F735) to detect the water stress. Mistele et al. (2012) used the laser-induced fluorescence to assess the water content of maize in the field. Gameiro et al. (2016) thought that the laser-induced fluorescence is a quick and non-destruction method to detect the water deficit of arabis. Fedotov et al. (2016) illustrated that it is feasible to monitor the vegetation stress using the laser-induced fluorescence.

#### 1.2.6.2 The response of chlorophyll fluorescence to ozone stress

Schreiber et al. (1978) used the chlorophyll fluorescence to assess the ozone-induced injury in bean leaves. Guidi et al. (1997) utilized the chlorophyll fluorescence and stomatal conductance parameters to study the bean leaves in response to ozone stress. Calatayud et al. (2001, 2002, 2004) took the tomato and lettuce as research objects to study the chlorophyll fluorescence in response to ozone stress. Flowers et al. (2007) developed the research about the sensitivity of chlorophyll fluorescence, photosynthesis and production to the ozone. Bussotti et al. (2011) studied the trees in response to the ozone stress. Thwe et al. (2014) illustrated the variation of the photosynthesis and chlorophyll fluorescence of the tomato under the different ozone state. Meroni et al. (2008a, 2008b) thought that the steady fluorescence could be as the effective indictor to monitor the early ozone stress. Gerosa et al. (2014) carried out an experiment on the bean in the open-air indoor to study the response of the chlorophyll fluorescence and reflectivity to the ozone stress.

#### 1.2.6.3 The response of chlorophyll fluorescence to nitrogen stress and the pest stress

Ciompi et al. (1996) studied the effects of the nitrogen deficit on the stomatal conductance and chlorophyll fluorescence of the sunflowers. Schächtl et al. (2005) and Crop et al. (2009) thought that the chlorophyll fluorescence is a good indictor to detect the nitrogen content of the maize and wheat. Middleton et al. (2008) compared the SIF and reflectance of a corn crop under nitrogen treatments with FluorMOD simulations. Agati et al. (2013, 2015) used the chlorophyll fluorescence index to detect the nitrogen content in Paspalum vaginatum, Zoysia matrella turfgrasses and hybrid bermudagrass.

Rodríguez-Moreno et al. (2008) used the chlorophyll fluorescence image to detect the soybean bacterial blight. Zhang (2009) used the chlorophyll fluorescence to detect the wheat stripe rust and nitrogen stress. Ranulfi et al. (2016) used the laser-induced fluorescence to diagnose the vegetation Huanglongbing (HLB).

#### 1.2.6.4 Estimation of GPP using chlorophyll fluorescence

Damm et al. (2012) assessed the variation of GPP with the different ecosystem. Damm et al. (2014) used the SIF to analyze the daily variation of GPP. Zhang et al. (2015) built the relationship between GPP and SIF based on the SCOPE model. Damm et al. (2015) illustrated the relationship between SIF and GPP by the theoretical analysis and experiment. Cheng et al.

(2015) and Perez-Priego et al. (2015) coupled the SIF with the photochemical index to estimate the GPP of maize. Zhang et al. (2015) estimated the GPP of maize using the SIF and flux tower method. Guan et al. (2015) used the SIF to estimate the production yield.

### 1.2.7 The existed problems

Until now, the chlorophyll fluorescence remote sensing has been paid with more attention, and has been used to monitor the vegetation, but there are still problems to be solved. This paper mainly focuses on the research about the multi-scale SIF detection.

In the leaf scale, the comparison between active and passive fluorescence is carried out under the same condition, and the comparison among them under the different water content still need to be done. The consistency between active and passive fluorescence illustrates the active and passive measurement reliable, and also shows that active fluorescence can validate the passive measurement results. Besides, the early water stress is paid the less attention than water stress. In the different site of the same leaf, chlorophyll fluorescence is different. Therefore, it is necessary to focus on the chlorophyll fluorescence in the same position of the same leaf to understand chlorophyll fluorescence response to the stress.

In the SIF retrieval methods near the ground, the radiance-based methods are widely used to retrieve the SIF, and the reflectance-based methods are less used because these methods can only provide qualitatively estimation of the SIF. Although the radiance-based methods can estimate the SIF accurately and quantitatively, the radiance-based methods may fail in some conditions, such as the artificial light, then the reflectance-based methods are only methods to estimate the SIF. The reflectance-based methods don’t estimate the SIF quantitatively, thus it is necessary to develop the reflectance-based methods to achieve the SIF quantitative retrieval.

To the airborne/space-borne SIF retrieval, it is necessary to consider the atmospheric effects on the SIF retrieval methods. Now, the SIF retrieval methods mainly exploit two features to retrieve the SIF, one is the oxygen absorption bands and other is fraunhofer lines. In the oxygen absorption bands, the atmospheric effects are the important factor to affect the SIF. It always uses the radiation transfer equation to compute the atmospheric effects in the SIF retrieval process. In the fraunhofer lines, the atmospheric effects can be neglected, thus the SIF is retrieved by the simplified radiation transfer equation. Because the oxygen

absorption bands are thought to be the good window of the SIF retrieval, it is important to develop the research about the atmospheric effects on the airborne/space-borne SIF detection.

## 1.3 Research objects and the structure of the thesis

At the leaf, we study the consistency between active and passive fluorescence, and analyze the different response of chlorophyll fluorescence and temperature to the early water stress; then we build the quantitative relationship between the fluorescence and the reflectance index near the ground; in the last, we analyze the effect of atmospheric absorption and scattering on the airborne/space-borne SIF retrieval methods, and provide the theory support for the multi-scale SIF detection.

Based on the research objects, the research flow is as follows (Figure 1-2):

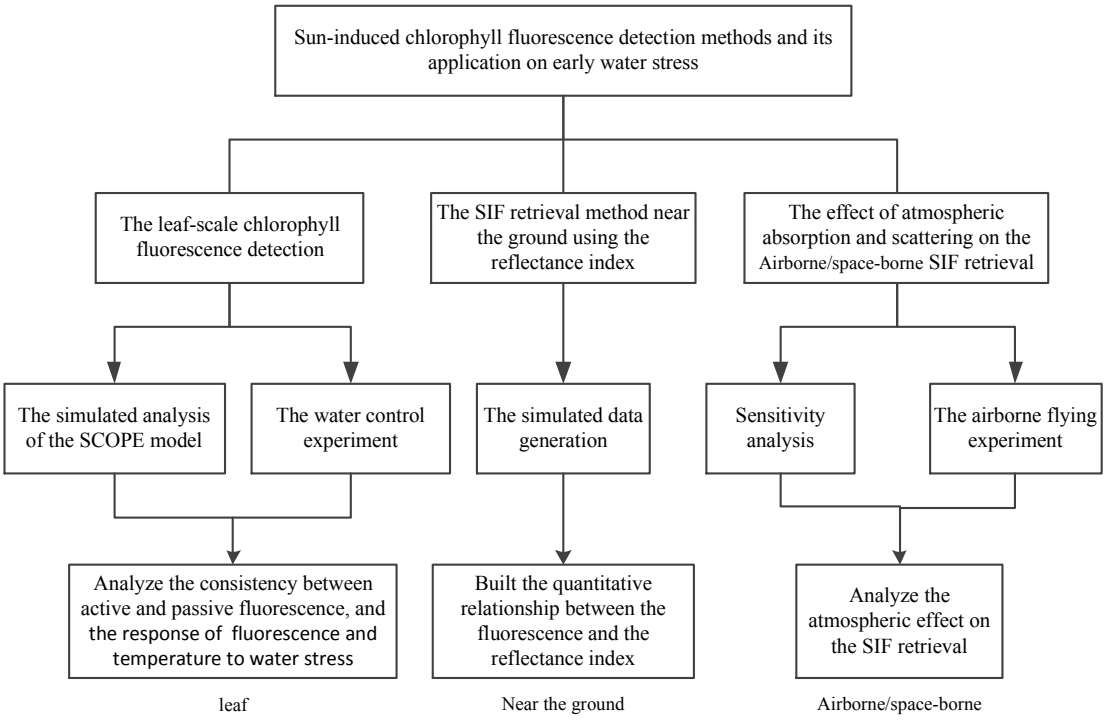


Figure 1-2 Flow chart

In this paper, there are six chapters and each chapter is introduced as follows:

The chapter 1 is the introduction. We introduce the research background, the research progress of chlorophyll fluorescence, the research objects and the structure of this paper.

The chapter 2 is the fundamental theory of chlorophyll fluorescence and chlorophyll fluorescence retrieval methods. In this paper, we fully introduce the generation of chlorophyll

fluorescence, measurement methods and the SIF retrieval methods near the ground or on the airborne/space-borne platform.

The chapter 3 is the leaf-scale chlorophyll fluorescence detection under the different water content. In this chapter, at first, we analyze the response of the sun-induced fluorescence and temperature to the different water stress state using the SCOPE model. Then, we introduce the water control experiment of the potted maize, and analyze the relationship amongst the active fluorescence, passive fluorescence, the leaf temperatures and soil water content of potted maize. In the last, we analyze the consistency between active and passive fluorescence, and the different response of active and passive fluorescence and temperatures to the early water stress.

The chapter 4 is the SIF retrieval method near the ground using the reflectance index. In the chapter, a research is developed based on the FluorMOD model, and the sensitivity analysis of FluorMOD model is carried out. Based on the results of sensitivity analysis, we select the sensitive parameters to use to generate the simulated data. Then we build the quantitative relationship between the fluorescence and the reflectance index using the simulated data, and compare the results using our methods with the traditional methods, such as FLD and 3FLD, to validate our methods.

The chapter 5 is about the effects of the atmospheric absorption and scattering on the airborne/space-borne SIF retrieval. In this chapter, we use the SCOPE and MODTRAN models to generate the simulated radiance at-sensor including the contribution of the fluorescence. Based on the simulated data, we select four indicators correlated with the fluorescence to analyze the atmospheric effects on these indicators. Because the oxygen absorption bands are the ideal window to retrieve the SIF, thus, we pay more attentions to analyze the atmospheric effects on the oxygen absorption depth. Moreover, we analyze the atmospheric effects on three SIF retrieval methods, and illustrate the necessity of atmospheric correction in the SIF retrieval algorithm. Besides, the airborne experiment is carried out to further illustrate that the accurate atmospheric parameters can improve the SIF retrieval accuracy. The results of this chapter can provide theoretical support of the development of SIF retrieval methods.

The chapter 6 is the conclusions. We summarize the main conclusions of the last five chapters, point out the existed problems in this paper, and give the prospects for the SIF remote sensing.

# Chapter2. Fundamental theory of chlorophyll fluorescence and chlorophyll fluorescence retrieval methods

## 2.1 The generation of chlorophyll fluorescence

It is well known that the complete leaf is composed of three layers: upper epidermis, lower epidermis and mesophyll cell, and mesophyll cell contains many chloroplasts. Chloroplast is a plastid in the cells of green plants and algae, which is surrounded by a double-celled composite membrane with an intermembrane space. Inside the plants, chloroplasts are usually disk-shaped and can reorient themselves in the cell to expose to sunlight. Chloroplast is the site of photosynthesis and is composed of chloroplast envelope, thylakoids and stroma. Thylakoids is the saclike membranes, which contain the chlorophyll and are arranged in stack-like structures, known as grana. Chlorophyll is the important pigment in the process of photosynthesis. From the point of view of the quantum theory, chlorophyll molecule absorbs the photon and then changes from the ground state to the excited state. When chlorophyll molecule absorbs red light (centered at the 670nm), it is excited to the first singlet state; when chlorophyll molecule absorbs blue light, it is excited to the second singlet state. Because the second singlet state only takes 10-12 s, the energy isn't able to do chemical work, and then the excited molecules emit heat and return the first singlet state. This first singlet state is much more stable than second singlet state, and it can last 4×10-9s (Heldt & Piechulla 2004).

The chlorophyll molecules in the first singlet state do chemical work to consume the energy, and return to the ground state. First and second singlet states are shown which occur by absorbing red and blue light. Fluorescence, phosphorescence, and heat emission are also shown as the energy emission ways from the excited states to the lower energy states. As shown in the figure 2-1, the electrons in the first singlet state have three ways to consume the energy and return to the ground state. The first way is to process photosynthesis; the second way is to emit energy; and the last way is to emit the larger wavelength electrons, known as fluorescence. These three processes compete against each other. If the photochemical reaction of photosynthesis is blocked, it means the energy for emitting fluorescence signal increase, and the fluorescence intensity will increase. Fluorescence can last 10-8-10-9 s.

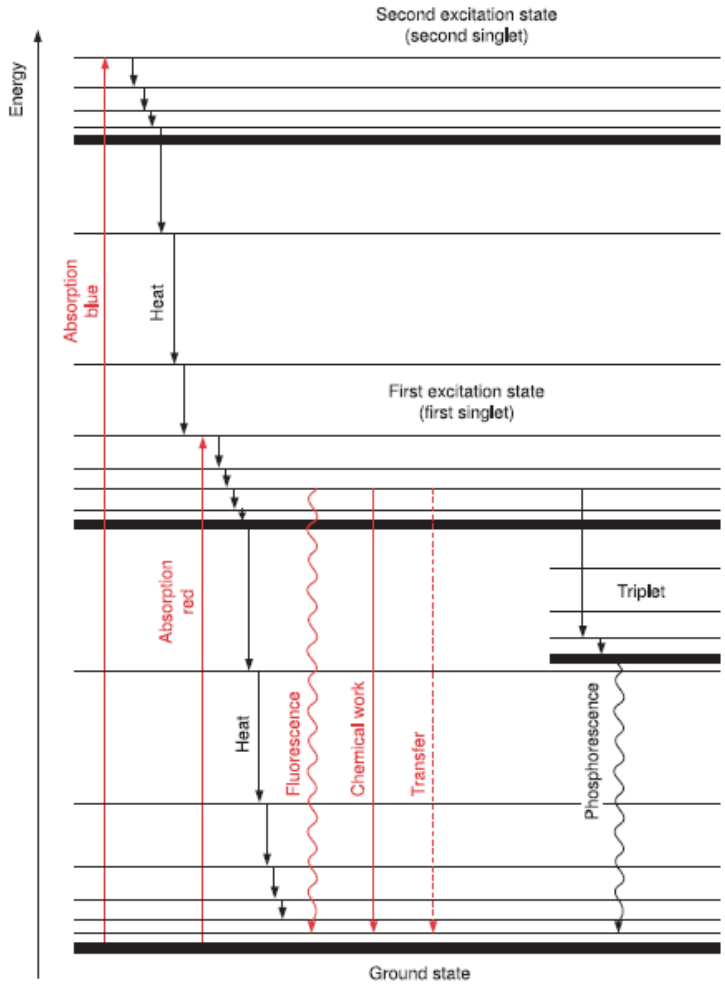


Figure 2-1 Energy levels of chlorophyll fluorescence (Heldt & Piechulla 2004)

Chlorophyll fluorescence is the production of the chlorophyll excited by natural sunlight, and the chlorophyll excitation is the first step of converting light energy to chemical energy, the absorbed energy is passed to the chlorophyll a in the reaction center to carry out photosynthesis. Because of the close relationship between Chlorophyll fluorescence and photosynthesis, chlorophyll fluorescence is thought to be a direct and effective probe to detect the vegetation physiological state.

## 2.2 Chlorophyll fluorescence measurements

### 2.2.1 Active chlorophyll fluorescence measurements

Active chlorophyll fluorescence measurements have two different measurement ways: 1) pulse modulated chlorophyll fluorimeter, 2) continuous excitation or prompt chlorophyll fluorimeters.

A modulated chlorophyll fluorimeter uses sophisticated electronics to separate chlorophyll fluorescence from ambient light. The systems achieve this using a rapid pulsing excitation light in order to induce a corresponding pulsed fluorescence emission. The fluorimeter uses a highly sensitive photodiode to detect and record the pulsed fluorescence signal and to ignore any non-pulsed signal

A continuous excitation fluorimeter is designed to measure the Kautsky Induction or Fast Chlorophyll Fluorescence Induction (Kautsky & Hirsch 1931).

2.2.1.1 Active chlorophyll fluorescence measurements

In 1983, the first Pulse Amplitude Modulation (PAM) fluorimeter was designed by Dr. Ulrich Schreiber (WALZ Corporation) using the modulation technique and the saturated pulse technology (Figure 2-2). The PAM can measure the fluorescent kinetic curve of vegetation.

Figure 2-2 PAM-2500

The so-called modulation technology uses the modulation measuring light to excite chlorophyll fluorescence, and only detects and records chlorophyll fluorescence which has the same frequency with measuring light. Therefore, modulation fluorimeter can be used to measure chlorophyll fluorescence under every physiological status, including the condition of the strong background light. Because of the modulation technology, the chlorophyll fluorescence measurement is feasible in the field experiments, and the research about chlorophyll fluorescence is also developed from physiology to the ecology.

The saturation pulse technology is using a strong light with very short duration (generally less than 1 s) to close all electronic doors to suppress the photosynthesis, thus chlorophyll fluorescence will achieve the maximum value. Saturation pulse can be regarded as a special

case of actinic light. The strong actinic light causes photosystem II (PSII) to release much more electrons and the electrons accumulate in plastoquinone (PQ). The electronic doors are in the closed state. In this condition, photosynthesis is suppressed, and chlorophyll fluorescence increases.

After fully dark acclimation, all electronic doors are in the open state. When we open measuring light, the minimum fluorescence ($F_0$) can be observed. If giving a saturation pulse, all electronic doors are closed. The energy for photosynthesis will be converted into chlorophyll fluorescence and heat. The chlorophyll fluorescence at this moment reaches the maximum value, marked as Fm. Fv is variable fluorescence, where Fv= Fm-F0. The maximum quantum yield of PSII reflects the potential maximum photosynthetic capacity, and can be expressed as follows:

$$F_v / F_m = (F_m - F_0) / F_m \quad (2\text{-}1)$$

When the plant is exposed to the sunlight, only a part of the electronic doors are in open state. If a saturated pulse is given, the electronic door opens and chlorophyll fluorescence increases. Chlorophyll fluorescence at this moment is marked as Fm' (Fm' is less then Fm). Chlorophyll fluorescence in the steady state is marked as Ft. The actual quantum yield of PSII in current illumination condition reflects the current actual photosynthetic efficiency of plant, and expressed as follows:

$$Yield = \Delta F / F_m' = (F_m' - F_t) / F_m' \quad (2\text{-}2)$$

Under the illumination of sun light, because of only a part of the electronic door opening, the real-time fluorescence Ft is lower than Fm. This process is also called fluorescence quenching. The light energy absorbed by plants only has three ways to go: photosynthesis, chlorophyll fluorescence and heat dissipation. Fluorescence quenching is divided into two categories: photochemical quenching (qP) and non-photochemical quenching (NPQ). In the other words, the decline of chlorophyll fluorescence yield (quenching) may be caused by the increase of photosynthesis or the increase of heat dissipation. The fluorescence quenching caused by the increasing of photosynthesis is photochemical quenching (qP), and the fluorescence quenching caused by the increasing of heat dissipation is non-photochemical quenching (NPQ). qP reflects the intensity of plant's photosynthetic activity. NPQ reflects the

plant's ability to convert the excess light energy into heat, or the ability of light protection. qP and NPQ can be expressed as follows:

$$qP = (F_m' - F_t) / (F_m' - F_0') \tag{2-3}$$

$$NPQ = \frac{F_m}{F_m'} - 1$$

$F_0$'is the minimum fluorescence in the illuminated state.

The figure 2-3 shows chlorophyll fluorescence induction kinetics curve. The common chlorophyll fluorescence induction kinetic parameters are $F_0$, Fv, Fm, Fv/ Fm, Ft, Yield (Y), qP and NPQ (seeing table 2-1).

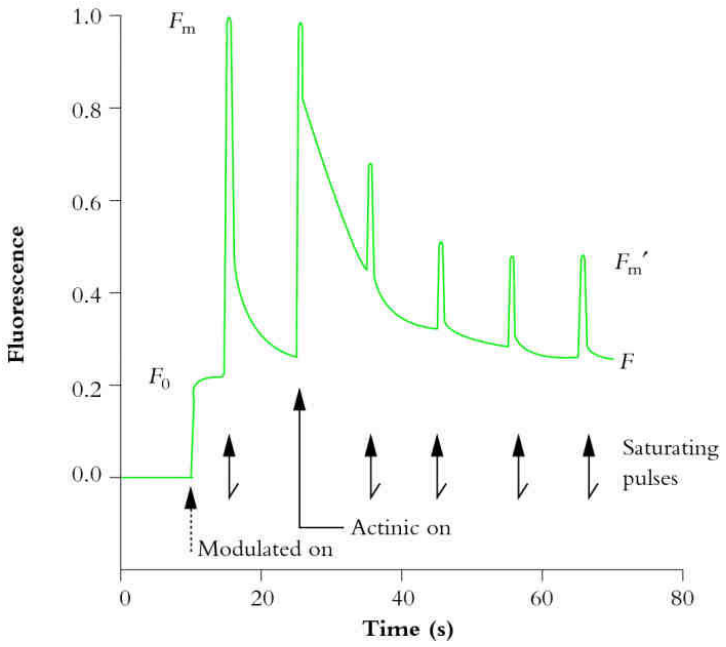


Figure 2-3 chlorophyll fluorescence induction kinetics curve measured by pulse modulation fluorometer

Table 2-1 Formulae and terms used in the analysis of the fluorescence induction dynamics curve

| Formulae and terms | Illustrations |
|---|---|
| $F_0$ | minimum fluorescence after dark acclimation |
| $F_0'$ | minimum fluorescence in the illuminated state |
| Fm | maximum value when all electronic doors are open |
| $Fm'$ | maximum value only a part of electronic doors are open |
| Fv | variable fluorescence |
| Ft | steady state chlorophyll fluorescence |
| $F_v/F_m$ | variable fluorescence yield |
| $\Delta F/F_m'$ | actual quantum yield of PSII |
| qP | photochemical quenching |
| NPQ | non-photochemical quenching |

Chlorophyll fluorescence is closely related with the photosynthetic process, and chlorophyll fluorescence induction kinetics curve can reflect various information of vegetation, such as, the survival status, the pathological condition and the physiology trends under the stress state. Therefore, chlorophyll fluorescence can be used to detect photo-inhibition, and nutrition, pest, low temperature, heat, environmental pollution, water and salt stresses.

2.2.1.2 Non-modulate fluorimeter

In 1931, a scientific paper about the changing process of chlorophyll fluorescence was published in Naturwissenschaften by Kautsky & Hirsch (1931). They found that, upon transferring photosynthetic material from the dark into the light, an increase in the yield of chlorophyll fluorescence occurred over a time period of around 1 s. This rise had subsequently been explained as a consequence of reduction of electron acceptors in the photosynthetic pathway, downstream of PSII, notably acceptor plastoquione QA. Once PSII absorbs light and QA has accepted an electron, it is not able to accept another until it has passed the first onto a subsequent electron carrier (QB). During this period, the reaction center is said to be ‘closed’. At any point in time, the presence of a proportion of closed reaction centers leads to an overall reduction in the efficiency of photochemistry and so to a corresponding increase in the yield of fluorescence. After a rapid polyphasic rise in

chlorophyll fluorescence, a slow (approximate 2 min) decline in fluorescence intensity to a steady state level of fluorescence. This induction phenomenon is often referred to as the Kausky Induction (Kautsky & Hirsch 1931; Maxwell & Johnson 2000; Li et al., 2005).

Kautsky Induction curves or OJIP induction curves must be plotted on a logarithmic axis in order to observe the polyphasic rise to the maximum chlorophyll fluorescence value (Figure 2-4). This is due to the reactions causing the different kinetics to occur typically in the first 300 milliseconds of illumination.

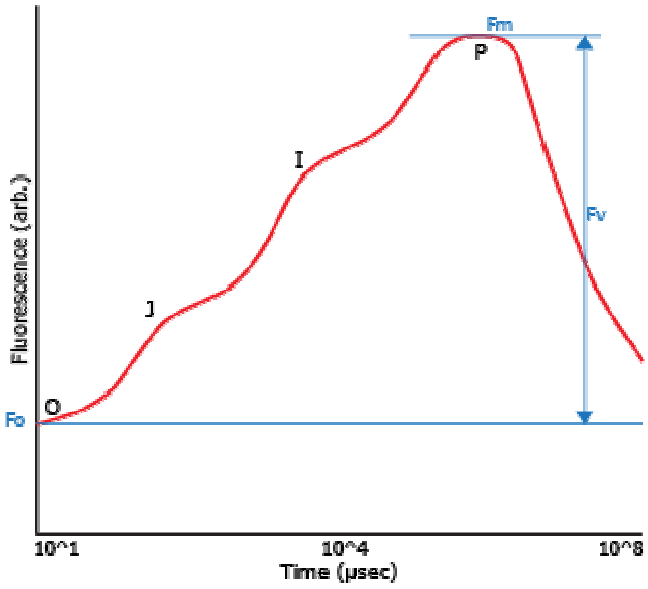


Figure 2-4 Kautsky curve

Non-modulate fluorimeters, such as Handy PEA, Pochet PEA and the new M-PEA Multi-Function Plant Efficiency Analyser, utilize a fast data acquisition system capable of recording every 10 s. An algorithm is then used to determine a line of best fit through the data points recorded immediately after the start of illumination. This line is extrapolated back to time zero when illumination commenced in order to derive F0.

The kinetics of fluorescence changes at the onset of illumination thus are related to primary electron transfer reaction in PSII and interpreted in terms of a two-state trapping model. It has been proposed that the polyphasic OJIP induction curve is composed of a photochemical (OJ) and a thermal (JIP) phase. The photochemical phase O-J phase reflects light-driven accumulation of reduced QA with QB being oxidized and the thermal JIP phase is associated with light-driven accumulation of QB- and QB2-, respectively, in addition to accumulation of QA- (Vredenberg & Pavlovič 2013).

### 2.2.2 Passive chlorophyll fluorescence measurement

Most energy absorbed by vegetation is used for photosynthesis, and the excess energy is dissipated by heat and chlorophyll fluorescence (Figure 2-5). Chlorophyll fluorescence locates in the range of 650-850 nm with two peaks values in 687nm (red) and 740nm (far-red) (Lichtenthaler 1992; Middleton et al., 2006; Meroni et al., 2009; Crop et al., 2003). In the figure 2-6, comparing with the true vegetation reflectance, it can be observed that apparent reflectance spectrum has two peaks in the $O_2$-A and $O_2$-B absorption band. The peak in the oxygen absorption bands can be attributed to the contribution of chlorophyll fluorescence.

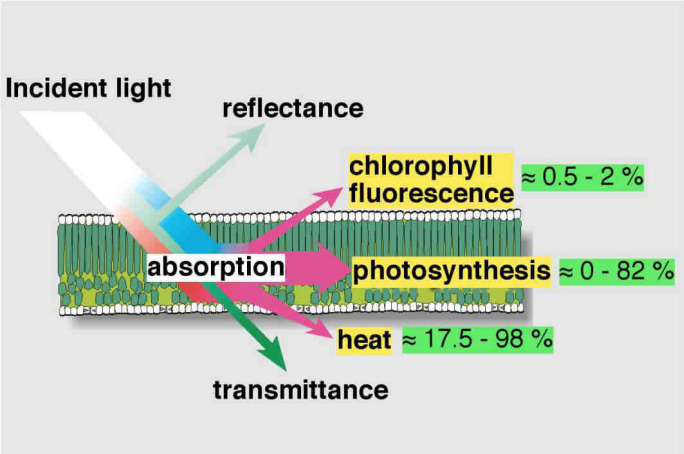


Figure 2-5 Interaction between sunlight and leaf

The figure 2-6 shows that three spectral windows existing in the solar spectrum are usually used to retrieve chlorophyll fluorescence, such as Ha absorption band (the central wavelength is 656.4 nm), $O_2$-B absorption band (the central wavelength is 687.0 nm) and $O_2$-A absorption band (the central wavelength is 760.0 nm). Because the oxygen absorption bands are closer to the fluorescence peak than Ha band, the oxygen absorption bands are more used to extract chlorophyll fluorescence. The width of $O_2$-A absorption band is much more wider and deeper than $O_2$-B, $O_2$-A absorption band is used more extensively. Although $O_2$-A absorption band (760nm) is not consistent with the peak of fluorescence spectrum (740nm), the fluorescence in the $O_2$-A absorption band can still explain 50% of the fluorescence peak (Moya et al., 2004).

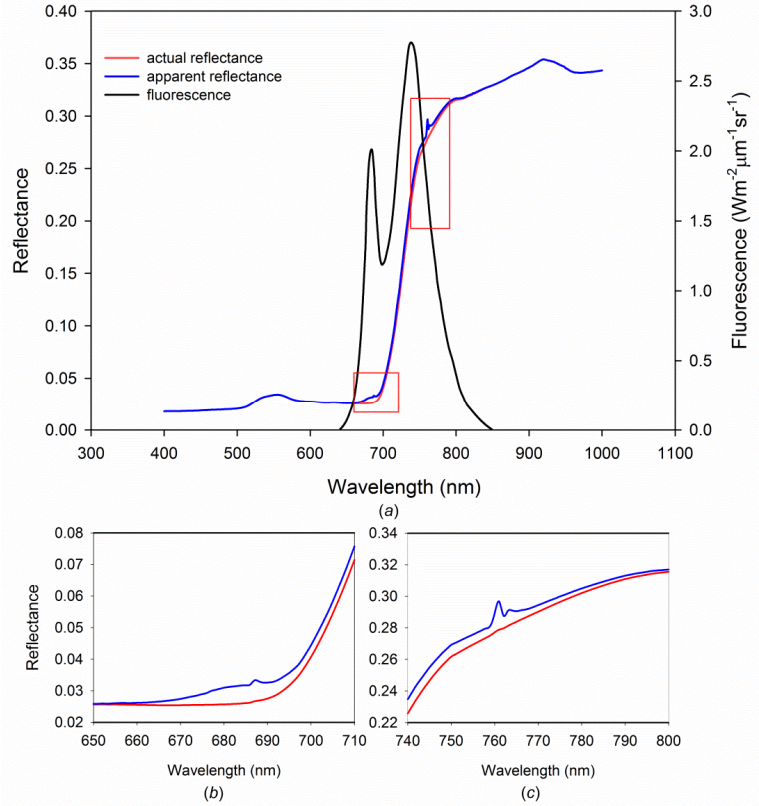


Figure 2-6 Reflectance and fluorescence spectra simulated by the FluorMOD model

The received signal at-sensor includes the reflected signal and the chlorophyll fluorescence excited by vegetation. Assuming the fluorescence emission and the surface reflectance follow the lambert's law, the radiance at-sensor (L) can be expressed as follows:

$$L(\lambda) = \frac{r(\lambda)E(\lambda)}{\pi} + F(\lambda) \tag{2-4}$$

Where λ is the wavelength, r is the real reflectance, and E is the total incident radiance. The contribution of chlorophyll fluorescence to the received radiance at-sensor is very little, and about only 1-5% of the reflected radiance. Some researches derive the range of chlorophyll fluorescence (seeing the table 2-2).

Table 2-2 The reported SIF values (Raychaudhuri Braun 2014)

| **Reference** | **Fluorescence emission** （**W $m^{-2}sr^{-1}\mu m^{-1}$**） | **Remark** |
|---|---|---|
| Meroni et al.(2009) | $O_2$-A: 0-20<br>$O_2$-B: 0-36 | Reviewed and compiled the results of many ground-based, airborne and satellite based measurements |
| Guanter et al.(2007) | $O_2$-A: 0-6 | Used both airborne (CASI) and satellite (MERIS) measurements |
| Zarco-Tejada et al. (2009) | 0-3.8(healthy vegetation)<br>0-2.2(stressed vegetation) | Airborne imagery and use of $O_2$-A band |
| Guanter et al.(2010) | $O_2$-A: 0-3<br>$O_2$-B: 0-2 | Ground-based measurement |
| Joiner et al.(2011) | 3.0 | Value used in simulation of GOSAT spectra |
| Frankenberg et al. (2011) | Up to 2.5% of the continuum level radiance | Simulated data |
| Guanter et al. (2012) | 0-1.8 | Global fluorescence mapping by spatial and temporal averaging |
| Joiner et al. (2013) | 0-6 | Simulated data |
| Barun Raychaudhuri (2014) | 0-1.87 | Derived from Hyperion images |

## 2.3 The fluorescence retrieval methods near the ground

The methods used to estimate chlorophyll fluorescence are divided into two categories: 1) the radiance-based approaches; 2) the reflectance-based approaches. The radiance-based approaches use fraunhofer line to disentangle the fluorescence signals from the reflected radiance in physical unit. The reflectance-based methods exploit the indices correlated with the fluorescence to estimate the fluorescence without physical meaning.

### 2.3.1 The radiance-based methods

The Radiance-based approaches exploit 2 or 3 spectral channels (at least one nearby the fraunhofer line) or the continuous bands extract the fluorescence quantitatively. These methods are developed based on the high spectral resolution data. Now, the radiance-based methods includes fraunhofer Line Depth (FLD), 3 bands FLD (3FLD), corrected FLD (cFLD), improved FLD (iFLD), extended FLD (eFLD) and spectral fitting method (SFM).

2.3.1.1 Fraunhofer Line Depth (FLD)

Plascyk (1975) and Plascyk & Gabriel (1975) proposed the FLD principle. All radiance-based methods are developed based on the FLD principle. As the figure 2-7 shown, the FLD uses two flux measurements, one inside and one outside the Fraunhofer line. Because of the fluorescence, an in-filling effect occurs on the real fluxes in the oxygen absorption bands ($O_2$-A and $O_2$-B bands). For application, FLD is computed using the mathematical operation of the solar irradiance and target radiance inside and outside the fraunhofer line:

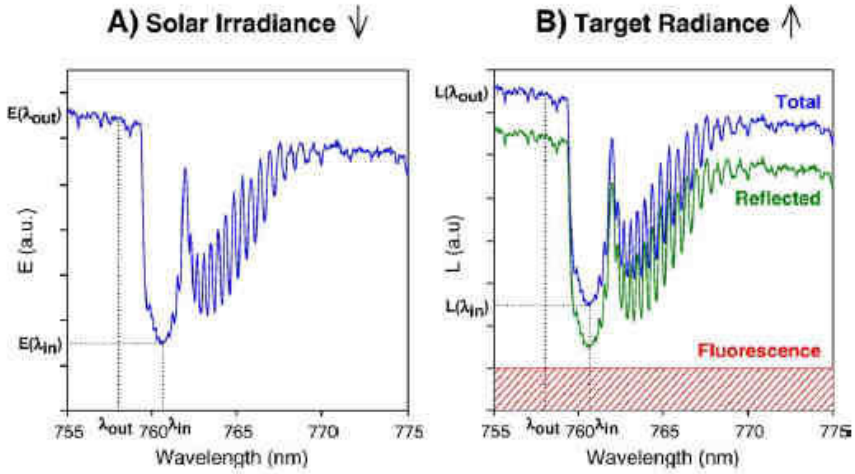


Figure 2-7 Standard FLD principle

Assuming that r and fluorescence are spectrally constant: an example is given at the $O_2$-A band investigated with a FWHM of 0.33 nm. A): Incident solar irradiance spectrum. B): Upwelling fluxes: the total radiance over the vegetated target (blue curve) is made up of the sum of fluorescence (red area) and pure reflection (green curve). The blue curves in A) and B) are the only measurement quantities.

$$L(\lambda_{in}) = \frac{r(\lambda_{in})E(\lambda_{in})}{\pi} + F(\lambda_{in}) \qquad (2\text{-}5)$$

$$L(\lambda_{out}) = \frac{r(\lambda_{out})E(\lambda_{out})}{\pi} + F(\lambda_{out})$$

Assuming the reflectance and fluorescence inside and outside the absorption line are constant, the expression can be arranged as following:

$$r = \frac{L(\lambda_{out}) - L(\lambda_{in})}{E(\lambda_{out}) - E(\lambda_{in})} \cdot \pi \tag{2-6}$$

$$F(\lambda_{in}) = \frac{E(\lambda_{out}) \cdot L(\lambda_{in}) - L(\lambda_{out}) \cdot E(\lambda_{in})}{E(\lambda_{out}) - E(\lambda_{in})}$$

This method is simple and only need requires two flux measurements in two spectral channels. In this method, the precondition is that the reflectance and fluorescence are constant in and out the fraunhofer band. In fact, despite the two spectral channels are enough close, the actual reflectance and fluorescence are not exactly the same. This assumption has been questioned by several authors (Meroni & Colombo 2006; Moya et al., 2006; Alonso et al., 2008).

2.3.1.2 3FLD

Maier et al. (2003) proposed a 3FLD method, which used three bands to estimate the fluorescence. In this method, the single reference band (λout) in FLD is replaced by the average of two bands out of the absorption line, at left and right wavelengths of the absorption band, respectively. In the 3FLD algorithm, r and F are assumed to vary linearly in the restricted spectral range. Therefore, the accuracy of this method is improved than that of FLD.

$$F(\lambda_{in}) = \frac{L(\lambda_{in}) \cdot \frac{E(\lambda_{in})\,(\omega_{left} \cdot L(\lambda_{left}) + \omega_{right} \cdot L(\lambda_{right}))}{\omega_{left} \cdot E(\lambda_{left}) + \omega_{right} \cdot E(\lambda_{right})}}{1 - \frac{E(\lambda_{in})}{\omega_{left} \cdot E(\lambda_{left}) + \omega_{right} \cdot E(\lambda_{right})}} \tag{2-7}$$

where $L(\lambda_{left})$ and $L(\lambda_{right})$ are the radiance at the left and right of fraunhofer lines, respectively; $E(\lambda_{left})$ and $E(\lambda_{right})$ are the irradiance of the bands at the left and right of fraunhofer lines, respectively; and $w_{left}$ and $w_{right}$ are the weight for the left and right wavelengths.

$$\omega_{left} = \frac{\lambda_{in} - \lambda_{left}}{\lambda_{right} - \lambda_{left}} \tag{2-8}$$

$$\omega_{right} = \frac{\lambda_{right} - \lambda_{in}}{\lambda_{right} - \lambda_{left}}$$

2.3.1.3 cFLD

On the basis of FLD algorithm, Gómez-Chova et al. (2006) and Moya et al. (2006) used two correction factors $\alpha_r^*$ and $\alpha_F$ to show the variation of the reflectance and fluorescence inside and outside the absorption bands.

$$r(\lambda_{in}) = \alpha_r \cdot r(\lambda_{out}) \qquad (2\text{-}9)$$
$$F(\lambda_{in}) = \alpha_F \cdot F(\lambda_{out})$$

This algorithm is cFLD algorithm:

$$r(\lambda_{in}) = \frac{\alpha_r^* \cdot E(\lambda_{in}) \cdot L(\lambda_{out}) - L(\lambda_{in}) \cdot E(\lambda_{out})}{\alpha_r^* \cdot E(\lambda_{in}) - \alpha_F \cdot E(\lambda_{out})} \qquad (2\text{-}10)$$

In cFLD, correction factor $\alpha_F$ is derived from the measurements of actual fluorescence at the leaf level; $\alpha_r^*$ is derived by interpolating apparent reflectance, one inside the Fraunhofer lines and at least two bands outside the Fraunhofer lines.

2.3.1.4 iFLD

Based on the existed methods, Alonso et al. (2007, 2008) developed the improved FLD algorithm (iFLD). There is a little peak in the apparent reflectance spectrum in the Fraunhofer lines due to the contribution of the fluorescence. In this method, $\alpha_r^*$ is computed by using the cubic or spline interpolation which overcomes the cFLD assumption of linearity expressed in Eq. 2.11. The relationship between$\alpha_r$* and fluorescent correction factor $\alpha_F^*$ is:

$$\alpha_r^* = \frac{R_{out}}{\tilde{R}_{in}}$$
$$\alpha_F^* \approx \frac{E(\lambda_{out})}{\tilde{E}(\lambda_{in})} \cdot \alpha_r^* \qquad (2\text{-}11)$$

where $R_{out}$ is the apparent reflectance outside the Fraunhofer lines, $\tilde{R}_{in}$ is the interpolated reflectance without the contribution of fluorescence in the Fraunhofer lines, $E(\lambda_{out})$ is the irradiance outside the fraunhofer lines, and $\tilde{E}(\lambda_{in})$ is the interpolated irradiance in the franuhofer lines to remove the atmospheric absorption effects.

2.3.1.5 eFLD

Mazzoni et al. (2007) proposed the eFLD (extended FLD) algorithm. In this algorithm, the reflected radiance spectrum is divided into two parts: inside and outside the absorption bands; and the reflectance spectrum is normalized by a base line which is fitted by using the bands outside the absorption bands (Figures 2-8).

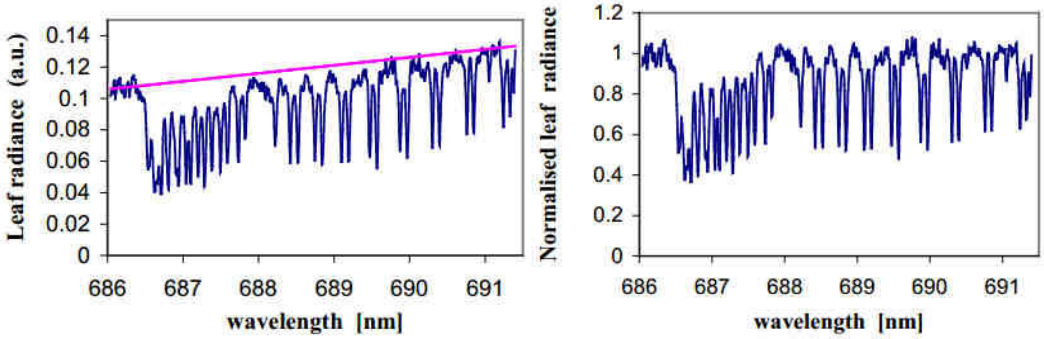


Figure 2-8 The leaf normalized radiance spectrum (Mazzoni et al. 2007)

Apparent reflectance can be expressed as:

$$R(\lambda) = \frac{LB(\lambda) - LS(\lambda)}{RB(\lambda) - RS(\lambda)} \tag{2-12}$$

LB and RB refer to the baseline of vegetation and reference board, respectively; and LS and RS refer to the spectrum of vegetation and reference board, respectively.

In the window of absorption bands, R(λ) is fitted, and the fitting coefficient FITR(λ) is obtained. The above formula can be written as:

$$F(\lambda) = LS(\lambda) - FITR(\lambda) \cdot RS(\lambda) \tag{2-13}$$

In this method, we only consider the variation of the reflectance along with the wavelength variation, and do not consider the variation of the shape of the fluorescence spectrum along with the wavelength variation.

2.3.1.6 SFM

Meroni & Colombo (2006) proposed the spectral fitting method (SFM), which assumed that r and F can be fitted by simple mathematical functions. Therefore, the vegetation radiance can be expressed as:

$$L^s(\lambda) = \rho(\lambda) L^i(\lambda) + F(\lambda) \quad (2\text{-}14)$$

Where $L^s(\lambda)$ is the terrestrial upwelling radiance, $L^i(\lambda)$ is the solar irradiance, $\rho(\lambda)$ is the terrestrial real reflectance, and $F(\lambda)$ is fluorescence.

Assuming $\rho(\lambda)$ and $F(\lambda)$ vary linearly in the adjacent bands, $L^s(\lambda)$ can be expressed as follows:

$$\begin{aligned} L^s(\lambda_0 + \Delta\lambda) &= (\rho(\lambda_0) + \frac{d\rho}{d\lambda}\Delta\lambda) L^i(\lambda) + F(\lambda_0) + \frac{dF}{d\lambda}\Delta\lambda \\ &= (a_1 + a_2\Delta\lambda) L^i(\lambda) + b_1 + b_2\Delta\lambda \end{aligned} \quad (2\text{-}15)$$

where $\lambda_0$ is the left border of selected window, and $\Delta\lambda$is step size. In the given wavelength range, reflectance $\rho$ and fluorescence F can be solved by using the least square method.

### 2.3.2 The reflectance-based methods

The reflectance-based methods mainly exploit 2 or 3 bands in the range of 650-800 nm to build reflectance index related with fluorescence. These methods only assess the fluorescence qualitatively, and the fluorescence has no physical units. The reflectance-based methods can be divided in three categories: reflectance ratio, derivative index and infilling index.

The reflectance ratio do not exploit the fraunhofer lines, and only uses two or three bands, at least one affected by the fluorescence or locating near by the fluorescence peak, and other bands not affected by the fluorescence. In the process of building the index, the band normalization is used to remove the influence of reflectance shape. The derivative index is the normalized index of first-derivative reflectance. Compared with the reflectance, the first-derivative reflectance can detect much more subtle variations in fluorescence. The infilling index exploits the little peak of the apparent reflectance at 760.5 nm, and is expressed as the reflectance at 760.5 nm minus the reflectance at 759.9 nm, marked as R760.5-R759.9. The filling index estimates the fluorescence by measuring the height of the little peak at 760.5 nm.

The advantage of the reflectance-based methods is the simplicity to derive the relative fluorescence value, but the estimated fluorescence has no physical meaning, and is prone to be affected by the chlorophyll content. Despite these limitations, the reflectance-based methods are often the only methods that allow passive remote sensing of fluorescence in the

laboratory, in which artificial light is used and where the radiance-based approaches failed. Meroni et al. (2009) had summarized the existed reflectance-based methods in the table 2-3.

Table 2-3 Summary of reflectance-based indices developed for estimating the fluorescence

| **References** | **Device name** | **Illumination** | **Scale** | **Index type** | **Index formation** |
|---|---|---|---|---|---|
| | | A/E | Leaf/Canopy | RR/D/I | |
| Ground level | | | | | |
| Zarco-Tejada et al.(2000a) | ST1000 Integ.Sphere Long-pass filter | A | L | RR<br>Td<br>RR<br>RR<br>RR | $(r675 \cdot r690)/r683^2$<br>$r740_{t1}$-$r740_{t2}$<br>r750/r800<br>r685/r655<br>r690/r655 |
| Zarco-Tejada et al.(2000b) | CASI Long-pass filter | A | C | RR<br>RR<br>RR/I<br>RR<br>RR<br>RR | r680/r630<br>r685/r630<br>r687/r630<br>r690/r630<br>$r685^2/( r675 \cdot r690)$<br>r685/r655 |
| Zarco-Tejada et al.(2003b) | ASD | A | C | D/I<br>D/I<br>D<br>D<br>D<br>D | $DPI=(D688 \cdot D710)/D697^2$<br>Area of D(688-710)<br>D705/D722<br>D730/D706<br>DλP/D720<br>DλP/D(λp+12nm) |
| Dobrowski et al. (2005) | ASD | A | C | RR<br>RR | R690/r600<br>R740/r800 |
| Perez-Priego et al. (2005) | HR2000 | E | C | I | R760.59-r759.5 |
| Airborne level | | | | | |
| Zarco-Tejada et al. (2000b) | CASI | E | C | D<br>D<br>RR<br>RR | D730/D706<br>DλP/D703<br>$r683^2/(r675 \cdot r691)$<br>r685/r655 |

A: Aritifical; E: Environmental; RR: Reflectance Ratio; D : Derivation; I : Infilling index. D is the first derivative of reflectance with respect to wavelength, whereas DλP is the derivative of the reflectance at the inflection point of

the red edge. Time difference (Td) refers to a laboratory method with the radiative magnitude of F is deduced from the reflectance difference determined between two times at which F is different.

## 2.4 The SIF retrieval methods on the airborne or space-borne

### 2.4.1 The airborne/space-borne SIF retrieval principle

When we detect the chlorophyll fluorescence on the leaf or the canopy, the propagation path of chlorophyll fluorescence is short. It can be thought that the observed chlorophyll fluorescence is not affected by the atmosphere, and it is the true plant chlorophyll fluorescence. If we detect the chlorophyll fluorescence from the airborne or the space-borne, chlorophyll fluorescence passes through the atmosphere, and is affected by atmospheric scattering and absorption. Compared with the vegetation reflected radiance, the intensity of the fluorescence signal is weak. If we want to extract chlorophyll fluorescence from the airborne scale or space, it is important to remove the effect of atmosphere. Therefore, the relevant knowledge of radiative transfer is introduced in this section.

#### 2.4.1.1 Atmospheric radiative transfer mode

The figure 2-9 illustrates the propagation of sunlight from the sun to the surface to the sensor. The radiation at the sensor include three parts: ① the sun and sky irradiation reflected by the target, 2a is the reflected sun irradiation, and 2b is the reflected sky irradiation; ② atmospheric path radiance; ③the irradiation reflected by the background, 3a is the reflected sun irradiation, and 3b is the sky irradiation; ④ chlorophyll fluorescence passed through the atmosphere to the sensor.

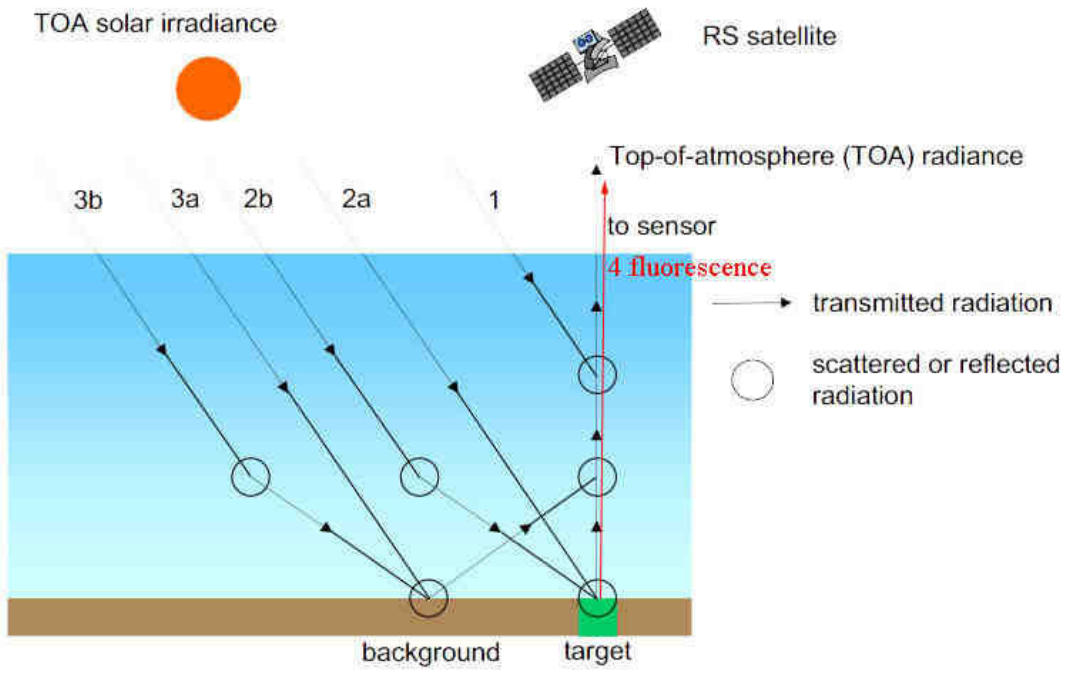


Figure 2-9 Radiation transfer process

Under the assumption that both surface reflectance and fluorescence emission are isotropic, the TOA (top of atmosphere) radiance signal $L_{TOA}$ can be formulated by a simple expression accounting for the interaction with the atmosphere of the radiation reflected and emitted by the surface.

$$L_{TOA} = \frac{E_0 \cos\theta}{\pi}\rho_{so} + \frac{E_0 \cos\theta}{\pi}\frac{\left(\tau_{ss} + \tau_{sd}\right) R \left(\tau_{do} + \tau_{oo}\right)}{1 - R\ \rho} + \frac{SIF\left(\tau_{do} + \tau_{oo}\right)}{1 - R\ \rho} \qquad (2\text{-}16)$$

On the right side of this equation, the first item is the atmospheric contribution to the TOA radiance signal, the second item is the surface-reflected radiance, and the last item is the fluorescence signal contribution to the TOA radiance. In the equation, $\rho_{so}$ is the hemispherical reflectance, $E_0$ is the extraterrestrial solar irradiance on a plane perpendicular to the sun's rays, $\theta$ is the solar zenith angle, R is the surface reflectance, SIF is the fluorescence radiance at the top-of-the-canopy (TOC), and $\rho$ is the spherical reflectance of the atmosphere back to the surface.

$\tau$ stands for transmittance. The first subscript indicates incident radiation, and the second subscript indicates scattered radiation. $\tau_{ss}+\tau_{sd}$ is the total irradiance transmittance (including direct and diffuse components), and $\tau_{do}+\tau_{oo}$ is the spherical transmittance from the surface to the TOA.

$\tau_{ss}$, the incident and scattered radiation are direct solar radiation;

$\tau_{sd}$, the incident radiation is direct solar radiation, and scattered radiation is hemispherical diffuse radiation;

$\tau_{do}$, the incident radiation is diffuse sky radiation, and the scattered radiation is the direct radiation in the observer's direction;

$\tau_{oo}$, the incident radiation is direct radiation, and the scattered radiation is the direct radiation in the observer's direction.

In equation 2-16, SIF and R come from the simulation of the SCOPE model, and the other parameters are computed by MODTRAN.

2.4.1.2 Effect of the atmosphere on the radiative transfer

The solar radiation reaches the ground surface through the atmosphere, and the electromagnetic waves emitted or reflected by the ground surface reach the sensor through again the atmosphere. The signal received by the sensor includes all kinds of distortion and attenuation due to the sun position and angle, the atmospheric conditions, the topography and the performance of the sensor itself. Therefore, the effect of various factors on the radiative transfer should be considered in the analysis of the surface signal.

In this process, the received signal at-sensor depends on the initial intensity of the light ($I_0(\lambda)$), the length of the light path through the absorber/scatters, the absorption/scattering ability of the gas molecules, so called extinction cross section ($\sigma_{ext}(\lambda)$ [$cm^2$/particle]), which is divided into two main terms of absorption cross section ($\sigma_{abs}$), and scattering cross section ($\sigma_{scatt}$), and the total concentration of absorber/scatters along the path (N) [particles/$m^3$]. Therefore, according to the Beer-Lambert's Law the general light extinction term is written as:

$$I(\lambda, s) = I_0(\lambda) \exp(-\sigma_{ext}(\lambda) N) \quad (2\text{-}17)$$

The product of extinction cross-section and the length of the light path are also known as Optical Depth (OD).

2.4.1.2.1 The atmospheric absorption

The solar radiation on the sun-surface path is affected by absorption and scattering effects from atmospheric gases and aerosols. Accurate modeling of these effects is required in order to derive surface reflectance spectra from imaging spectrometer data. Among the approximately thirty atmosphere gases, only eight gases, namely water vapor ($H_2O$), carbon dioxide ($CO_2$), ozone ($O_3$), nitrous oxide ($N_2O$), and nitrogen dioxide ($NO_2$) produce observable absorption features in imaging spectrometer data over the range 0.4 to 2.5 μm with a spectral resolution between 1 and 20 μm. Gao et al. (2009a) gave an example of simulated atmospheric transmittances for the eight gases (Figure 2-10). Approximately half of the spectral region between 0.4 and 2.5 μm is affected by atmospheric water vapor absorption. The effects from the other seven gases are generally located in the narrow wavelength. Each gas absorbs the light at some specific wavelengths due to their absorption cross section. Absorption is always paired with emission. Gas absorbs energy in a spectral wavelength and emits energy at a longer spectral wavelength. In our interest wavelengths (600-800nm), the main absorbers are oxygen ($O_2$) and water vapor ($H_2O$) (Khosravi 2012).

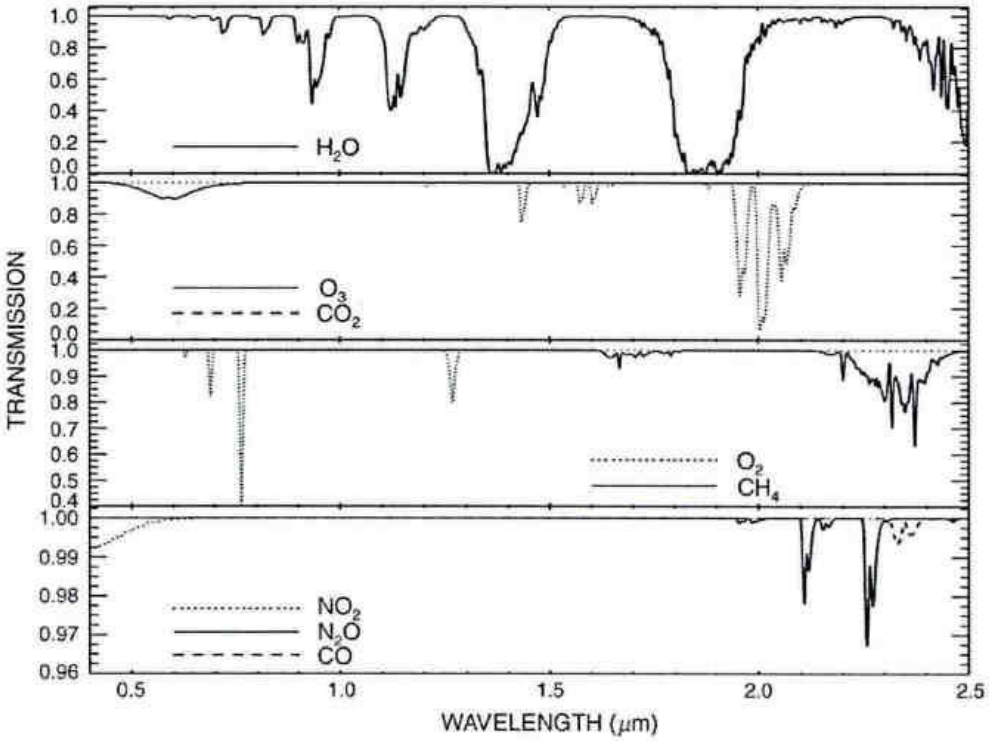


Figure 2-10 Simulated transmittance spectra of atmospheric water vapor, carbon dioxide, ozone, nitrous oxide, carbon monoxide, methane, oxygen and nitrogen dioxide in (Gao et al. 2009a)

2.4.1.2.2 Atmospheric scattering

Scattering is the process that when electromagnetic radiation encounters small particles, it changes its transmission direction, and spreads to other directions, thus radiation intensity in original direction weakens, and radiation intensity in other directions strengthens. The wavelength region between 0.4 and 0.7 μm is strongly affected by molecular scattering (Rayleigh scattering). Its effect decreases rapidly with increasing wavelength ($\lambda^{-4}$). The aerosol scattering effect also decreases with increasing wavelength, but at a slower rate (typically $\lambda^{-2}$ to $\lambda^{-1}$). There are two kinds of scattering: elastic scattering (preserving the incident energy) and inelastic scattering (changing the incident energy). Elastic scattering is divided into Mie scattering and Rayleigh scattering with respect to the light and particles properties. Scattering dominates the light received at TOA by both adding and subtracting photons to or from it.

1). Elastic scattering

Elastic scattering is a scattering process in which the kinetic energy of an incident particle is conserved. The incident particle does not change the frequency of the light and only changes the raveling direction by changing the phase function. The scattering cross-section can vary with wavelength. Due to the particle size and wavelength, it can be divided into two kinds: Mie scattering and Rayleigh scattering.

a. Mie scattering

Mie scattering occurs when the particles are just about the same size as the wavelength of the radiation. Dust, aerosol, smoke and water vapor are common causes of Mie scattering. The directivity of Mie scattering is obvious, and scattering intensity is stronger in the forward direction than that in the backward direction, which is inverse proportion to the square of the wavelength. Effects of Mie scattering can be observed from visible to near infrared bands.

b. Rayleigh scattering

Rayleigh scattering is the scattering that occurs when the particles are smaller than the wavelength than the wavelength of the light. It states that the light will be scattered is inversely proportional to the fourth power of the wavelength. Small particles will inversely much higher percentage of short wavelength light than long wavelength light. Because the mathematical relationship involves the fourth power of the wavelength, thus a small wavelength difference can mean a large difference in scattering efficiencies. Rayleigh scattering is mainly caused by molecules such as ozone, oxygen, carbon dioxide and nitrogen,

which are very obviously present in visible light. When sunlight passes through the atmosphere, the loss of energy in visible light can reach more than 10%. Rayleigh scattering often occurs in the visible region.

2) Inelastic scattering

Elastic scattering is an important factor affecting the fluorescence extraction. However, the influence of inelastic scattering can't be ignored. In the process of inelastic scattering, there is no change in the composition of the atom, but the internal state changes, some of the photon energy shift to the long wave or short wave direction when the collision occurs between incident photon and atom. Inelastic scattering is also called Raman scattering.

In the process of Raman scattering, the atom is affected by the incident photon, which is excited to a higher energy state. Excited atom emits a photon that is longer than the wavelength of the incident photon along with the energy transfer. If the atoms are in the excited state, it is also possible to launch a shorter or longer wavelength of the photon, and then return to the ground state. When the excited state atom emits a photon, it will return to a rotating or oscillating state that is different from ground state. If only the vibration state occurs, it is called Rotational Raman Scattering (RRS). If it is accompanied by a rotational and vibration state, it is called Vibrational Raman Scattering (VRS).

The effect of Raman scattering on the short wavelength region is relatively large, such as in Ultraviolet bands (UV), and it is not dominant in the long wavelength region, for example in Infra-Red bands (IR). In practice, the intensity of RRS is about one order of magnitude higher than that of the VRS in the UV-visible region. The effect of VRS is relatively weak, and the RRS is the dominant in the Raman scattering. Therefore, in many scientific studies, the influence of VRS is often neglected (Joiner et al., 2012). Raman scattering is often called the ring effect, which will cause the filling effect of the fraunhofer lines, accounting for about 4% of all scattering effect (Vountas et al., 1998). Therefore, the effect of Raman scattering is considered in the extraction of the space-borne fluorescence (Khosravi 2012).

### 2.4.2 The airborne/space-borne SIF retrieval methods

The intensity of chlorophyll fluorescence signal is relatively weak compared with the reflected solar radiation in the same spectral region. In the near infrared (NIR) spectral region, the chlorophyll fluorescence just occupied 2% - 5% of reflected solar radiation. It is so weak

that decoupling fluorescence radiation from reflected radiation is challenging. Campbell et al. (2008) drew a conclusion that the steady-state fluorescence was about 1.5 to 3.4 $mW \cdot m^{-2} \cdot sr^{-1} \cdot nm^{-1}$ at 685 nm, and 2.4 to 5.4 $mW \cdot m^{-2} \cdot sr^{-1} \cdot nm^{-1}$ at 740 nm. This conclusion was consistent with other researchers' results (Middleton et al., 2006; Amoros−Lopez et al., 2008; Zarco-Tejada et al., 2009). How to remove the atmospheric effects and to improve the accuracy of SIF retrieval has attracted researchers' attentions. In recent years, many methods have been developed to measure chlorophyll fluorescence from the space. Based on the past literatures, methods of retrieving SIF from space always exploit atmospheric absorption features, primarily the oxygen absorption band or the fraunhofer lines. The figure 2-11 gives the common use windows to retrieve the SIF, and the SIF retrieval methods are summarized in the table 2-4.

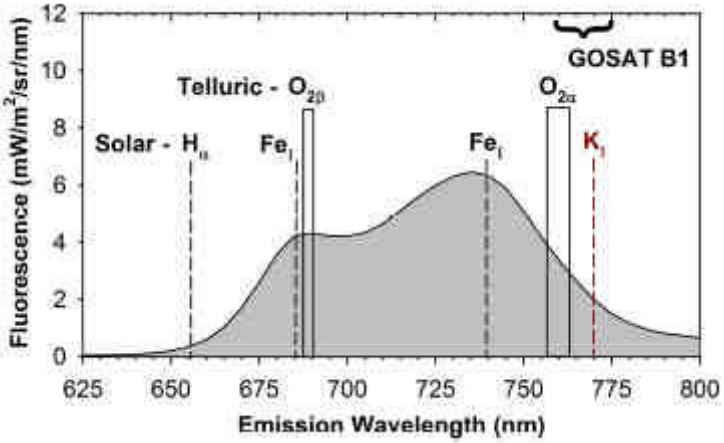


Figure 2-11 Simulated solar-induced fluorescence as a function of the emission wavelength with locations of oxygen absorption bands and several solar fraunhofer lines including the K I line used here (Joiner et al. 2011)

2.4.2.1 The SIF retrieval methods exploiting the atmospheric absorption bands

When the light wave passes through the atmosphere, the wave at the particular wavelengths is absorbed by the different kinds of gas, such as $O_2$, $H_2O$, $CO_2$, $O_3$ and so on, and the dark features (or dark lines) in the solar spectrum are generated due to the gas absorption. The influence generated by the $CO_2$ or $O_3$ is often neglected due to their relatively small content in the atmosphere. In $O_2$-A bands, the oxygen is the only absorbing gas; the dynamic range of the transmittance of $O_2$-A bands is very wide; and the $O_2$-A bands is close to the fluorescence peak. Thus, the oxygen absorption bands are the ideal window to retrieve the fluorescence. Currently the satellites in orbit with the capability of detection in the oxygen

absorption band include SeaWiFS, GOME, POLDER, MERIS, SCIAMACHY, OCO, and GOSAT and so on. In this chapter, we introduce the airborne/space-borne SIF retrieval methods and its applications on the satellite imageries.

(1) Damm algorithm

The FLD algorithm is only used to extract fluorescence in the leaf or on the canopy due to its original design neglecting the atmospheric effects. Damm et al. (2014) combined 3FLD with atmospheric parameters to build the SIF retrieval algorithm. At airborne or aerospace scale, the fluorescent signal can be regarded as an additional term of received radiance at-sensor. If the surface reflectance and the fluorescence emission follow the Lamber's law, the at-sensor radiance can be calculated with the following equation:

$$L = L^{p} + \frac{E^{g} \cdot \rho / \pi + SIF}{1 - S \cdot \rho} \cdot \tau_{\uparrow} \tag{2-18}$$

The radiance inside and outside the oxygen absorption band can be expressed as follows:

$$\begin{aligned} L_{i} &= L^{p}{}_{i} + \frac{E^{g}{}_{i} \cdot \rho_{i} / \pi + SIF_{i}}{1 - S_{i} \cdot \rho_{i}} \cdot \tau_{\uparrow i} \\ L_{o} &= L^{p}{}_{o} + \frac{E^{g}{}_{o} \cdot \rho_{o} / \pi + SIF_{o}}{1 - S_{o} \cdot \rho_{o}} \cdot \tau_{\uparrow o} \end{aligned} \tag{2-19}$$

where i is inside $O_2$-A band (760 nm), o is outside $O_2$-A (753 nm), L is the radiance at-sensor, $L^p$ is the path radiance, $E^g$ is the irradiance including the direct and the scatter flux, S is the land surface reflectance, ρ is the hemisphere albedo, τ↑ is the up-welling transmittance, SIF is the land surface fluorescence.

Combining the two above-mentioned equations, the Fs can be calculated as follows:

$$SIF_{i} = B\left[\frac{X_{i}(E^{g}{}_{o} + \pi X_{o}S_{o}) - AX_{o}(E^{g}{}_{i} + \pi X_{i}S_{i})}{B(E^{g}{}_{o} + \pi X_{o}S_{o}) - A(E^{g}{}_{i} + \pi X_{i}S_{i})}\right] \tag{2-20}$$

in which：

$$
\begin{aligned}
X_j &= \frac{L_j - L_j^p}{\tau_{\uparrow j}}, j = i, o \\
\rho_i &= A \cdot \rho_o \\
SIF_i &= B \cdot SIF_o
\end{aligned}
\tag{2-21}
$$

A is the factor relating $\rho_i$ with $\rho_o$, and it is derived from the linear interpolation of ρ of the left and right $O_2$-A band shoulders. B is the factor relating $SIF_i$ and $SIF_o$ (inside and outside the $O_2$-A band) and is fixed to a value of 0.8 (Alonso et al., 2008; Rascher et al., 2009). This conclusion about B is also confirmed using the simulated data in this paper by the ratio of inside and outside fluorescence.

$$
\begin{aligned}
A &= \frac{\rho_{758} \cdot \omega_1 + \rho_{771} \cdot \omega_2}{\rho_{758}} \\
\omega_1 &= \frac{771 - 760}{771 - 758} \\
\omega_2 &= \frac{760 - 758}{771 - 758}
\end{aligned}
\tag{2-22}
$$

In this method, there is an assumption that the variation of the reflectance and the fluorescence are linear in the oxygen absorption bands and the changes of spectral shape of fluorescence and reflectance have not been taken into account. This method is often used combined with the MODTRAN model, which can simulate the atmospheric profiles. This method can get an accurate fluorescence radiance value in radiance unit. However, the atmospheric profiles are necessary for this method, and it is very difficult to obtain accurate atmospheric profiles. The simulated atmospheric profiles by MOTRAN have an error to some extent comparing with the true atmospheric profiles. Thus, there is an error with the results of the fluorescence radiance and the source of the errors is difficult to explain.

Guanter et al. (2007) used FLD and MODTRAN to retrieve the SIF in the oxygen-A bands from the MERIS and CASI-1500 imagery, and compared the retrieved fluorescence with the ground measurement fluorescence, and then illustrated that it is feasible to retrieve the fluorescence in the airborne/space-borne. Guanter et al. (2010) analyzed the effects of the atmospheric parameters on the SIF retrieval methods in the oxygen-A and –B bands. Damm et al. (2010) exploited FLD and MODTRAN to retrieve the fluorescence from the ASD spectrum in the airborne, and then Damm et al. (2014) used the semi-empirical method to

estimate the fluorescence from the ASD data, and analyzed the effects of atmospheric parameters on the oxygen absorption depth in the oxygen-A bands.

(2) Barun method

Barun Raychaudhuri (2014) exploited the radiance ratio which is composed by the radiance in the vegetation region and the radiance in the non-vegetation region to retrieve the fluorescence from the Hyperion imagery. Radiance at-sensor can be thought to be a linear combination of the radiance reflected by vegetation and fluorescence radiation (Meroni et al., 2009). Assuming that the effects of the atmosphere parameters are the same in the same district and, then, through comparing the vegetation region with the non-vegetation region, the effect of atmosphere scattering can be cancelled out, and fluorescence radiation can be expressed in the following equations:

$$SIF = (A_V - A_{NV})(\omega_L L_L + \omega_R L_R) \tag{2-23}$$

In which:

$$\begin{aligned} A_i &= \frac{D}{\omega_L L_L + \omega_R L_R} = 1 - \frac{L_F}{\omega_L L_L + \omega_R L_R}, \mathrm{i} = V, NV \\ \omega_L &= \frac{\lambda_R - \lambda_F}{\lambda_R - \lambda_L} \\ \omega_R &= \frac{\lambda_F - \lambda_L}{\lambda_R - \lambda_L} \end{aligned} \tag{2-24}$$

where $A_V$ is the percentage of reflected radiance inside the absorption band for vegetation, including reflected radiance, path radiance and fluorescence radiation; $A_{NV}$ is the contribution of surface reflectance and path radiance due to atmospheric scattering in the absorption band; $L_L$ and $L_R$ are radiance on the left and right sides of the oxygen-A band, respectively; $L_F$ is the radiance in the oxygen-A band; and $\lambda_L$, $\lambda_F$ and $\lambda_R$ are 758.03 nm, 760.46 nm and 771.01 nm, respectively.

(3) Joiner method

Joiner et al. (2013) assumed that the reflectance and fluorescence follow Lambert's laws, the radiance at-sensor is as follows:

$$L_{TOA} = \frac{E_0 \cos\theta}{\pi} \cdot \rho_{so} + \frac{E_0 \cos\theta}{\pi} \cdot \frac{T_{\uparrow} \cdot R \cdot T_{\downarrow}}{1 - R \cdot \rho_{dd}} + \frac{SIF \cdot T_{\uparrow}}{1 - R \cdot \rho_{dd}} \quad (2\text{-}25)$$

in which, $T_{\uparrow}$is the spherical transmittance from the surface to TOA, $T_{\downarrow}$is the total irradiance transmittance (including direct and diffuse components).

The total reflectance $\rho_{tot} = \frac{\pi \cdot L_{TOA} \cdot d^2}{E \cdot \cos\theta}$ , in which d is Sun-Earth distance (astronomical unit), and is often set to 1, then can be computed as follows:

$$\rho_{tot} = \rho_{so} + \frac{T_{\uparrow} \cdot R \cdot T_{\downarrow}}{1 - R \cdot \rho_{dd}} + \frac{\pi \cdot SIF \cdot T_{\uparrow}}{(1 - R \cdot \rho_{dd}) \cdot E_0 \cdot \cos\theta} \quad (2\text{-}26)$$

The basic idea behind this method is to separate the spectral features into three basic components: atmospheric absorption ($T_{\downarrow}$,$T_{\uparrow}$), surface reflectivity (R), and fluorescence radiance ($F_s$). Assuming that the effects of atmospheric scattering are small ($\rho_{so}\approx 0$ and $R*\rho_{dd} << 1$), the above equation can be expressed as follows:

$$\rho_{tot} = T_{\uparrow} \cdot R \cdot T + \frac{\pi \cdot SIF \cdot T_{\uparrow}}{E_0 \cdot \cos\theta} \quad (2\text{-}27)$$

where $T_{\uparrow}$ and $T_{\downarrow}$include atmospheric molecular absorption only. The parameters $T_{\uparrow}$ and $T_{\downarrow}$ can be expressed as one parameter $T(\lambda)$ ($T(\lambda)= T_{\uparrow}* T_{\downarrow}$). $T(\lambda)$ is the sun-to-satellite (two-way) atmospheric transmittance, and can be expressed as follows:

$$T(\lambda) = \exp\left[-A_2(\lambda)\right] \quad (2\text{-}28)$$

where $A_2(\lambda)$ is the two-way absorptance, $A_V(\lambda)$ is the vertical absorptance, $\theta$ is sun zenith angle, $\theta_0$ is view zenith angle (Figure 2-12), then the Eq. 2-28 can be expressed in the following equation:

$$T(\lambda) = \exp\left[-A_v(\lambda)\left\{\sec\theta + \sec\theta_0\right\}\right] \quad (2\text{-}29)$$

The upward absorptance $A_{\uparrow}(\lambda)$ can be expressed as follows:

$$\bar{A}(\lambda) = A_v(\lambda)\sec\theta_0 = A_2(\lambda)\frac{\sec\theta_0}{\sec\theta + \sec\theta_0} \quad (2\text{-}30)$$

In the last, the transmitance can be expresses as follows:

$$T_{\uparrow}(\lambda) = \exp\left[-\bar{A}(\lambda)\right] = \exp\left[-A_2(\lambda)\frac{\sec\theta_0}{\sec\theta + \sec\theta_0}\right]$$
$$= \exp\left[\ln T(\lambda)\frac{\sec\theta_0}{\sec\theta + \sec\theta_0}\right] \quad (2\text{-}31)$$

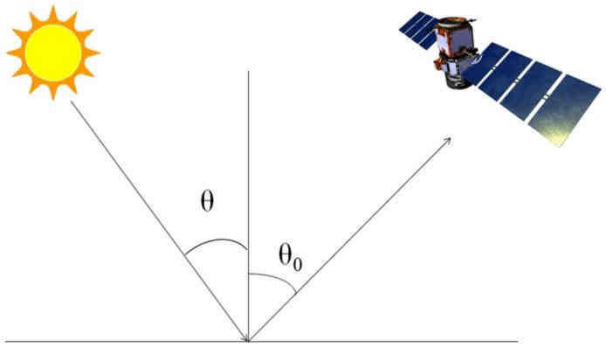


Figure 2-12 Schematic diagrams of sun zenith angle and view zenith angle

By the above simplification, the total reflectance is expressed as follows (Joiner et al., 2013):

$$\rho_{tot} = R \cdot T + \frac{\pi \cdot SIF}{E_0 \cos\theta} \cdot \exp\left[\ln T(\lambda)\frac{\sec\theta_0}{\sec\theta + \sec\theta_0}\right] \quad (2\text{-}32)$$

Note that the above equations are strictly valid only for monochromatic radiation. It should note that $\rho_{so}$, $\rho_{dd}$, $T_{\uparrow}$ and $T_{\downarrow}$in the presence of atmospheric scattering and in the absence of atmospheric molecular absorption, are a spectrally smooth function of wavelength. Therefore, when atmospheric scattering is present, R and $F_s$ in Eq. 2.32 can be thought of as effective TOA spectral components of surface reflectance and fluorescence that have been modified by spectrally smooth atmospheric scattering; the spectral structure of $\rho_{so}$ can be incorporated into the components of the first term of Eq. 2.32.

To solve R, Fs and T(λ), Joiner et al. (2013) assumed that each of them has a distinct spectral structure. Fs is a Gaussian function of λ centered at 736.8 nm with σ= 21.2 nm. Within our limited spectral fitting window, R is spectrally smooth, and is modeled as a low-order polynomial in λ. Previous works suggest that small errors in the prescribed shape of the fluorescence emission have a little impact on the estimated peak fluorescence value (Daumard et al., 2010; Guanter et al., 2013). Spectral structure of $A_2$ (λ) (or T(λ)) is using principal components (PCs) to be expressed.

This method may be applied to the entire fluorescence emission band containing both the red and far-red features. Alternatively, different fitting windows could be used to estimate fluorescence within smaller wavelength ranges. This method focuses on retrievals of the far-red fluorescence.

(4) Differential Optical Absorption Spectroscopy (DOAS)

Differential Optical Absorption Spectroscopy (DOAS) is a method to determine concentrations of trace gases by measuring their specific narrow band absorption structures in the UV and visible spectral region. DOAS is based on Beer-Lambert'law of light extinction and determines the amount of molecular absorbers along the effective optical light path by fitting and scaling spectra within a given wavelength window. Khosravi (2012) thought the fluorescence as a trace gases, and rewrote the DOAS equation as follows:

$$-\ln\frac{L(\lambda,\theta)}{E_g(\lambda,\theta)} = \sum_{n=1}^{N}\sigma_n^{'}(\lambda)S_n + \sigma_{Ray}(\lambda)S_{Ray} + \sigma_{Mie}(\lambda)S_{Mie} + \sigma_f(\lambda)S_f + \sum_{m=1}^{M}a_m\lambda_m \qquad (2\text{-}33)$$

Where $I(\lambda)$ and $I_0(\lambda)$ are the measured backscattered radiance and extraterrestrial irradiance; $S_n$ is the number density of either molecules or aerosol particles along the slant optical path; $\sigma'_n(\lambda)$ is the rapid part of the absorption cross-section of the nth atmospheric absorber; N is the number of absorbers; $\sigma_{Ray}(\lambda)$, $\sigma_{Mie}(\lambda)$ and $\sigma_f(\lambda)$ are the reference spectra of Rayleigh scattering, Mie scattering and fluorescence, respectively; $\sum_{m=1}^{M}\alpha_m\lambda^m$ is the low order polynomial, typically of the order M<4. Note, in here $\sigma_f(\lambda)$ is the fluorescence reference spectrum and acts as a pseudo emission across section for DOAS method, and $S_f$ is a DOAS fluorescence fit factor, and reacts like a fluorescence column showing how much the pseudo emission cross-section (Khosravi 2012). The absorption cross-section of a given molecule can be split into two parts: rapid and slow variations with wavelength. The rapid part $\sigma_n$' shows rapid variations with $\lambda$, mostly due to an absorption line, and the slow part $\sigma_n$ varies monotonically with the wavelength $\lambda$, and can be merged into the scattering item (Mie Scattering and Rayleigh Scattering).

Khosravi (2012) chose the 745-758nm fitting window in his study. He thought that this window seem to be affected only by Fraunhofer lines but no deep absorption feature from oxygen and water vapor. The Rayleigh and Mie scattering are removed by a low-degree polynomial that is also fitted. In the last, the Eq. 2-33 can be simplified as follows:

$$-\ln\frac{L(\lambda,\theta)}{E_g(\lambda,\theta)} = \sigma_f(\lambda)S_f + \sum_{m=1}^{M} a_m\lambda_m \tag{2-34}$$

In the Eq.2-34, L and $E_g$ are known, $\sigma_f(\lambda)$ is the fluorescence spectrum, m is set to 3, the coefficients $a_m$ and $S_f$ are fitted using the least-squares algorithm.

2.4.2.2 The SIF retrieval methods exploiting the fraunhofer lines

(1) Joiner method

Joiner et al. (2011) used the Potaium (K) I absorption line to retrieve the fluorescence from GOSAT TANSO-FTS. K I line locates among several weak oxygen absorption bands. Because GOSAT has the super-fine spectral resolution, K I line can be observed in the GOSAT TANSO-FTS data. Based on the previous researches, Joiner et al. (2012) exploited two windows (769.9-770.25 nm and 758.45-758.85 nm) to extract the fluorescence from the GOSAT data. He thought that a wide window can improve the SNR, but it should consider the reflectance and fluorescence varying with length. Besides, the fitting window 863.5-868.8 nm including the CaII line near 866nm was used to retrieve the fluorescence from the SCIAMACHY data.

In the interest spectral region, the satellite-observed radiance can be approximated using a Lambertian-equivalent reflectivity surface model and fluorescence is also here assumed to be spectrally constant. The radiance at-sensor can expressed in the Eq. 2-16.

Assuming that the effects of atmospheric scattering and absorption are negligible on the fitting window ($\rho_{so}$=0, $\rho$=0, $\tau_{ss}+\tau_{sd}$=1, $\tau_{do}+\tau_{oo}$=1), the observed total intensity can be simplified to

$$(L_{TOA})^* = \left(\frac{R \cdot E_0 \cdot \cos\theta}{\pi} + SIF\right)^* = K \cdot E^* + F \tag{2-35}$$

in here, * represents convolution with the ILSF (instrumental line shape function).

Similarly, if assuming that atmospheric scattering and absorption are spectrally constant over the wavelengths of interest, then the observed intensity can be rewritten as follows (Joiner et al., 2011, 2012):

$$(L_{TOA})^* = [\frac{E_0 \cdot \cos\theta}{\pi} \cdot (\rho_{so} + \frac{(\tau_{ss} + \tau_{sd}) \cdot R \cdot (\tau_{do} + \tau_{oo})}{1 - R \cdot \rho})]^* + \frac{SIF \cdot (\tau_{do} + \tau_{oo})}{1 - R \cdot \rho} \quad (2\text{-}36)$$
$$= K' \cdot E^* + \in F$$

The Eq. 2-36 is in similar with the Eq. 2.35. Note that the value of K (or K' or R) is of no importance for determining fluorescence. Similarly, a constant calibration offset in the solar irradiance will not affect the derive fluorescence as the error will be absorbed in the retrieved value of K (or K'). Neglecting the scattering and absorption will produce a slight scaling error $\epsilon$ in F (for R=0.3, the error is approximately 0.6%). Standard weighted least squares fitting procedure is used to solve this equation.

(2) Guanter method

Guanter et al. (2012) assumed that the SIF-free radiance spectrum can be expressed as the linear combination of the singular vectors describing the SIF-free set of measurements, and retrieved the fluorescence radiance from the GOSAT FTS data using this method from two windows centered 750nm and 770nm respectively. Using the concept of singular vectors, the forward model fluorescence consisting of the SIF-free plus the TOA Fs contribution can be written as

$$F(\omega, F_s) = \sum_{i=1}^{n_v} \omega_i V_i + F_s^{TOA} I \quad (2\text{-}37)$$

where $\omega_i$ is the weight of the singular vector $v_i$, $F_s^{TOA}$ is the TOA fluorescence intensity in radiance units, I is the identity vector of size n, and $n_v$ is the number of singular vectors used to model the input radiance spectrum. The fit coefficients are the $n_v$, weights $\omega_i$ and $F_s^{TOA}$. Concerning $n_v$, in view of the percentage of captured variance by each singular vector, a number $n_v$ of 4 and 5 singular vectors has been selected for the forward modeling of the 755 and 770 nm windows, respectively. It must be noted that the strongest atmospheric features in the 770nm window are removed from the inversion due to the fact that physical formulation of atmospheric absorption and scattering is not included in the forward model. The Eq. 2.37 is inverted by linear least squares without spectral weights.

Guanter et al. (2013) improved the Guanter et al. (2012) method, and enlarged the application range to 717-780nm. In this spectral range, due to the LAI and the effects of

chlorophyll absorption, the spectral structure of vegetation changes. Therefore, the Eq. 2-37 can be modified as following:

$$F(\alpha, b, c, \mathrm{F}_s^{760}) = \nu_1 \sum_{i=1}^{n_p} \alpha_i \lambda^i + \nu_2 \sum_{i=1}^{n_p} b_i \lambda^i + \sum_{i=1}^{n_v} c_i \nu_i + F_s^{TOA} h_f \quad (2\text{-}38)$$

In the Eq. 2-38, the first and second items are low-frequency information, and compose of the SIF-free information; the third item is high-frequency information, and is about the spectral structure information. In which, nv is the number of single vectors standing for high-frequency information, $n_p$ is the number of single vectors standing for low-frequency information, α, b and c is the coefficient of $n_p$、 $n_p$ and $n_v$.

(3) Frankenberg method

Isolated fraunhofer lines are affected only by fluorescence (not scattering) and allow for an unambiguous retrieval. Frankenberg et al. (2011) thought that the depth of fraunhofer lines near the oxygen absorption bands can be expresses as following:

$$\vec{f}(\mathrm{F}_s^{rel}, \alpha) = \log\left(\left\langle \vec{I}_0 + \mathrm{F}_s^{rel} \right\rangle\right) + \sum_{i=0}^{n} \alpha_i \cdot \lambda^i \quad (2\text{-}39)$$

Where $\overrightarrow{I_0}$ is the high-resolution solar transmission spectrum, $F_s^{rel}$ is the relative fluorescence signal, the summation term is an n'th order polynomial describing the continuum radiance. < > applies the convolution with the instrumental line-shape as well as the mapping of the high resolution model grid to the lower resolution spectrometer grid. As atmospheric scattering and surface albedo only affect the low-frequency behavior of the reflectance in the absence of telluric $O_2$ absorption lines, they can be efficiently characterized by the polynomial term, avoiding the need to run computationally expensive multiple-scattering radiative transfer calculations. In the small retrieval windows (a few nanometers wide), $F_s^{rel}$ is assumed to be wavelength-independent, hence a scalar. A nonlinear weighted least-squares algorithm provides the solution for ($F_s^{rel}$, α) that minimize the Euclidian norm of the measurements-model difference vector (spectral residuals) inversely weighted by the respective 1σ noise estimates:

$$\arg\min \left\| S_\epsilon^{-1/2} (\vec{\mathrm{y}} - \vec{\mathrm{f}}(\mathrm{F}_s^{rel}, \alpha)) \right\|_2 \quad (2\text{-}40)$$

In the Eq. 2-40, $\vec{y}$ is the measurement vector (=log(R($\vec{\lambda}$ ))) and Sϵ is the strictly diagonal measurement error covariance matrix. In this setup (if $I_0$ is defined as transmission spectrum),

$Fs^{rel}$ is unit-less and the retrieved fluorescence flux Fs in radiance units can be approximated by $F_s = F_s^{rel} / (1 + F_s^{rel}) \cdot R_{cont}$ . (Rcont is the continum radiance).

(4) Köhler method

Köhler et al. (2014) assumed a lambertian reflecting surface in a plane-parallel atmosphere, the TOA radiance measured by a satellite sensor can be described by:

$$T_{TOA} = \frac{R_p}{\pi} \cdot E_0 \cdot \cos\theta \cdot T_{\uparrow} \cdot T_{\downarrow} + F_s \cdot h_f \cdot T_{\uparrow} \tag{2-41}$$

where $R_p$ is the planetary reflectance. Verhoef and Bach (2003) spited $R_p$ into contributions due to atmospheric path radiance, adjacency effect (path radiance from objects outside the field of view), reflected sky-light by the target and reflected sunlight by the target. $F_s$ is the amount of sun-induced fluorescence at 740 nm (second peak of the emission spectrum). $h_f$ is a normalized reference fluorescence emission spectrum and $T_{\uparrow}$ is the atmospheric transmittance in the upward direction.

In Eq. 2-41, Rp is expressed by a combination of a third-order polynomial in wavelength to account for the spectrally smooth part, and the transmittance is composed by a set of atmospheric principal components (PCs), then the equation can be expressed as follows (Köhler et al., 2014):

$$T_{TOA} = \frac{E_0 \cdot \cos\theta}{\pi} \cdot \sum_{i=0}^{3} \alpha_i \cdot \lambda_i \cdot \sum_{j=1}^{nPC} \beta_j \cdot PC_j + F_s \cdot h_f \cdot T_{\uparrow} \tag{2-42}$$

where $\alpha_i$, $\beta_j$, $F_s$ and $T_{\uparrow}$ are the unknowns which are necessary to generate a synthetic measurement.

Besides, Köhler et al. (2015) proposed a similar method aimed to the GOSAT (GARLiC). The spectral range 755-759nm was selected to retrieve the fluorescence. In this spectral window, the upward transmittance in the clear day is about 1, the equation 2-42 can be simplified in the following:

$$T_{TOA} = \frac{E_0 \cdot \cos\theta}{\pi} \cdot (\rho_{so} + R \cdot T_{\downarrow}) + F_s \tag{2-43}$$

In the Eq. 2-43, assuming the atmospheric scattering and surface reflectance are the function of the wavelength, the Eq. 2-43 can be further simplified as follows:

$$T_{TOA} = \langle I_{sc} \rangle \cdot (\alpha_0 + \alpha_1 \cdot \lambda) + F_s \quad (2\text{-}44)$$

in which, $I_{sc}$ is the high-resolution solar irradiance spectrum from Kurucz and it is convolved to the lower resolution spectrometer grid, which is represent by the < > operation. $\alpha_0$ and $\alpha_1$ are for the modeling of atmospheric scattering and surface reflectance. The least squares fit is used to obtain $\alpha_0$, $\alpha_1$ and $F_s$.

Table 2-4 Review of the methods of retrieving the fluorescence from the space-borne data

| Reference paper | Band | Method | Application |
|---|---|---|---|
| **Fraunhofer lines** | | | |
| Joiner et al. (2011) | 769.9-770.25nm (K I) | (Seeing Eq. 2-35) | GOSAT TANSO-FTS |
| Joiner et al. (2012) | 769.9-770.25nm<br>758.45-758.85nm<br>863.5-868.5nm( Ca II) | (Seeing Eq. 2-36) | GOSAT SCIAMACHY |
| Guanter et al. (2012) | 755-775nm (K I) | (Seeing Eq. 2-37) | GOSAT-FTS |
| N. Khosravi (2012） | 660-683nm<br>745-758nm | DOAS | |
| Guanter et al. (2013) | 745-759nm(fraunhofer line)<br>717-759nm(red-edge)<br>745-780nm($O_2$-A band)<br>717-780nm(full-range) | (Seeing Eq. 2-38) | GOSAT-FTS<br>HR4000 |
| Köhler et al. (2014) | 590-790nm (GOME-2)<br>604-805nm( SCIAMACHY) | (Seeing Eq. 2-42) | GOME-2<br>SCIAMACHY |
| Köhler et al. (2015) | 755-759nm | GARLiC | GOSAT |
| **Oxygen absorption band** | | | |
| Guanter et al. (2007) | 760.6nm<br>753.8nm | FLD<br>MODTRAN-4 | MERIS<br>CASI-1500 |
| Damm et al. (2010) | 760.6nm<br>755nm | FLD<br>MODTRAN-4 | ASD |
| Guanter et al. (2010) | 745-775nm<br>672-702nm | SFM<br>FLD-S | FIMAS-like<br>TOA radiance |
| Mazzoni et al. (2010) | 677-697nm<br>750-770nm | DS=NSENSOR_RADn-NSENSOR_RADm | OCO<br>TANSO-FTS |
| Frankenberg et al. (2011) | $O_2$-A | (Seeing Eq. 2-39) | GOSAT<br>OCO-2 |
| Joiner et al. (2013) | 715-745nm<br>750-780nm | (Seeing Eq. 2-27) | GOME-2 |
| Damm et al. (2014) | $O_2$-A | FLD-like<br>MODTRAN-5 | ASD |
| Braun Raychaudhuri (2014) | $O_2$-A | $F= A_V - A_{NV}$ | EO-1 |
| Liu et al. (2015) | 650-800nm | F-SFM | simulated data |

## 2.5 Summary

In this chapter, the basic theory of chlorophyll fluorescence is introduced. First, the generation of chlorophyll fluorescence is described. Chlorophyll fluorescence is the production of the chlorophyll excited by natural sunlight illumination, and the chlorophyll fluorescence is excited is the first step of converting light energy to chemical energy. Therefore, Chlorophyll fluorescence has a close relationship with the photosynthesis, and is thought to be the ideal probe for detecting the vegetation ecosystem. In the second, two types of measurements, passive and active measurements, are thought to be the main ways to detect chlorophyll fluorescence. Active fluorescence measurements use the external energy to motivate the plant to emit the fluorescence signal. Passive measurements exploit the remote sensing method to measure the fluorescence excited by natural solar light illumination. In the third, the methods of retrieving the fluorescence near the ground are introduced. The radiance-based methods and the reflectance-based methods are two categories to estimate the fluorescence. Finally, the fluorescence retrieved methods from the space-borne is proved to be possible, and mostly exploit the atmospheric absorption bands or Fraunhofer lines.

# Chapter3. Detection of leaf chlorophyll fluorescence under the different water content

## 3.1 Background

Chlorophyll fluorescence, photosynthesis and heat dissipate are three ways to consume the leaf absorbed energy. By measuring the chlorophyll fluorescence, we can obtain the information about the plant physiological state. The traditional remote sensing always exploits the information of vegetation reflectance, emission and scattering to retrieve the vegetation biochemical parameters, such as chlorophyll content, LAI and so on, and assesses the vegetation physiological state from the biochemical parameters. Because of the close relationship between the chlorophyll fluorescence and photosynthesis, chlorophyll fluorescence is thought as a direct and effective way to monitor the vegetation physiological state.

Chlorophyll fluorescence is affected by the canopy structure, chlorophyll content and illumination and so on. At the leaf scale, the chlorophyll fluorescence detection can avoid to consider the effects of canopy structure, and obtain the actual fluorescence. The chlorophyll fluorescence measurement includes the active measurement and passive measurement. The active and passive measurements are all used to measure the chlorophyll fluorescence, and the consistency among them shows the measurement reliable (Zarco-Tejada et al., 2000c, 2009). Chlorophyll fluorescence can reflect the variation of vegetation physiological state quickly. When plant is in stress state, the plant tissue can increase heat dissipate to consume the extra energy, in the same time decrease the chlorophyll fluorescence yield (Flexas et al., 2000, 2002).

In this chapter, we develop the research about the leaf chlorophyll fluorescence detection, and investigate the consistency between active and passive fluorescence under the different water content, besides, we observe the chlorophyll fluorescence's response to the variation of water content. In the figure 3-1, we first use the SCOPE model to simulate the daily variation of chlorophyll fluorescence and temperature under water stress, in order to understand the chlorophyll fluorescence and temperature's response to water stress. Besides, we develop the field experiments to observe the leaf active and passive fluorescence, and to analyze the variation of the fluorescence and temperature with the water content change. The theoretical and experimental conclusions show that chlorophyll fluorescence and temperature can better reflect the vegetation water stress.

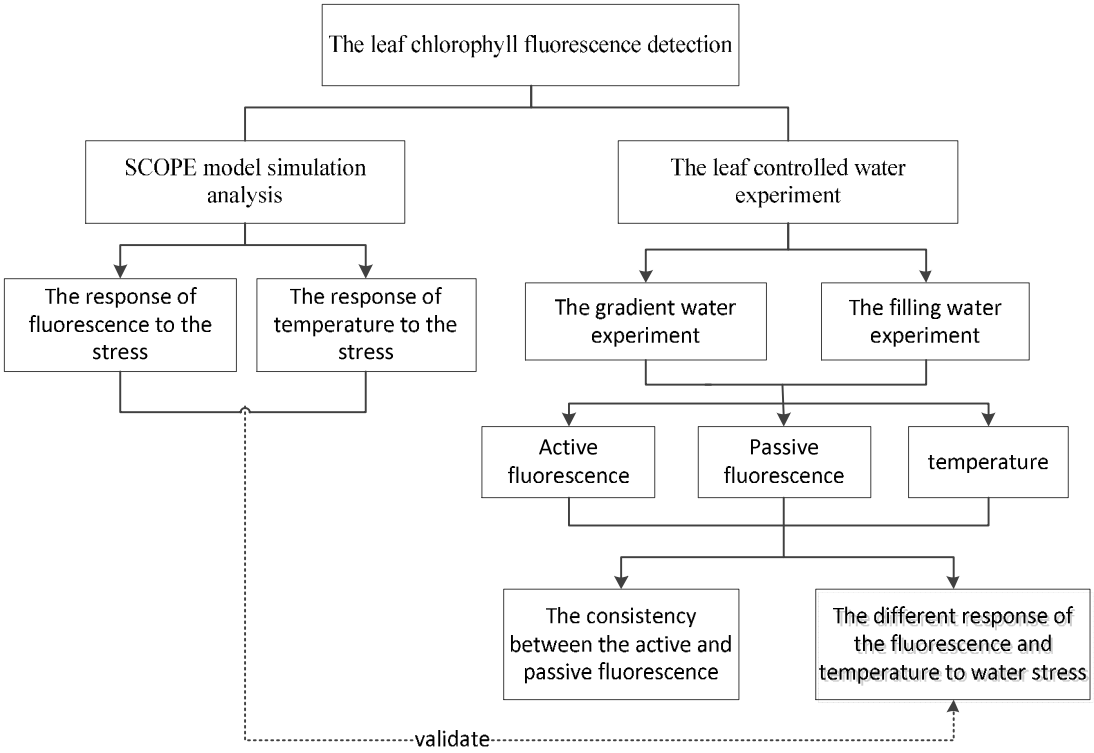


Figure 3-1 Flow chart of chapter 3

## 3.2 The response of fluorescence and temperature to the stress

### 3.2.1 SCOPE model

Figure 3-2 depicts a flowchart of SCOPE model. It shows the relationship between the various modules. First, we need read the soil and leaves information and time information which are recorded in the input file, marked as input_data.xlsx. SCOPE model can be run using two ways: a single simulation and time series simulation. Each simulation starts from the leaf optical model FLUSPECT, and then enters to the radiative transfer model SAIL in which it can complete the simulation from the leaf to the canopy; in the last, the simulation enters the energy balance module. In the energy balance module, turbulent heat flux, photosynthesis, leaf and soil temperature for each leaf layer under the sun and in the shadow can be calculated in the vertical direction and each leaf azimuth, respectively. This module is a continuous iterative process. If the closure error of the energy balance is within the required range, the cycle stops, and the final temperature is obtained. In addition, this module can also calculate the fluorescent radiation, thermal infrared emission spectrum (2.5-50 μm) and BRDF.

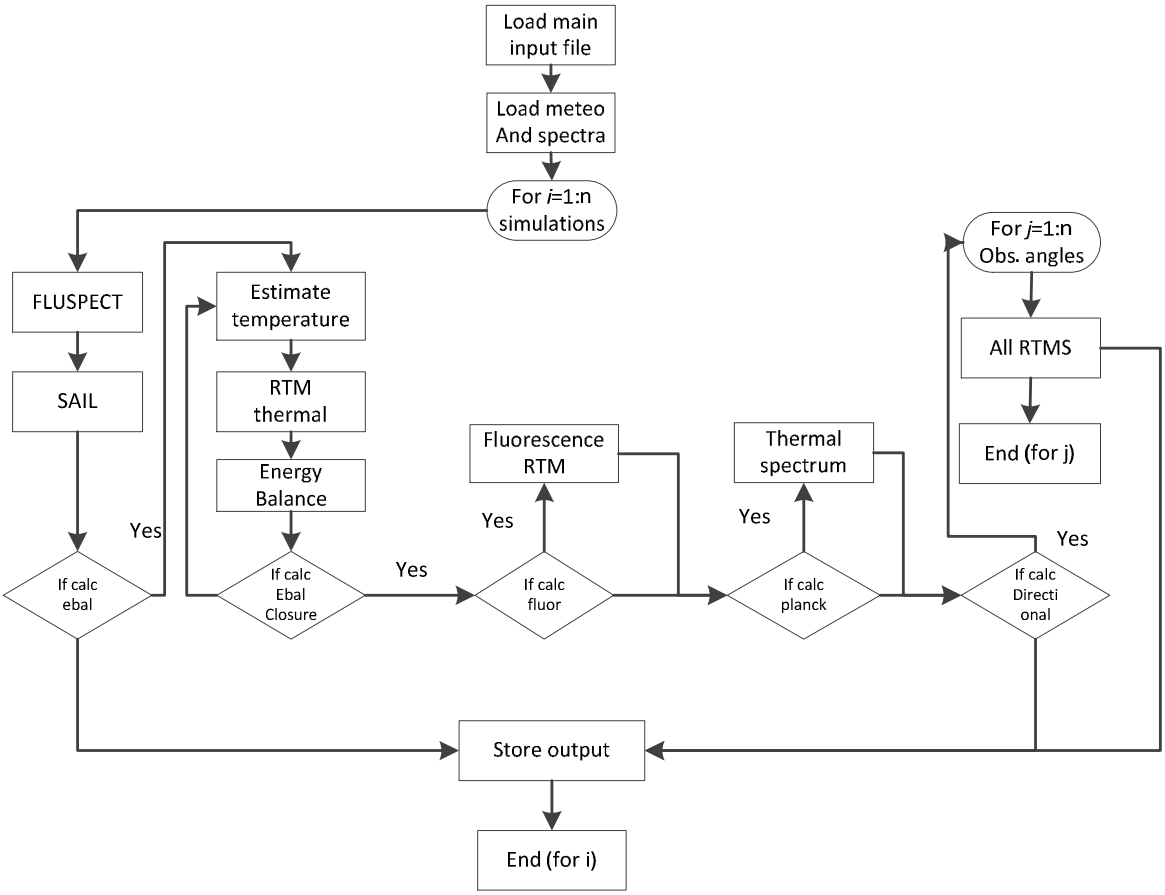


Figure 3-2 SCOPE model (From the SCOPE document)

In this study, SCOPE is used to illustrate the variation tendencies of fluorescence and canopy temperature under stress conditions. The input parameters of SCOPE include the Prospect parameters, leaf biochemical parameters, fluorescence quantum yield, soil parameters, canopy geometry parameters, meteorological data, aerodynamic data, time series information, solar zenith angle, observation angle and the azimuthal difference between solar and observation angles (seeing Table 3-1). Table 3-1 lists the default parameters of the model. In addition, the meteorological data in Baoding, Hebei province, China, was used as input to derive the SCOPE model, and the results showed that the variations of some input parameters did not result in significant variations in fluorescence or temperature trends; therefore, these results were not presented here.

The SCOPE model can simulate the vegetation fluorescence variation not only under the healthy condition, but also under the stress condition. In the model, the parameter 'stressfactor' is factor to reduce the maximum carboxylation rate (Vcmax), for example soil moisture, leaf age, and the default value is 1 (healthy condition). Vcmax is the maximum CO2 fixation per time unit and per area unit (μmol $m^{-2}$ $s^{-1}$), and decides the vegetation net

photosynthesis ratio and photorespiration. Vcmax changes with the ambient environment conditions change.

Table 3-1 SCOPE input parameters (Van der Tol 2013)

| Parameters | Values | Unit | Description |
|---|---|---|---|
| **Prospect** | | | |
| Cab | 40 | ug $cm^{-2}$ | Chlorophyll a+b |
| Cdm | 0.012 | gcm-2 | Dry matter content |
| Cw | 0.09 | Cm | Leaf water equivalent layer |
| Cs | 0 | fraction | Scenecent material fraction |
| N | 1.4 | | Leaf thickness parameters |
| rho_thermal | 0.01 | | Broadband thermal reflectance |
| tau_thermal | 0.01 | | Broadband thermal transmittance |
| **Leaf_Biochemical** | | | |
| Vcmo | 30 | umol $m^{-2}$ | maximum carboxylation capacity(at optimum temperature ) |
| m | 8 | | Ball-Berry stomatal conductance parameter |
| Type | 0 | | photochemical pathway: 0=C3,1=C4 |
| kV | 0.6396 | | extinction coefficient for Vcmax in the vertical (maximum at the top). 0 for uniform Vcmax |
| Rdparam | 0.015 | | Respiration = Rdparam*Vcmcax |
| Tparam | 0.2 0.3 281 308 328 | | These are five parameters specifying the temperature response. |
| **Leaf_Biochemical (magnani model)** | | | |
| Tyear | 15 | ºC | mean annual temperature |
| beta | 0.507 | | fraction of photons partitioned to PSII (0.507 for C3, 0.4 for C4; Yin et al. 2006; Yin and Struik 2012) |
| kNPQs | 0 | $s^{-1}$ | rate constant of sustained thermal dissipation (Porcar-Castell 2011) |
| qLs | 0.5 | | fraction of functional reaction centres (Porcar-Castell 2011) |
| stressfactor | 0.1 | | optional input: stress factor to reduce Vcmax (for example soil moisture, leaf age). Default value = 1. |
| **Fluorescence** | | | |

| | | | |
|---|---|---|---|
| fqe | 0.02 | | fluorescence quantum yield efficiency at photosystem level |
| **Soil** | | | |
| spectrum | 1 | | Spectrum number (column in the database soil_file) |
| rss | 500 | s $m^{-1}$ | soil resistance for evaporation from the pore space |
| rs_thermal | 0.06 | | broadband soil reflectance in the thermal range (1-emissivity) |
| cs | 1.18E+03 | $Jm^{-2}$ $K^{-1}$ | volumetric heat capacity of the soil |
| rhos | 1.80E+03 | kg $m^{-3}$ | specific mass of the soil |
| lambdas | 1.55 | $Jm^{-1}$ $K^{-1}$ | heat conductivity of the soil |
| SMC | 0.25 | | volumetric soil moisture content in the root zone |
| **Canopy** | | | |
| LAI | 3 | $m^2$ $m^{-2}$ | Leaf area index |
| hc | 2 | m | vegetation height |
| LIDFa | -0.35 | | leaf inclination |
| LIDFb | -0.15 | | variation in leaf inclination |
| leafwidth | 0.1 | m | leaf width |
| **Meteo (values in data files, in the time series option, can overrule these values)** | | | |
| z | 10 | m | measurement height of meteorological data |
| Rin | 800 | W m-2 | broadband incoming shortwave radiation (0.4-2.5 um) |
| Ta | 20 | T | air temperature |
| Rli | 300 | W m-2 | broadband incoming longwave radiation (2.5-50 um) |
| p | 970 | hPa | air pressure |
| ea | 15 | hPa | atmospheric vapour pressure |
| u | 2 | m s-1 | wind speed at height z |
| | | | atmospheric CO2 concentration |
| | | | unit is mg m-3 in a time series file, because that is what you |
| Ca | 380 | ppm | usually get from EC (LI7500) data |
| Oa | 209 | per mille | atmospheric O2 concentration |
| **Aerodynamic** | | | |
| zo | 0.246 | m | roughness length for momentum of the canopy |
| d | 1.34 | m | displacement height |
| Cd | 0.3 | | leaf drag coefficient |
| rb | 10 | s m-1 | leaf boundary resistance |
| CR | 0.35 | | Verhoef et al. (1997) Drag coefficient for isolated tree |
| CD1 | 20.6 | | Verhoef et al. (1997) fitting parameter |

| | | | |
|---|---|---|---|
| Psicor | 0.2 | | Verhoef et al. (1997) Roughness layer correction |
| CSSOIL | 0.01 | | Verhoef et al. (1997) Drag coefficient for soil |
| rbs | 10 | s m-1 | soil boundary layer resistance |
| rwc | 0 | s m-1 | within canopy layer resistance |
| **timeseries (this option is only for time series)** | | | |
| startDOY | 169 | | Julian day (decimal) of start of simulations |
| endDOY | 170 | | Julian day (decimal) of end of simulations |
| | | decimal | |
| LAT | 52.25 | deg | Latitude |
| | | decimal | |
| LON | 5.69 | deg | Longitude |
| timezn | 1 | hours | east of Greenwich |
| **Angles** | | | |
| tts | 30 | deg | solar zenith angle |
| tto | 0 | deg | observation zenith angle |
| psi | 90 | deg | azimuthal difference between solar and observation angle |

### 3.2.2 Daily variations in the fluorescence and temperature under the stress condition

As shown in Figure 3-3a, fluorescence from the morning to afternoon gradually increases to a maximum value in the first and then decreases to nearly zero, and the fluorescence has a peak at approximately midday. During the early morning or late night hours, no fluorescence signal is emitted over a short period because the leaves don't absorb sunlight and only process respiration without photosynthesis. When plants are in a healthy environment (stressfactor=1.0), the fluorescence is much higher than when plants are in water stress. As a drought becomes more severe, the fluorescence decreases quickly. Comparing with fluorescence under different water stress conditions, variations in the fluorescence are relatively large around midday, while small during the early morning and late afternoon.

The variations of canopy temperature are shown in the Figure 3-3b. From the Figure 3-3b, it can be seen that canopy temperature first decreases to its lowest point during the early morning (close to 5:00am) and gradually increases to reach its peak at 14:00 pm and then decreases again. A small trough was observed at 13:00 pm, potentially due to stomatal closure to protect the plant from damage, known as the midday depression of photosynthesis. When

vegetation is under stress condition, the canopy temperatures are larger than when vegetation is in well-watered conditions. Canopy temperature is directly determined by canopy energy and water balance. Canopy temperatures can also be used to indirectly determine the level of surface water status. When the plants are in water stress, in order to reduce water loss due to transpiration, leaf stomata close, and then latent heat flux reduce. According to the energy balance principle, sensible flux will increase, and leaf temperature rises. Therefore, the abnormal of canopy temperature can be used as the good indicator for detecting the vegetation drought (Gao et al., 2007).

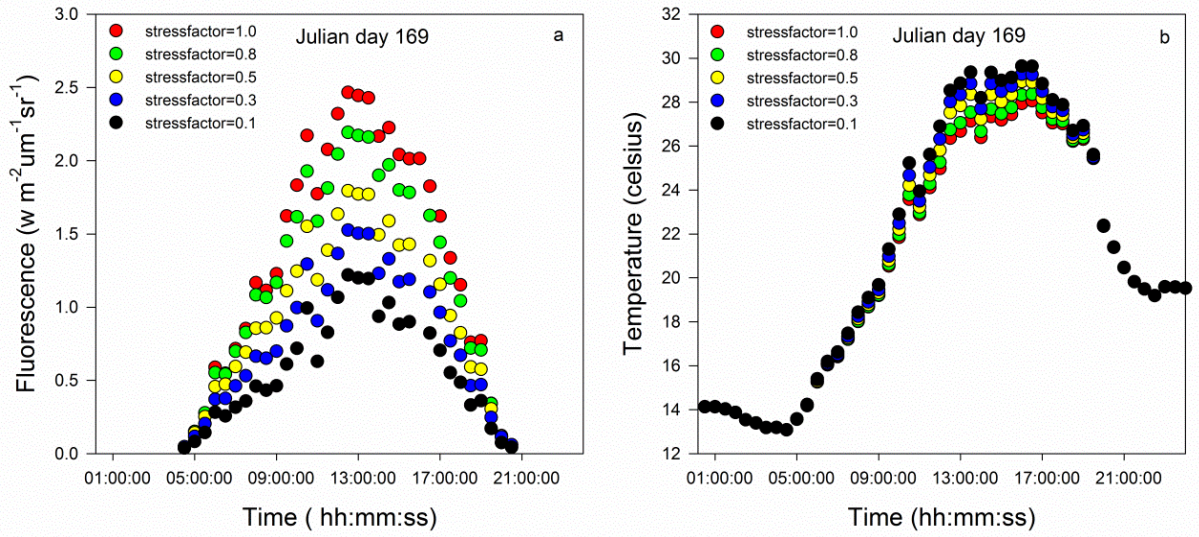


Figure 3-3 The variation of chlorophyll fluorescence (a) and canopy temperature (b)

## 3.2.3 Relationships between the fluorescence and temperature

Chlorophyll fluorescence and canopy temperature are positively related before becoming negatively related (Figure 3-4a). A turning point occurs during the daily cycle. Before mid-day, a good linear relationship is observed between the fluorescence and canopy temperature. The slope of this linear relationship varies with the water status (Figure 3-4b). In this period, chlorophyll fluorescence and temperature gradually increases. The rate of the chlorophyll fluorescence increase declines slowly as stress became more severe, and the rate of temperature remains stable. After midday, the relationship between the fluorescence and canopy temperature is nonlinear and complex (Figure 3-4c), and varies with the stress level change. When the maize is in healthy condition, the maximum temperature is 27 ºC, and temperature varies gradually. In addition, the chlorophyll fluorescence declines remarkably in this case. As the stress becomes more severe (stress factor was from 1.0 to 0.1), the maximum

temperature slightly increases, and the range of temperature variation gradually increases. Simultaneously, the range of chlorophyll fluorescence decreases. This decrease reveals that heat dissipation plays an important role in energy consumption in the afternoon. In brief, using the temperature and chlorophyll fluorescence together can more accurately assess water stress.

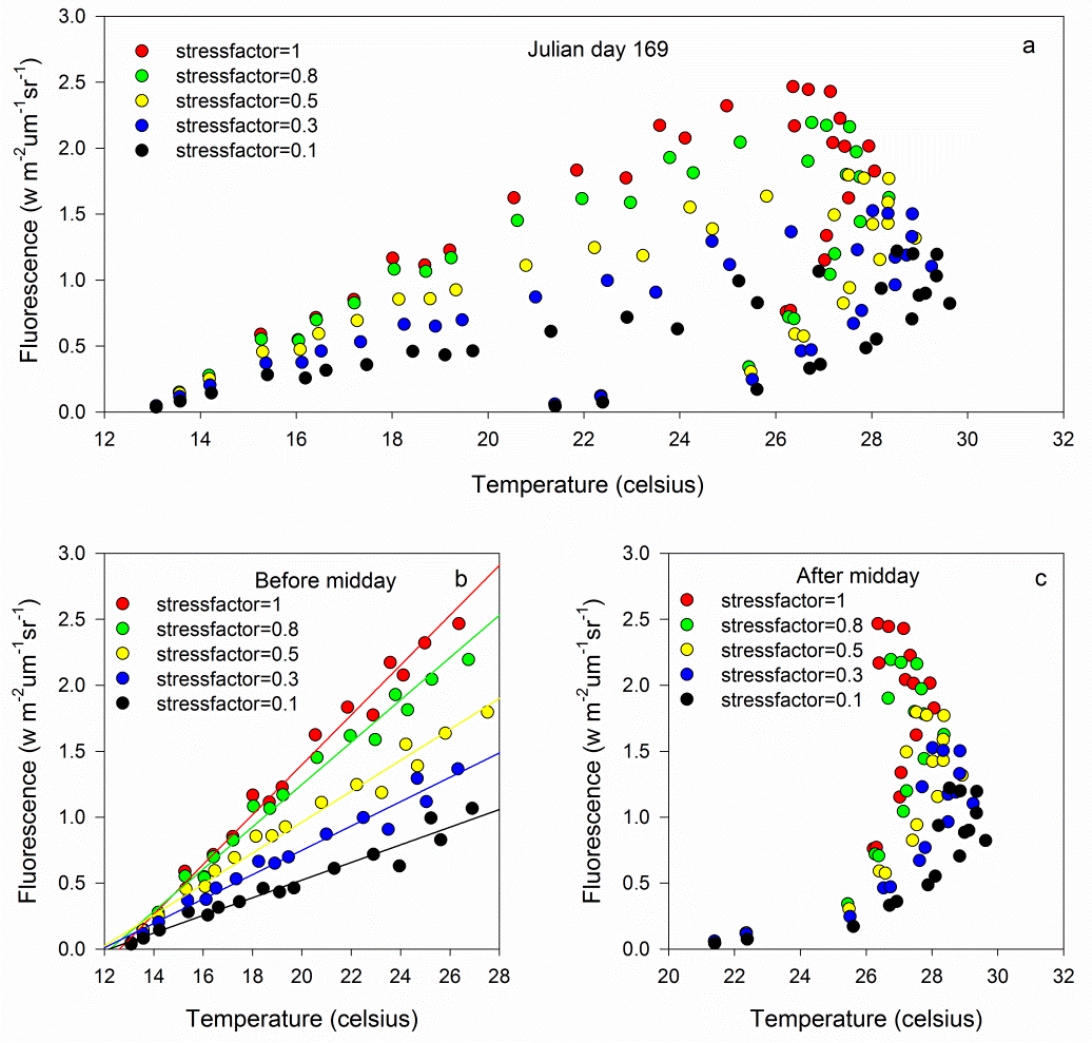


Figure 3-4 Relationships between the fluorescence and canopy temperature: (a) Full day, (b) before midday and (c) after midday

## 3.3 The leaf active and passive fluorescence measurement

To observe the variation of chlorophyll fluorescence, the field experiments are designed. In the field experiments, the gradient and filling experiments are carried out to show the variation of chlorophyll fluorescence under the different water conditions.

### 3.3.1 Experimental setup

The experimental site is located in the biological park in Beijing Normal University, which is in a sunny position with no high objects to block the sunlight. Potted maize is selected as the object of research. The soils in the plots at the study site have all typical silt loam profiles with uniform texture. Maize plants were planted in 20 plastic buckets in June 2013 and fertilized at the V6 stage (vegetative stage, 6 collars). Three maize plants were grown in each plastic bucket, and after some time, the best plants were kept and the others were removed. In the last, there was one maize plant in on plastic bucket. In addition, all maize was protected from rainfall using an umbrella to guarantee the accuracy of the water stress experiment. The water conditions were controlled during the maize growth process. The normal maize water consumption is 1860-4440 m3/ha over the entire life of the plant (Marcassa et al., 2006). The maize was watered four times during the following stages: before planting, V12 (vegetative stage, 12 collars), V15 (vegetative stage, 15 collars) and R (reproductive stage) (Zadoks et al., 1974). During the V12 stage, lacking water or nutrients will drastically affect yield; thus, it was important to add water at this stage. Generally, 1/4 of the normal watering amount was applied at each of the maize growth stages mentioned above. In this experiment, we assumed that the normal maize water consumption at one stage was 750 m3/ha, and according to the volume of plastic bucket (height 40cm, diameter 30cm), 5×10-3 m3 water was considered as the normal amount of water during the V12 stage. All maize was divided into four groups, S1, S2, S3 and S4. The four groups were treated as explained in Table 3-2.

Table 3-2 Watering conditions

| Date | Water condition | Water consumption($m^3$/per barrel) | | | |
|---|---|---|---|---|---|
| | | S1 | S2 | S3 | S4 |
| 2nd July | The gradient watering | 0 | $1.25\times10^{-3}$ | $2.5\times10^{-3}$ | $5\times10^{-3}$ |
| 5th July | The filled watering | $5\times10^{-3}$ | $3.75\times10^{-3}$ | $2.5\times10^{-3}$ | 0 |

In this experiment, three measurements were carried out. These measurements were used to analyze the relationships between chlorophyll fluorescence and the plant physiological state. For each measurement, the leaf spectrum, leaf chlorophyll fluorescence, PAR and soil water content were collected. The measurement arrangement were described in Table 3-3:

Table 3-3 Measurement timetable

| date | stage | water | Measure parameters | time |
|---|---|---|---|---|
| 2nd July | V12 | at night | Leaf spectrum, | 9:00 am |
| | | | chlorophyll fluorescence, | 11:40 am |
| | | | PAR and soil water content | 14:30 pm |
| | | | | 16:40 pm |
| 5th July | V12 | at night | Leaf spectrum, | 9:30 am |
| | | | chlorophyll fluorescence, | 11:30 am |
| | | | PAR and soil water content | 14:30 pm |
| | | | leaf temperature | 16:00 pm |
| 6th July | V12 | | Leaf spectrum, | 10:00 am |
| | | | chlorophyll fluorescence, | |
| | | | PAR and soil water content | |
| | | | leaf temperature | |

## 3.3.2 Data collection

### 3.3.2.1 PAR

In the photosynthesis process, the absorbed solar radiation whose spectral ranges from 380 to 710 nm can excite the chlorophyll in excited state. Photosynthetic active radiation is the energy source of plant life activities, organic material synthesis and crop yield; and it directly affects the plant growth, development, production and product quality. In this study, PAR was measured using a QSO-S PAR Photon Flux sensor (Decagon Devices, USA). QSO-S PAR sensor can measure PAR in all domains in μmol $s^{-1}$ $m^{-2}$, and it can be used outside for a long-term continuous time period owing to its waterproof features. It should be noted that the probe is in the horizontal direction.

### 3.3.2.2 Soil moisture content

Soil moisture content generally refers to the absolute soil water content which is the water content in 100g dry soil, also known as soil moisture. It is an important parameter for agricultural production. Generally there are two representations for soil water content: volumetric water content and water content by weight. In this experiment, the soil water content was measured using an EC-5 volumetric water content sensor. The data are registered by an EM50 digital/analog data logger. The EC-5 volumetric water content sensor is set at a depth of 5 cm below the soil surface.

3.3.2.3 Leaf spectral data collection

Leaf spectral data are acquired using a high-resolution spectrometer (HR4000) (Ocean Optics, USA), which has been widely used to measure plant spectral information and extract fluorescence data (Meroni et al., 2008; Suárez et al., 2009; Zarco-Tejada et al., 2009; Zarco-Tejada et al., 2013). The HR4000 spectrometer shows a spectral range of 720-800 nm and a spectral resolution of 0.05 nm. Absolute radiance calibration was performed by the Institute of Atmospheric Physics at the Chinese Academy of Sciences. To protect the HR4000 machine from the effects of air temperature, the HR4000 machine was housed in a thermally insulated box to maintain a stable internal temperature and reduce dark current drift (Meroni et al., 2008). The middle of one leaf from one bucket was measured three times, and the mean value was used for analysis. Radiance-based methods, including FLD and 3FLD, were used to retrieve the fluorescence.

3.3.2.4 Leaf fluorescence measurements

In the chapter 2.2.1, we introduce the active fluorescence measurement in detail. In this chapter, we used the pulse amplitude modulation PAM-2500 to measure the chlorophyll fluorescence of the potted maize. PAM-2500 is highly selective and sensitive, so that even in a strong or non-treated filter environment (e.g., full sunlight even 10000 μmol $s^{-1}$ $m^{-2}$) may also determine the fluorescence yield without intervention. Therefore, PAM-2500 is not only suitable for using in the laboratory under the manual environment, but also be effective in the natural environment and even strong light conditions.

PAM-2500 is equipped with a dark-adapted clip DLC-8. Its weight is 4g, and can be clipped on the majority of the leaves directly without damage. Leaf clip is equipped with a slip sheet which can prevent the leaf exposure to light during dark adaptation. When measurement, open clip sheet, and the leaf only absorbs the light from an optical fiber without interference by ambient light. Only after a reasonable dark adaptation, it is better to obtain the maximum quantum yield Fv / Fm and dark-light-induced kinetic curves.

After 20 mins dark adaptation, the Fo and Fm are recorded in the dark-acclimated state. In this case, Fo is the basic chlorophyll fluorescence yield recorded under low measuring light intensities and Fm is the maximum chlorophyll fluorescence yield when the photosystem II reaction centers are closed by a Saturation Pulse. The three following parameters were recorded in the light-exposed state: (i) Fo is the minimum chlorophyll fluorescence yield in

the state of open photosystem II reaction centers; (ii) Fm is the maximum chlorophyll fluorescence yield when the photosystem II reaction centers are closed due to a strong light pulse; and (iii) Ft represents the fluorescence during steady-state photochemical levels, which are also marked as Fs. Here, the Fs parameter was used to indicate the stable fluorescence. The result with the leaf that was measured by PAM was consistent with that measured by HR4000.

#### 3.3.2.5 Leaf temperature measurement

The leaf temperatures are measured using the infrared thermometer, Testo 845. The emissivity is set to 0.99, and the accuracy is ±0.75 °C between -35 and +75 °C. To ensure the accuracy and comparability of the experiment result, leaf temperature measurements collected time is consistent with the other measurements. Air temperature was obtained from the automatic weather station in the Beijing Olympic park which is close to the experimental site (Beijing Normal University). Leaf temperature is affected by air temperature; therefore, air temperature was used to correct leaf temperature, marked as Tleaf-Tair.

### 3.3.3 The active and passive fluorescence retrieval methods

In this study, FLD and 3FLD are used to retrieve the chlorophyll fluorescence. These two methods are belonging to the radiation-based methods, which are formatted by one band inside the fraunhofer line and at least one band outside the fraunhofer line. They measure the chlorophyll fluorescence with physical meaning in radiance unit. The formulas are introduced in the Chapter 2. When the FLD method is used, the band inside the fraunhofer line is set at 760.45 nm, and the band outside the fraunhofer line at 766.84 nm; with the 3FLD method, the band inside that is set at 760.45 nm, the band in the left at 759.22 nm, and the band in the right at 766.84 nm.

Here, the fluorescence, measured by PAM, is marked as Fs, and the fluorescence that is computed from the leaf spectrum using the FLD or 3FLD method was marked as FLD or 3FLD, respectively. The normalized fluorescence is computed by FLD or 3FLD and divided by Photosynthetic active radiation (PAR), marked as FLD/PAR or 3FLD/PAR. In this experiment, the maize is divided into four groups, with four barrel maize plants in each group. In the following analysis, the mean value of each group is used.

## 3.4 Analysis of the field data

### 3.4.1 Time series of active fluorescence and temperature under the different stress

To analyze the variations in chlorophyll fluorescence and leaf temperature under water stress conditions, three days of field data are used for comparative analysis.

On July 2, similar soil water contents for the four groups were measured (Figure 3-5a). However, the Fs values for the four groups are different during the morning and similar in the afternoon (Figure 3-5b). When the measurement was finished, gradient watering was applied. The S1 group was treated with no water, the S2 group was treated with ¼ of the normal water volume, the S3 group was treated with ½ of the normal water volume, and the S4 group was treated with the normal water volume.

On July 5, the Fs in S1 was low and the Fs in the S4 group varied from small to large relative to the values observed on July 2. Because S3 was treated with more water than S2, the Fs in the S3 group was larger than that in S2 (Figure 3-5c). The results of the gradient watering indicated that well-watered maize plants had a greater fluorescence than those under water stress. The results of the simulation using the SCOPE model indicated that the fluorescence increased before decreasing, and Zarco-Tejada et al. (2000c) demonstrated that these results, obtained at the field canopy level from an airborne CASI hyperspectral sensor, were consistent with leaf, laboratory, and theoretical levels. Therefore, a comparison can be performed between field data and the SCOPE results. Under water stress conditions, chlorophyll fluorescence decreased and the leaf temperature increased. This result can be observed in the analysis of field data and the simulation analysis of SCOPE model. However, this daily trend of chlorophyll fluorescence was not found in the analysis results of Fs, possibly due to the limited number of measurements. The gradient watering experiment indicated that the Fs value was low under water stress but high in well-watered conditions.

After measuring during the day on July 5, the filled watering was applied at night. According to the normal water volume of maize and the first water volume, the second watering was performed (Table 3-1). After the filled watering, four groups were treated with the same water volume, and the Fs values in these four groups were similar (Figure 3-5d). For the S1 group, filled water relieved the water stress condition, and the maize recovered from

water stress and reached a relatively healthy state. The Fs in the S1 group recovered to the same level as that in the S4 group when filled watering occurred. In addition, the Fs recovered in the S2 and S3 groups, but several differences were observe relative to the S1 group, potentially due to the low soil water content, which resulted in the need for water in the S1 group. The filled watering experiment demonstrated that it was possible to exploit the Fs to detect when the plant is under early water stress. The Fs can detect subtle variations in the plant physiological state.

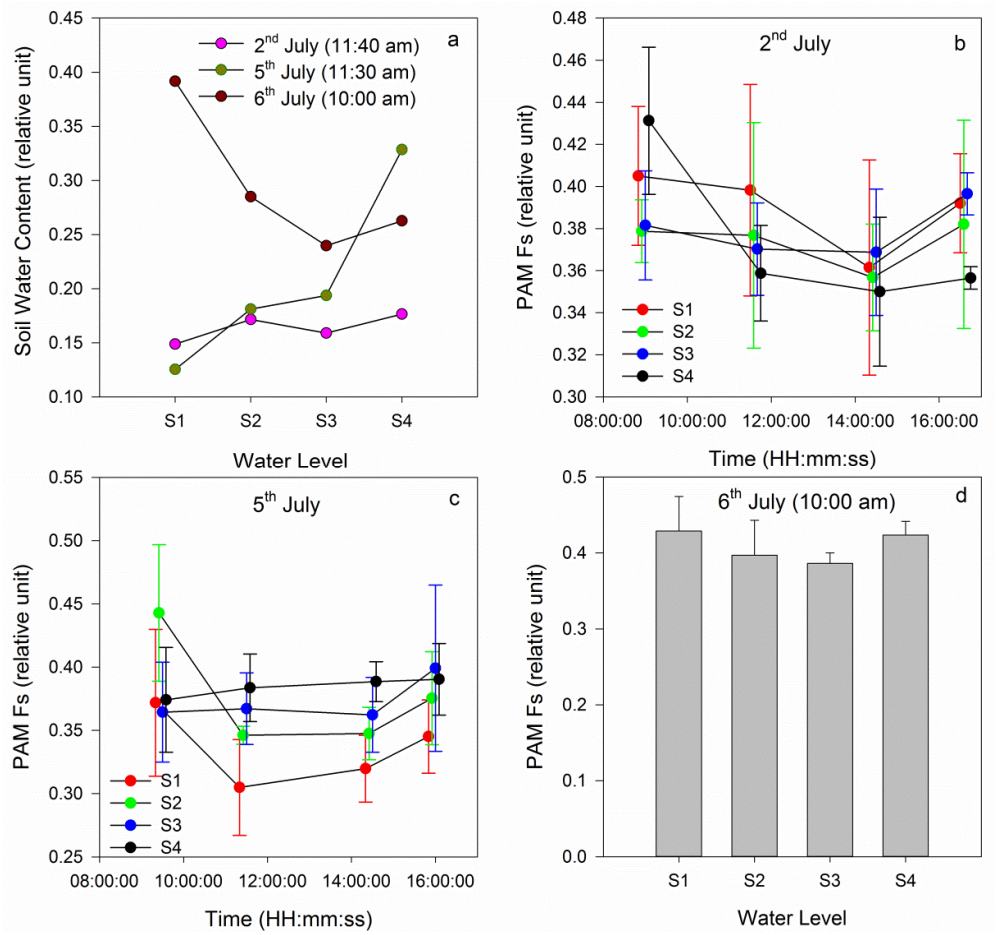


Figure 3-5 (a) Comparison of the soil water content; (b) Daily variations in the PAM Fs on July 2; (c) Daily variations of PAM Fs on July 5; (d) PAM Fs for the 4 groups on July 6

When we measured chlorophyll fluorescence, we also used the thermal infrared thermometer to measure the leaf temperature, and used air temperature recorded in nearby meteorological station to correct the leaf temperature. In process of the plant's growth, the moisture not only involves in the physiological processes of plants, but also regulates the plant temperature by leaf transpiration. Thus the crop canopy temperature can be used to

detect water status. Monteith & Szeicz (1962) and Tanner (1963) were the first to use infrared thermometry to determine plant temperatures. With the development of infrared temperature measurement technology, canopy temperature has been paid more attention for monitoring crop water status, and leaf-air temperature difference is also known as an important indicator of the observed soil moisture conditions. Under the condition of adequate water supply, leaf-air temperature difference is stable; while under conditions of water stress, it shows an increasing trend.

In this experiment, the leaf temperature on July 2 was measured using the NiCr-Ni thermocouple equipped in the PAM-2500, and that on July 5 and 6 was measured using an infrared thermometer. To keep the accuracy of the result, we only chose the data on July 5 and 6 to compare the leaf temperature. We used the air temperature to correct the leaf temperature, marked as Tleaf-Tair. Tleaf-Tair on July 5 and on July 6 was analyzed. On July 5, the four groups were treated with gradient watering. As shown in Figure 3-6a, Tleaf-Tair for S4 had small change within the range of -9 ~ -4 °C; and Tleaf-Tair for other groups treated as the gradient watering had the increasing trend compared with that for S4. The daily variation of Tleaf-Tair for all groups first increased and then decreased. At 12:00 am on July 5, Tleaf-Tair for S1 was obviously higher than that of the other groups, while at 14:30 pm and 16:30 pm, and Tleaf-Tair for S2 was higher than that in S1. This result indicated that the relationships between the temperature and water stress level are complicated (Zarco-Tejada et al., 2013) and that the temperature cannot accurately reflect variations in the physiological state. Figure 3-6b showed that after filled watering there were some differences for Tleaf-Tair between four groups. It may have two raisons: 1) the inadequate water absorption owing to the close measurement time; 2) complicated relationship between the Tleaf-Tair and water stress level.

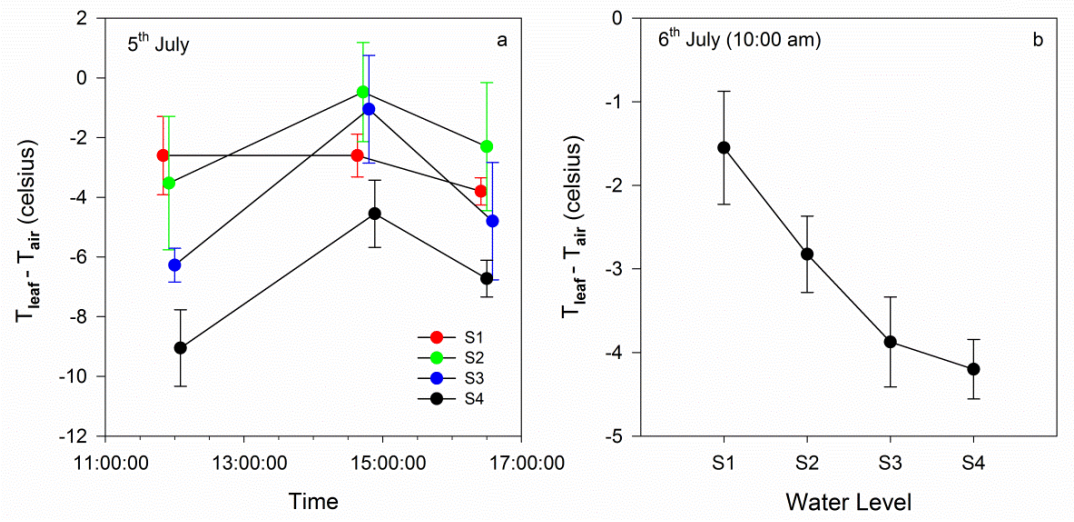


Figure 3-6 (a) Daily variations in $T_{leaf}$-$T_{air}$ on July 5. (b) Variations in $T_{leaf}$-$T_{air}$ at 10:00 am on July 6

### 3.4.2 Comparison of active fluorescence and leaf-air temperature difference between gradient watering and filled watering

To explain the variations in fluorescence and temperature after gradient watering or filled watering, the soil water content, Fs, and temperature data at a certain time within three days were compared. From Figure 3-5a, the soil water contents in the four groups changed during the two watering times. After the gradient watering, the soil water content in S4 increased quickly, and the soil water content in S2 or S3 increased slightly. In addition, some variations were found in the fluorescence (Figure 3-7a). On July 5, the Fs in the S4 group, which was treated with a normal water volume, was greater than that in the S1 group. According to the water volume, the Fs values in the four groups were arranged in gradient order. When comparing the Fs on July 2 with that on July 5, the Fs in S4 obviously increased, while that in S1, S2 and S3 decreased. This finding indicated that S1, S2 and S3 are under different degrees of water stress. During the measuring phase, maize was in the V12 stage. At this stage, maize requires water to maintain normal growth. During the addition of filled water, the maize plants in the four groups were given the same volume of water. When comparing the Fs values on July 6 and July 5, the Fs values of the four groups increased, despite S4 not being given water. The maize in the S4 group remained in a healthy state through the first watering. The same amount of water was given to these four groups, but differences were observed between the Fs values among these four groups. It demonstrated that there are differences in the maize physiological state.

Variations in temperature at different water levels can be observed in Figure 3-7b. When the four groups were given different water volumes, Tleaf-Tair in the lowest water content group was the highest. After filled watering, $T_{leaf}$-$T_{air}$ still increased due to inadequate water absorption. Compared $T_{leaf}$-$T_{air}$ on July 5 with that on July 6, it was found that the relationship between the temperature and water level is complex, and that the temperature was not sensitive to the variation of soil water content.

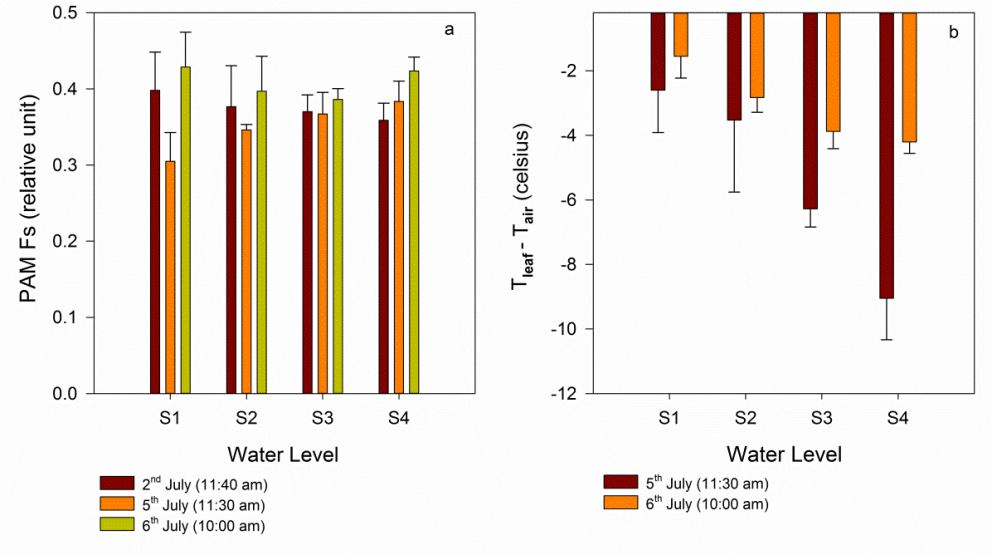


Figure 3-7 Comparision of PAM Fs (a) and $T_{leaf}$-$T_{air}$ (b) for four groups maizes

## 3.4.3 The response of passive fluorescence to the different water content

Radiation-based methods (FLD and 3FLD) were used to extract fluorescence from the leaf spectrum measured by HR4000. Illumination conditions are important for fluorescence. The normalization was calculated by dividing the PAR by the extracted fluorescence from the spectrum (marked as FLD/PAR, 3FLD/PAR) (Meroni et al., 2008).

On July 2 (Figure 3-8a), the daily variation trend of FLD/PAR was the same as that shown in the SCOPE model. The FLD/PAR increased before gradually decreased. The FLD/PAR in the four groups changed over a small range. After gradient watering (Figure 3-8b), the FLD/PAR in the S4 group was larger than that in the other groups. The FLD/PAR in S1 was the lowest because S1 group was not given any water. However, the FLD/PAR in S3 was sometimes larger than that in S4. These observations potentially result from measured errors in the spectrum and PAR measurements. After the filled watering (Figure 3-8c), the FLD/PAR values in the four groups were similar to each other, and the FLD/PAR in S1 recovered to that of S4. In addition, the 3FLD/PAR in the four groups showed the same

results. An analysis of the FLD/PAR and 3FLD/PAR in the four groups explained that chlorophyll fluorescence was closely related with the plant physiological state, and could reflect early water stress (Figure 3-8d, e and f).

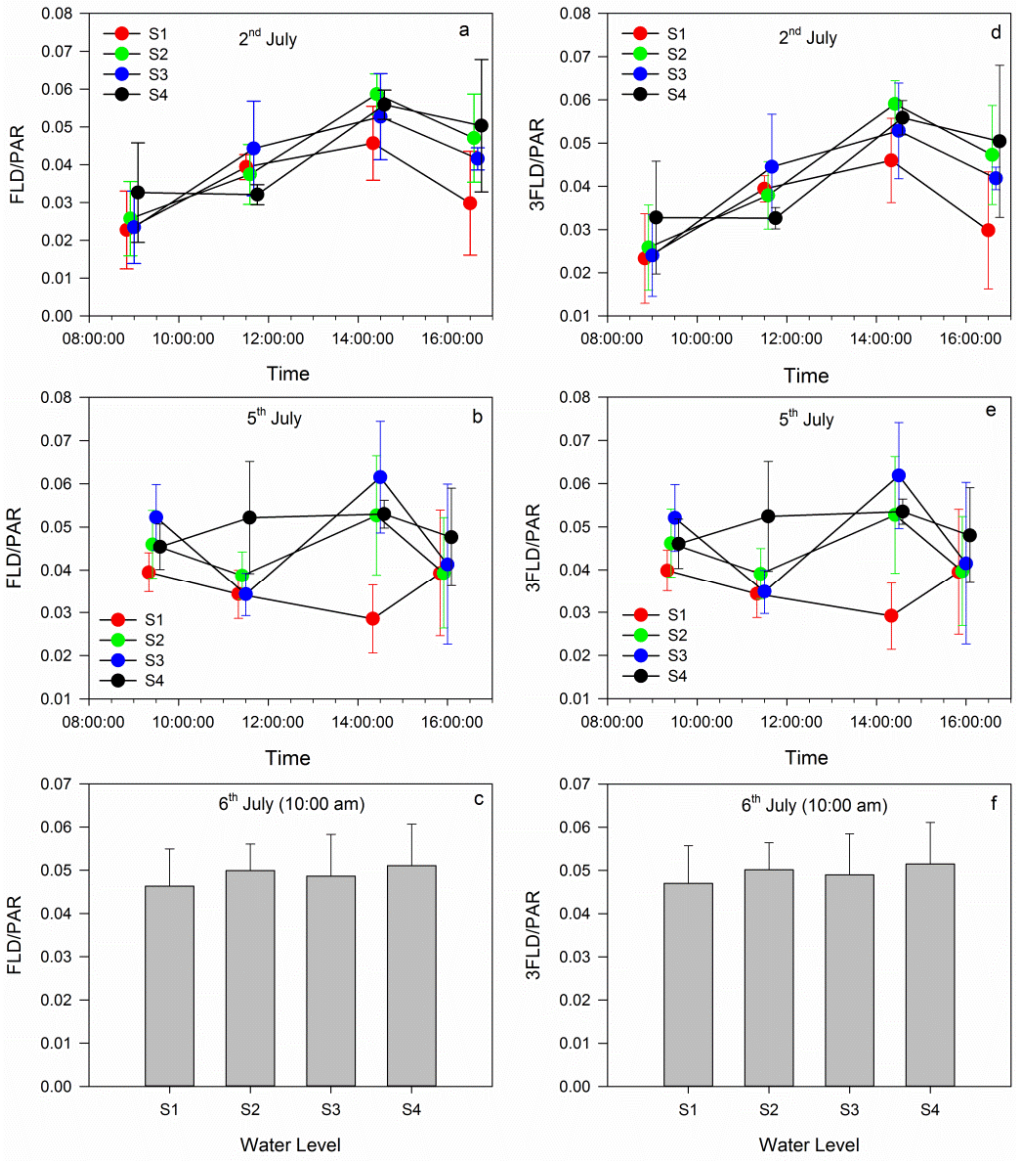


Figure 3-8 Daily variation in the fluorescence as retrieved by passive measurements: a, b and c: variations in the fluorescence using FLD on July 2, 5 and 6; d, e and f: variations in the fluorescence using 3FLD on July 2, 5 and 6.

## 3.4.4 Comparison of the active and passive fluorescence

The data obtained at 12:00 am on July 5, including the Fs, temperature, fluorescence retrieved by FLD and 3FLD, and water content, are used to analyze the relationship between the active and passive measurements. The four groups are combined to analyze the relationships among the measured parameters. The relationships between the fluorescence and

other parameters are analyzed, with $R^2$=0.54 for Fs vs. FLD/PAR (Figure 3-9a); $R^2$=0.48 for Fs vs. $T_{leaf}$-$T_{air}$ (Figure 3-9b); $R^2$=0.48 for FLD/PAR vs. $T_{leaf}$-$T_{air}$ (Figure 3-9c); and $R^2$=0.71 for Fs vs. soil water content (Figure 3-9d). The performances of FLD/PAR and 3FLD/PAR are similar; therefore, only the comparisons of FLD/PAR with the other parameters are given.

From the Figure 3-9a, it can be seen that PAM Fs has a good relationship with FLD/PAR. It demonstrates the consistency of active and passive measurements, and also reveals that the passive measurement results are reliable. Passive measurement is a common method to estimate chlorophyll fluorescence. The consistency of active and passive measurements confirms that chlorophyll fluorescence retrieved using the passive measurement is credible.

Figure 3-9b and d show the good relationship between PAM Fs or FLD/PAR and Tleaf-Tair. Chlorophyll fluorescence, heat dissipates and photosynthesis are three ways to consume the absorbed energy. Their close relationship shows that the variation of chlorophyll fluorescence can cause the variation of temperature, and also reveals that two parameters can be linked to reflect the vegetation photosynthesis.

Figure 3-9c shows that PAM Fs has a close relationship with soil water content. It demonstrates that the variation of soil water content can be observed from chlorophyll fluorescence, and also states that it is feasible to detect the water stress using chlorophyll fluorescence.

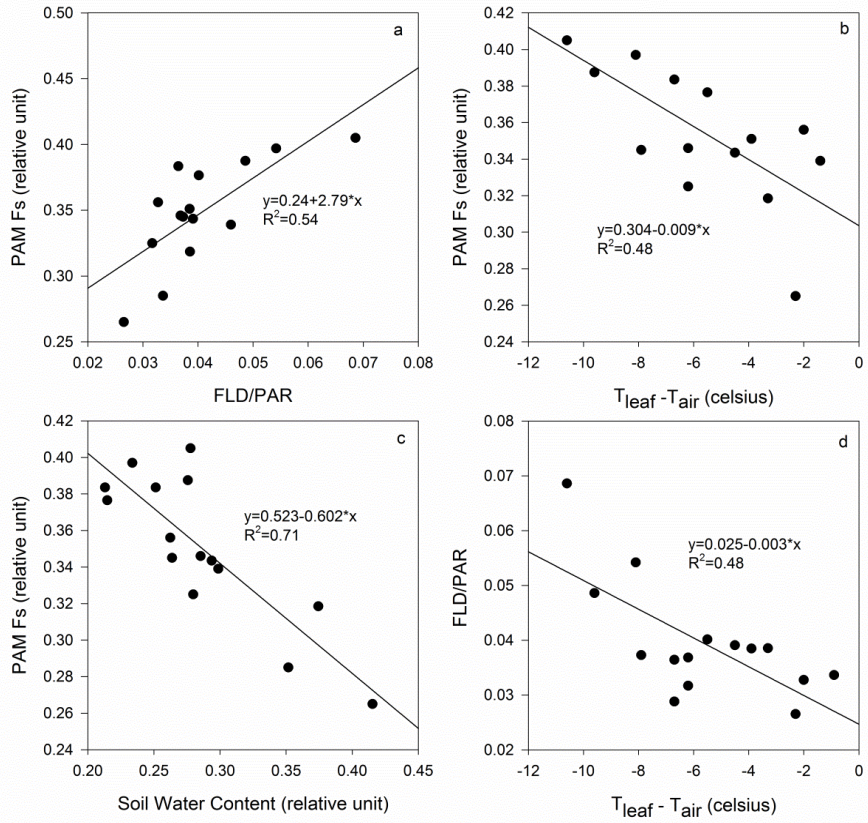


Figure 3-9 Comparison of the active and passive measurements (a) PAM Fs vs. FLD/PAR; (b) PAM Fs vs. $T_{leaf}$-$T_{air}$; (c) PAM Fs vs. Soil water content; and (d) FLD/PAR vs. $T_{leaf}$-$T_{air}$

## 3.5 Conclusions

Through the study of the leaf chlorophyll fluorescence, we explain that active and passive fluorescence are consistency under the condition of water content change, and the active and passive fluorescence can reflect the water content change. Besides, we analyze the temperature's response to the water content change, and illustrate that chlorophyll fluorescence and temperature can reflect the vegetation early water stress.

In this study, the main conclusions are as follows:

(1) The SCOPE model is used to simulate the daily variation of chlorophyll fluorescence and temperature under the water stress. Comparing with plants in healthy condition, the chlorophyll fluorescence decreases under the condition of the stress and the temperature increases. The relationship between chlorophyll fluorescence and temperature shows that there is a good linear relationship among them before noon, and complicated after noon.

(2) The gradient watering experiment shows that the fluorescence for maize is low under water stress. As the water stress becomes more severe, the temperature gradually increases. The active fluorescence is closely related with the water level. In the filled watering experiment, the different response of active fluorescence and temperature to water content change illustrate active fluorescence is much more sensitive to water content change than the temperature, and the temperature can reflect the early water stress.

(3) The normalized passive fluorescence of maize increases firstly and then decreases, and is consistency with the SCOPE simulated results. The controlled experiments illustrate that the normalized passive fluorescence can reflect the water content change, and recover to the healthy condition when the vegetation stress relieves.

(4) The comparison between active and passive fluorescence in the whole experiment illustrate the consistency of active and passive fluorescence under the condition of water content change. It shows that the measurement results of two ways are reliable, and the leaf active fluorescence can used to validate the passive measurement results.

# Chapter4. The SIF retrieval method near the ground using the reflectance index

## 4.1 Background

The sun-induced fluorescence is the effective probe to monitor the vegetation physiological state and early environmental stress. Chlorophyll fluorescence, photosynthesis and heat dissipate are three ways to consume the absorbed energy. Chlorophyll fluorescence spectrum locates in the range of 650-850 nm with two peaks, one in the 687 nm, and other nearby the 740 nm. Therefore, the reflectance index is used to detect the chlorophyll fluorescence, such as red/infrared red. The study of the leaf chlorophyll fluorescence make people begin to understand the chlorophyll fluorescence, and develop the chlorophyll fluorescence from the leaf to the canopy. The fluorescence model can help people better understand the relationship between the chlorophyll fluorescence and other parameters. Now the fluorescence models have FluorMOD and SCOPE models. These two models can simulate the variation of the fluorescence. The fluorescence intensity changes with the variation of vegetation state (species, phenology and so on) and the photosynthesis affective radiation. Under the different illumination condition, the red fluorescence near the ground changes in the range of 0.5-10.5 mW $m^{-2}$ $nm^{-1}$ $sr^{-1}$, and the infrared red fluorescence near the ground changes in the range of 0.5-12.0 mW $m^{-2}$ $nm^{-1}$ $sr^{-1}$ (Theisen 2000; Moya et al., 2003; Liu et al., 2005; Dobrowski et al., 2005; Louis et al., 2005; Meroni & Colombo 2006; Corp et al., 2006). The results of the variation of sun-induced fluorescence can attributed to the illuminate change and measurement error.

Sun-induced chlorophyll fluorescence (SIF) near the ground includes the radiance-based methods and the reflectance-based methods. The radiance-based method can retrieve the fluorescence quantitatively, and the retrieved fluorescence has physical meaning with the radiance unit. These methods exploit the filling of SIF in the franhofer line to extract the SIF, and are widely used to retrieve the SIF. The reflectance-based methods use two or three bands to build the reflectance index to assess the SIF quickly and simply. Despite the reflectance-based methods only assess the SIF qualitatively, they are only methods under the certain conditions, such as artificial light or the radiance-based methods failing. It also shows that it is necessary to develop the reflectance-based methods.

This chapter aims to develop the SIF quantitative retrieval method using the reflectance index under the natural sun illuminate. Figure 4-1 shows the flow chart of this chapter. In the first, we carry out the sensitivity analysis of FluorMOD, and select the sensitive parameters; then based on the results of sensitivity analysis, the simulated data is generated using the

FluorMOD; in the following, we select the optimal reflectance index and build the quantitative relationships amongst the fluorescence@761nm, the reflectance index and other parameters. Because the FluorMOD can simulate the reflectance and fluorescence under natural illumination and no-stress condition, these methods presented in this study also have this limitation.

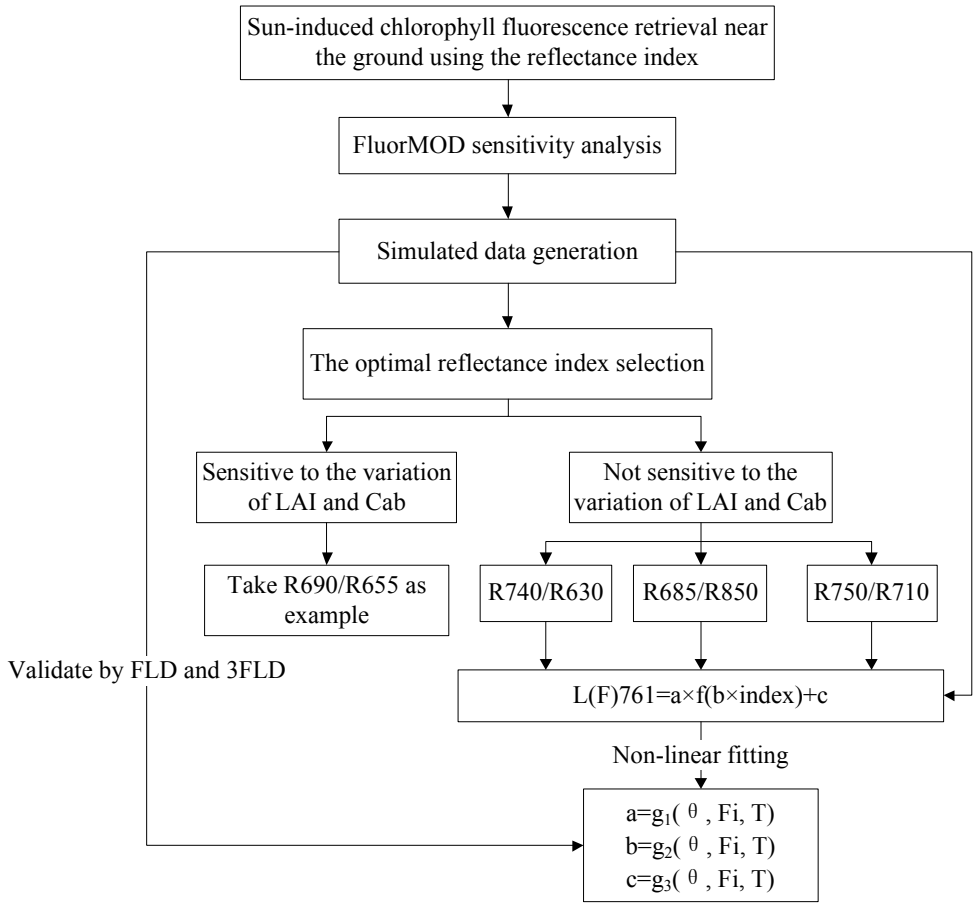


Figure 4-1 Flow chart

(θ: sun zenith angle, Fi: the fluorescence quantum field, LIDF: leaf distribution function, T: temperature, LAI: leaf area index, Cab: chlorophyll content)

## 4.2 Fluorescence and reflectance spectrum

In a photosynthetically active leaf, the emission of fluorescence light is one way of de-excitation and accompanies photochemical reactions at the reaction centres and light-induced heat production (Buschmann & Kocsányi 1989). The fluorescence emission spectrum of a green leaf induced by natural light is characterized by two bands with maxima or shoulders near 690 nm (red) and 740 nm (far-red; Figure 4-2) (Lichtenthaler 1992).

The solar spectrum has three main absorption bands: Ha hydrogen absorption (centered at 656.4 nm), $O_2$-B absorption (centered at 687.0 nm), and $O_2$-A absorption (centered at 760.0 nm; Figure 4-3). The oxygen absorption bands have been used more extensively than Ha because they are closer to the peaks in the chlorophyll fluorescence emission spectrum (690 nm and 740 nm). Among the oxygen absorption bands, the $O_2$-A absorption bands have been used more than the $O_2$-B absorption bands because the $O_2$-A absorption bands are much wider (spectral absorption band-width) and deeper (spectral absorption band-depth) than the $O_2$-B absorption bands. Although the $O_2$-A absorption band is not consistent with the fluorescence peak (740 nm), the fluorescence in the $O_2$-A absorption bands still account for 50% of the fluorescence peak (Moya et al., 2004). Therefore, the fluorescence radiance at 761 nm is chosen in this study and marked as L(F)761.

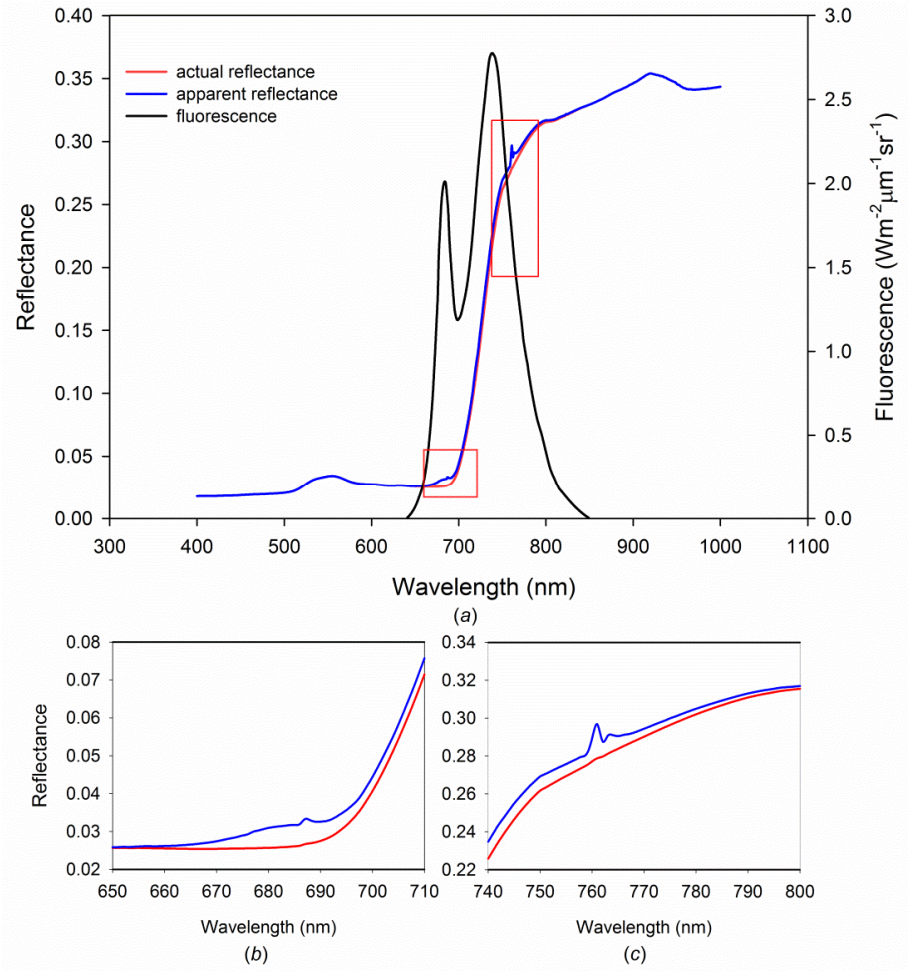


Figure 4-2 Reflectance and fluorescence spectra simulated by the FluorMOD model

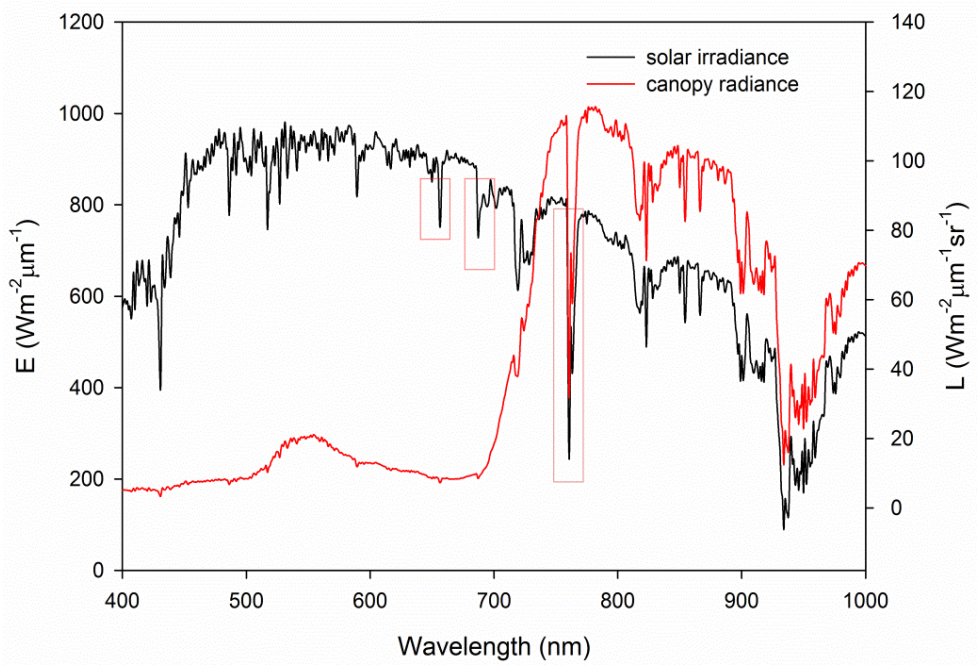


Figure 4-3 Solar irradiance (E) and canopy radiance (L) simulated by FluorMOD

## 4.3 The simulated data generation near the ground

### 4.3.1 FluorMOD model

FluorMOD is used to generate the simulated data in this research in which the fluorescence radiance of the plant on the canopy is computed under non-stress, favourable environmental and natural illumination conditions. The model has two modules: FluorMODleaf, developed based on PROSPECT to simulate the fluorescence at the leaf, and FluorSAIL, developed from SAIL and used to simulate natural solar-induced fluorescence on the canopy level. The input parameters of FluorMOD are atmospheric parameters, leaf parameters, and canopy parameters. The input parameters of the FluorMOD model are shown in Table 4-1; default values are used for all other parameters.

Table 4-1 Input parameters for the FluorMOD model

| Parameter | Description | Value | Units |
|---|---|---|---|
| **Atmosphere file** | | | |
| FlUORMOD10v23.MEP-FlUORMOD70v23.MEP | Consider the sun zenith angleθ changing from 10 to 70 deg | | |
| **Leaf input parameters** | | | |
| N | Number of layers | 1-3 | -- |
| Cab | Leaf chlorophyll a+b content | 5-100 | μg $cm^{-2}$ |
| Cw | Water equivalent thickness | 0-0.05 | cm |
| Cm | Dry matter content | 0.01 | g $cm^{-2}$ |
| Fi | Fluorescence quantum efficiency | 0.002-0.02 | - |
| T | Temperature | 5-25 | $^{o}C$ |
| S | Species | broad bean<br>bean<br>ficus<br>tomato<br>pea | -- |
| Sto | Stoichiometry of PSII to PSI reaction centers | 1-3 | -- |
| **Canopy input parameters** | | | |
| Raz | Relative Azimuth Angle | 0 | deg |
| Vza | Viewing Zenith Angle | 0 | deg |
| h | Hot Spot parameter | 0.1 | -- |
| LAI | Leaf area index | 0-8 | $m^2/m^2$ |
| LIDFa;LIDFb | Leaf inclination distribution function | 1: spherical<br>2: planophil<br>3: eretophile<br>4: plagiophile<br>5: extremophile<br>6: uniform | -- |

## 4.3.2 Sensitivity Analysis

Sensitivity analysis is the study of how the uncertainty in the output of a mathematical model can be apportioned to different sources of uncertainty in its inputs (Saltelli et al., 2008). The software Gaussian Emulation Machine for Sensitivity Analysis (GEM-SA) is used for sensitivity analysis. GEM-SA applies the BACOO approach to derive the sensitivity analysis (O'Hagan 2006). First, the input parameters are assessed to ensure that they are evenly distributed. Second, these parameters are input into the model, and the result is output. Finally,

the input parameters and the output results are entered into GEM-SA to derive the sensitivity analysis. In the sensitivity analysis, the indicator total effect is applied to evaluate the effect that each input parameter has on the output.

The results of the sensitivity analysis of the FluorMOD model show that sun zenith angle $\theta$, fluorescence quantum efficiency *Fi*, leaf inclination distribution function *LIDF*, leaf temperature *T*, leaf area index *LAI* and leaf chlorophyll a+b content *Cab* account for most of the variation in L(F)761.

Figure 4-4 indicates that $\theta$ accounts for 42.32% of the variation in L(F)761, making it the most important parameter because $\theta$ affected the total intensity of the incoming sunlight. *Fi* is the second most important parameter, accounting for 34.62% of the variation in L(F)761. *Fi* could assess the fluorescence emitting ability of the leaf and relate with light absorption and plant physiological status. The canopy structure parameters (*LAI* and *LIDF*) are thought to the third most important parameters; these parameters directly affect the light intensity accepted by the canopy. Fluorescence induction emphasizes the fact that sunlight is important for the fluorescence emission, and fluorescence has a direct and close relationship with photosynthesis (Krause & Weis 1984; Larcher 1994; Zarco-Tejada et al., 2003; Pérez-Priego et al., 2005).

Other parameters such as leaf temperature *T* and leaf chlorophyll a+b content (*Cab*) account for close to 10% of the variance in L(F)761. The chlorophyll present in the molecules of the photosynthetic antennae in the thylakoid membranes of green plants absorbs most of the light energy (Misra et al., 2012). Most of this energy is used for photosynthesis, while the extra energy dissipates in the form of heat and fluorescence emission. The leaf chlorophyll content is related to the fluorescence yield, and heat dissipation has a very close relationship with photosynthesis and fluorescence. Therefore, these two parameters should be considered in the generation of simulated data.

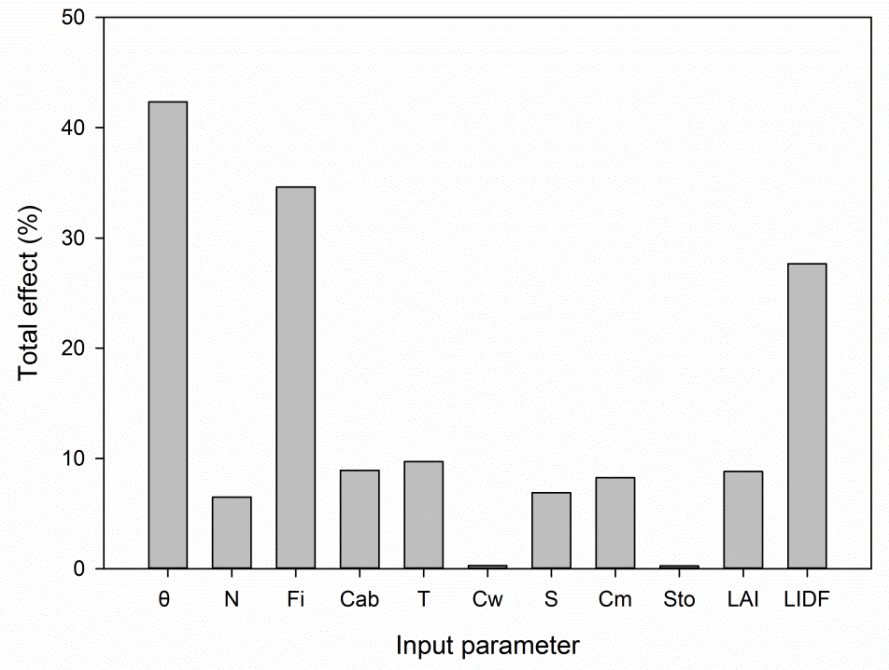


Figure 4-4 Sensitivity analysis results for FluorMOD

### 4.3.3 The simulated data generation

The sensitivity analysis shows that some parameters have great impacts on L(F)761 and should be given special attention in the generation of the simulated data. Other parameters whose variations have smaller effects on L(F)761 can be set to constant values. A large amount of simulated data including input parameters, reflectance indices, and L(F)761 composes a database. Assuming that LIDF has a spherical distribution, the FluorMOD model is used to generate the simulated data using fixed-step input parameters (Table 4-2) and 13 types of atmosphere files with different sun zenith angles θ. The 26,000 simulated data generated by FluorMOD are used to compose a database including input parameters (θ, Fi, T, LAI and Cab), reflectance indices, and L(F)761.

Table 4-2 The selected parameters in the sensitivity analysis

| Parameter | Range | Step |
|---|---|---|
| Fi | 0.01-0.10 | 0.01 |
| T | 5-25°C | 5 |
| LAI | 0.1-8.0 $m^2/m^2$ | 1 |
| Cab | 10-90μg/$cm^2$ | 20 |

## 4.4 Building the relationship between the fluorescence and the optimal reflectance index

### 4.4.1 Selection of the optimal reflectance index

In this study, the optimal reflectance indices from Table 4-3 are selected to build the quantitative relationship between L(F)761 and the related parameters using simulated data. In this paper, the reflectance indices are investigated, while derivative ratios and in-filling parameters are beyond the scope of this study. Table 4-3 lists the reflectance indices used in previous studies (Zarco-Tejada et al., 2000a; Meroni et al., 2009; Zarco-Tejada et al., 2009).

Table 4-3 Reflectance-based methods used in previous studies (Meroni et al. 2009)

| References | Reflectance Indices |
|---|---|
| Zarco-Tejada et al. (2000a) | R750/R800, $R683^2$/R675*R691, R685/R655, R690/R655 |
| Zarco-Tejada et al. (2000b) | R680/R630, R685/R630, R687/R630, R690/R630 |
| Pérez-Priego et al. (2005) | R760.5-R759.5 |
| Dobrowski et al. (2005) | R690/R600, R740/R800 |

We select the optimal reflectance index, and build the relationships between reflectance indices (Table 4-2) and L(F)761 based on the simulated data. We analyse the relationships between reflectance indices (Table 4-2) and L(F)761 for different values of Fi, T, LAI, Cab, and θ. To select the optimal reflectance index, the relationship between L(F)761 and the reflectance index is analysed as follows.

First, the relationship between R740/R630 and L(F)761, which corresponds to the input parameters θ = 30 deg, Fi = 0.04, T = 20 $^{o}$C, LAI = 4, and Cab = 10-90 μg $cm^{-2}$, is analysed. Both R740/R630 and L(F)761 increases gradually with increasing Cab (Figure 4-5a). When θ = 30 deg, Fi = 0.04, T = 20 $^{o}$C, LAI = 0.1-8, and Cab = 10-90 μg $cm^{-2}$, R740/R630 and L(F)761 increases with increasing LAI (Figure 4-5b). The relationship between R740/R630 and L(F)761 is insensitive to LAI and Cab, and L(F)761 is a function of R740/R630: $L(F)761 = a(1 - e^{-bIndex_{R740/R630}}) + c$ . Thus, the reflectance indices that are insensitive to Cab should be considered.

Figure 4-5c compares R740/R630 with L(F)761 for Fi = 0.04, T = 5-25 $^{o}$C, LAI = 0.1-8, and Cab = 10 to 90 μg cm$^{-2}$, L(F)761 decreases with increasing T, and the relationship between R740/R630 and L(F)761 varies regularly. The variation in T is opposed to the variation in fluorescence radiance. Figure 4-5d shows the results when Fi = 0.01-0.1, T = 20 $^{o}$C, LAI = 0.1-8, and Cab = 10-90 μg cm$^{-2}$. The variation in L(F)761 is proportional to the variation in Fi. In Figure 5e, L(F)761 decreases with increasing sun zenith angle, and the relationship between L(F)761 and R740/R630 also changes regularly.

Based on the above analysis, L(F)761 is expressed as the non-linear function of R740/R630, θ, Fi and T, and along with their variations, the relationship between L(F)761 and R740/R630 has slightly and regularly varied (Figure 4-5). Thus, the relationship could be expressed as $L(F)761 = a(1 - e^{-bIndex_{R740/R630}}) + c$ in Figure 5, where a, b, and c are functions of θ, Fi, and T.

The relationship between R690/R655 and L(F)761 is also analysed, and Figure 4-6 is generated using the same preconditions as in Figure 4-5. Figure 6a shows that the R690/R655 and L(F)761 exhibits different responses to variation in chlorophyll content; with increasing Cab, L(F)761 gradually increases, while R690/R655 decreases gradually after a quick increases. Figure 6b illustrates that the relationship between R690/R655 and L(F)761 changed with the variation in LAI and Cab and cannot be expressed as a non-linear or linear function. Figures 4-6c, d, and e also illustrate this conclusion. The reflectance indices, whose wavelengths are all located in the range of 650-690 nm, are affected by Cab. Gitelson & Merzlyak (2003) demonstrated that reciprocal reflectance (Rλ)-1 in the spectral range of λ = 520-550 nm and 695-705 nm was closely related to the total chlorophyll content in the leaves of all species; it was considered that these reflectance indices were contaminated by chlorophyll content. Therefore, R690/R655 is not considered to be a good reflectance index for the following analysis.

On the basis of 26,000 simulated data, the reflectance indices, such as R740/R630, R685/R850 and R750/R710, are observed that they are insensitive to variation in LAI and Cab (Figure 4-5), while the rest of indices are sensitive to LAI and Cab (Figure 4-6). LAI and Cab has close relationship with vegetation physiological status in the nature environment, such as soil water content, crop nitrogen status and so on. Many reflectance indices which are used to measure the fluorescence have close relationship with LAI and Cab. Therefore, the all reflectance indices in Table 4-3 are analysed to find optimal indices which are insensitive to

variation in LAI and Cab. R740/R630 and R690/R655 are selected as the representative indices, and Figures 5 and 6 show the relationships between these indices and L(F)761, respectively. It is clear that R740/R630, R685/R850, and R750/R710 achieve the research objective of identifying the quantitative relationship between reflectance index and L(F)761.

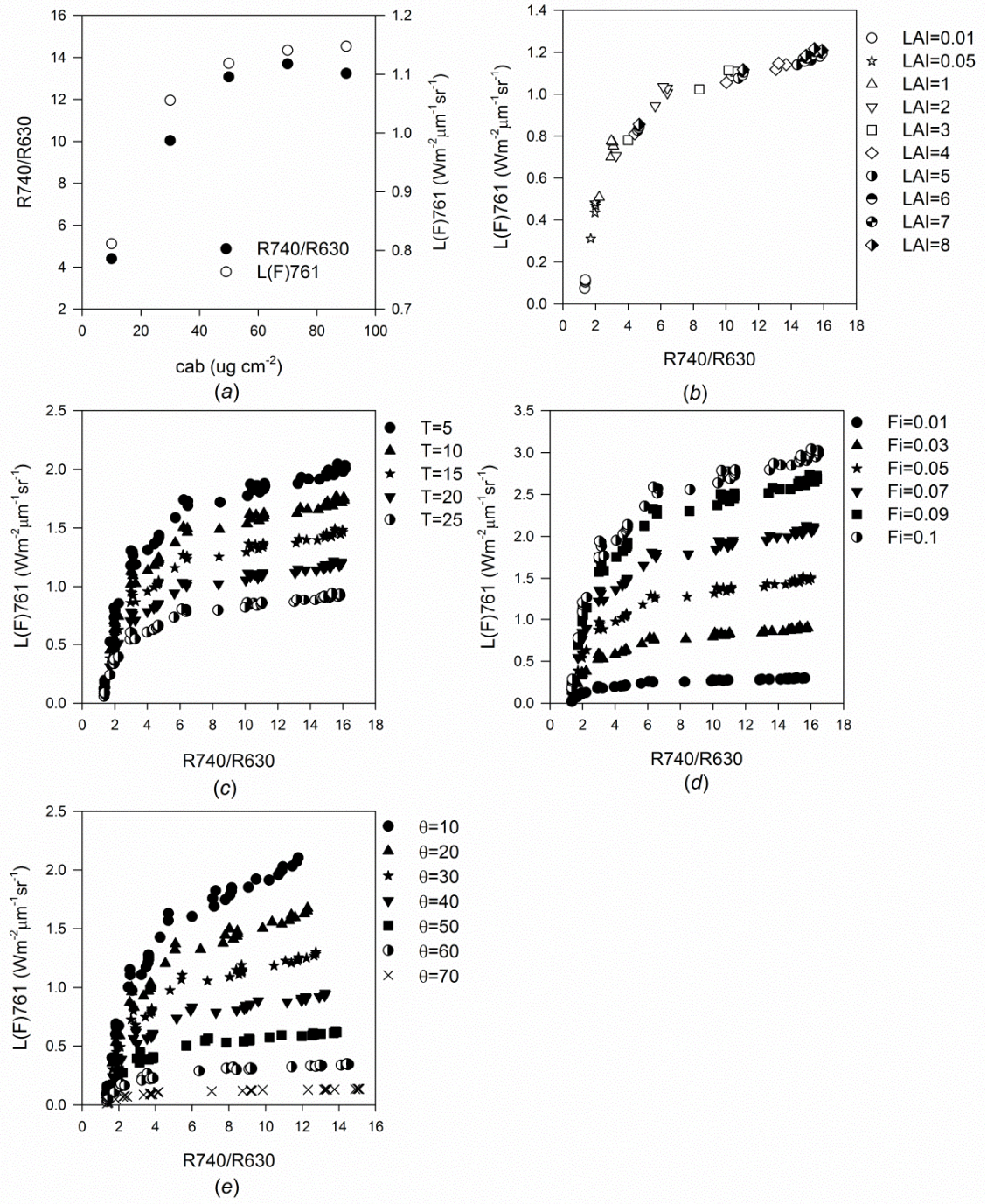


Figure 4-5 Relationship between L(F)761 and R740/R630:

(a) θ (sun zenith angle) = 30 deg, Fi (fluorescence quantum efficiency) = 0.04, T (leaf temperature) = 20 $^{o}$C, LAI (leaf area index) = 4, and Cab (leaf chlorophyll a+b content) = 10-90 μg cm$^{-2}$; (b) same as (a) but LAI = 0.1-8; (c) same as (a) but T = 5-25 $^{o}$C; (d) same as (a) but Fi = 0.01-0.1 ; (e) same as (a) but θ = 10-70 deg.

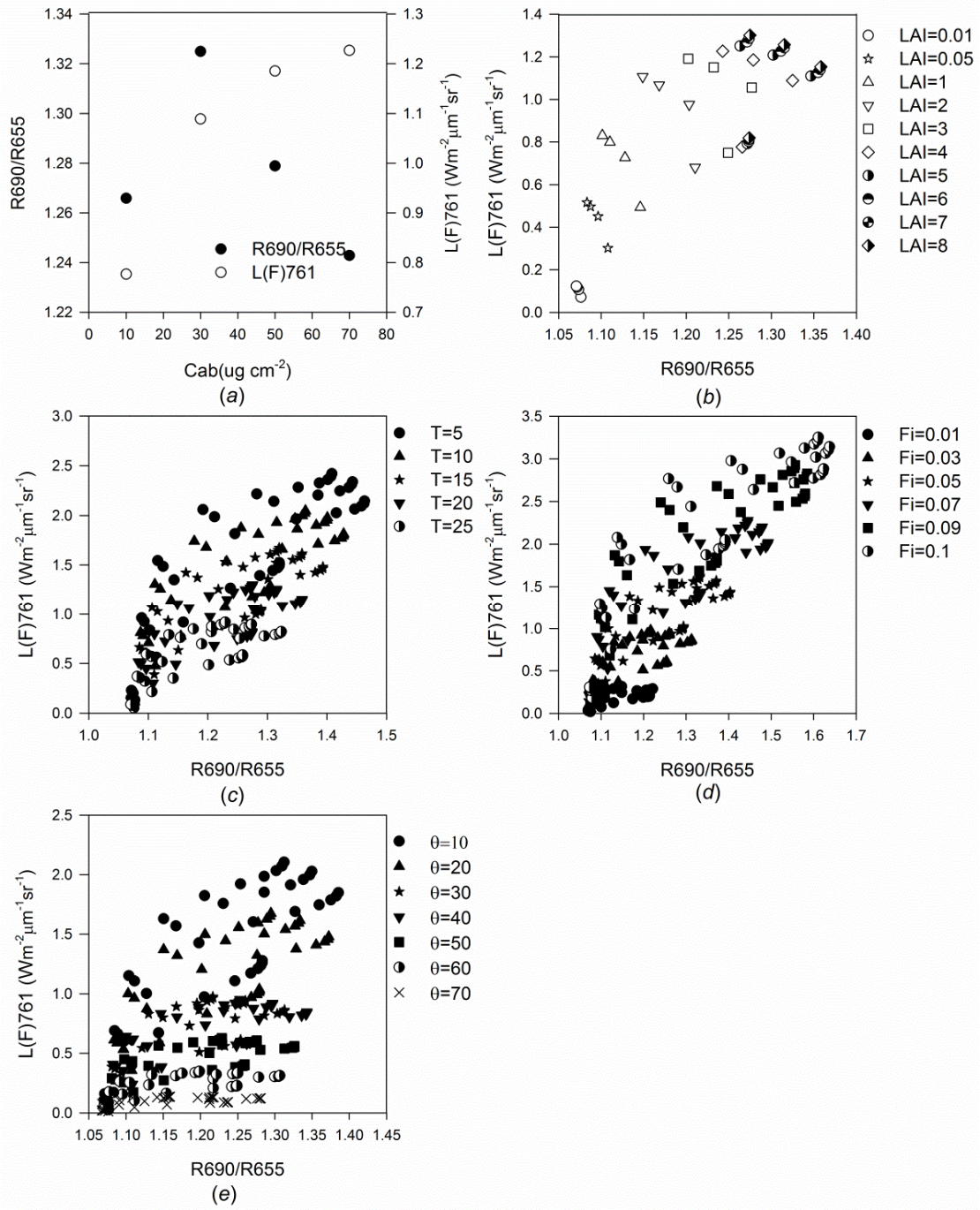


Figure 4-6 Relationship between L(F)761 and R690/R655:

(a) θ (sun zenith angle) = 30 deg, Fi (fluorescence quantum efficiency) = 0.04, T (leaf temperature) = 20 $^{o}$C, LAI (leaf area index) = 4, and Cab (leaf chlorophyll a+b content) = 10-90 μg cm$^{-2}$; (b) same as (a) but LAI = 0.1-8; (c) same as (a) but T = 5-25 $^{o}$C; (d) same as (a) but Fi = 0.01-0.1 ; (e) same as (a) but θ = 10-70 deg.

## 4.4.2 The quantitative relationship between the reflectance index and L(F)761

The fluorescence retrieved by the reflectance indices R685/R850, R740/R630, and R750/R710 are compared with L(F)761, and quantitative relationships are sought between L(F)761 and R685/R850, R740/R630, and R750/R710. Figure 4-5 shows that the relationship between L(F)761 and the reflectance index R740/R630 is exponential relationship, and the figure 4-7 and 4-8 illustrate the relationship between the other optimal reflectance indices and L(F)761. In the figure 4-7, L(F)761 has a liner relationship with the reflectance index R685/R850; and in the figure 4-8, L(F)761 has an exponential relationship with the reflectance index R750/R710.

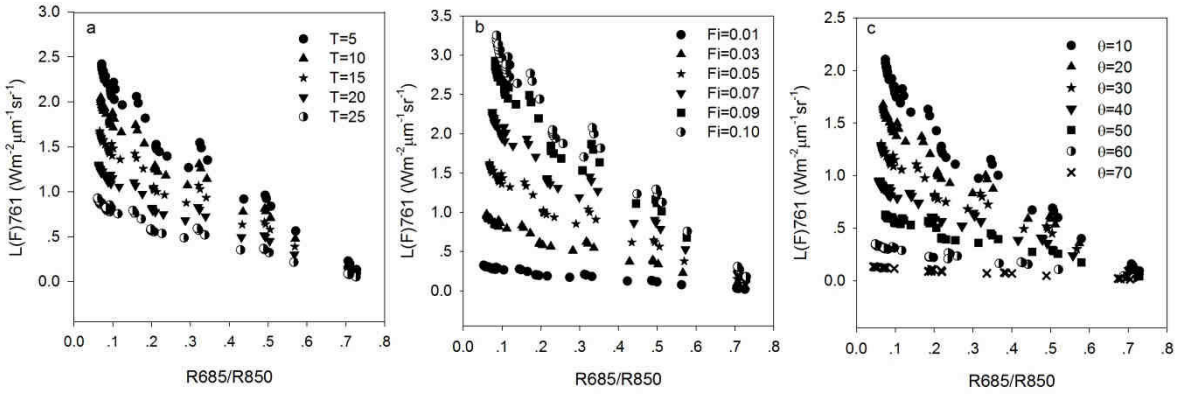


Figure 4-7 The relationship between L(F)761 and R685/R850

(a)θ=30 deg, Fi=0.04, T=5-25 $^{o}$C, LAI=4 $m^2/m^2$, Cab= 10-90 μg $cm^{-2}$; (b)θ=30 deg, Fi = 0.01-0.1, T=20 $^{o}$C, LAI=4 $m^2/m^2$, Cab= 10-90 μg $cm^{-2}$; (c)θ = 10-70 deg, Fi = 0.04, T=20 $^{o}$C, LAI=4 $m^2/m^2$, Cab= 10--90 μg $cm^{-2}$

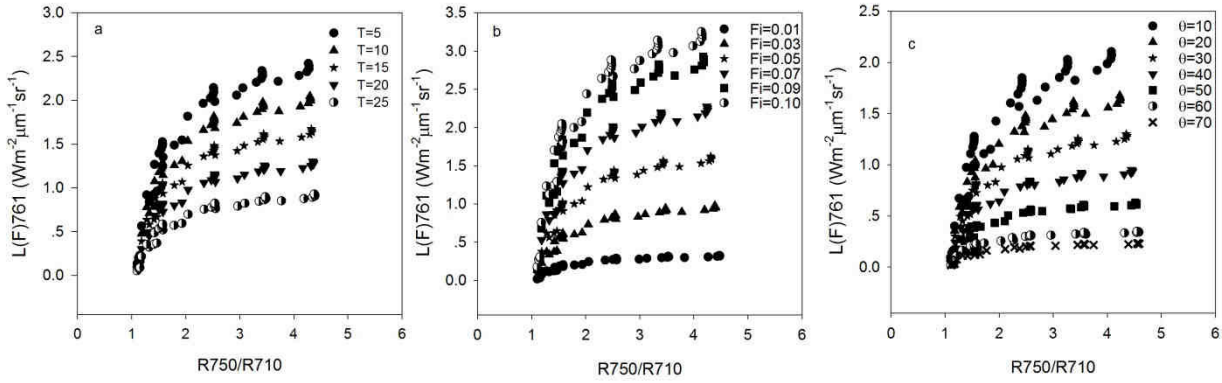


Figure 4-8 The relationship between L(F)761 and R750/R710

(a)θ=30 deg, Fi=0.04, T=5-25 $^{o}$C, LAI=4 $m^2/m^2$, Cab= 10-90 μg $cm^{-2}$; (b)θ=30 deg, Fi = 0.01-0.1, T=20 $^{o}$C, LAI=4 $m^2/m^2$, Cab= 10-90 μg $cm^{-2}$; (c)θ = 10-70 deg, Fi = 0.04, T=20 $^{o}$C, LAI=4 $m^2/m^2$, Cab= 10--90 μg $cm^{-2}$

Take R740/R630 as an example. When θ, Fi, and T are fixed, the relationship between L(F)761 and R740/R630 appear insensitive to variation in LAI and Cab (Figure 4-5b), and L(F)761 could be expressed as the function of R740/R630. The relationship between the reflectance index and L(F)761 changes correspondingly with variation in θ, Fi, and T, and it could be considered that the coefficients of the formula (a, b, and c) are functions of θ, Fi, and T, respectively. Based on the simulated data and the selected reflectance indices, quantitative expressions relating the reflectance indices and L(F)761 are obtained, and the formulas obtained by non-linear fitting are as follows:

$$L(F)761 = \alpha Index_{R685/R850} + b \quad (4\text{-}1)$$
$$\alpha = 0.05\theta - 3.79 + (1.57\theta - 108.86)Fi + (-0.004\theta + 0.27)T$$
$$b = -0.04\theta + 2.80 + (-1.15\theta + 80.49)Fi + (0.003\theta - 0.20)T$$

$$L(F)761 = \alpha(1 - e^{-bIndex_{R740/R630}}) + c \quad (4\text{-}2)$$
$$\alpha = -0.06\theta + 3.95 + (-1.47\theta + 104.83)Fi + (0.004\theta - 0.26)T$$
$$b = 0.001\theta + 0.41 + (0.004\theta - 0.45)Fi + 0.001T$$
$$c = 0.02\theta - 1.37 + (0.48\theta - 34.58)Fi + (-0.001\theta + 0.08)T$$

$$L(F)761 = \alpha(1 - e^{-bIndex_{R750/R710}}) + c \quad (4\text{-}3)$$
$$\alpha = -0.20\theta + 15.22 + (-5.82\theta + 438.47)Fi + (0.014\theta - 1.06)T$$
$$b = 0.006\theta + 1.56 + (-0.003\theta - 0.55)Fi + (-0.00004\theta + 0.00000)T$$
$$c = 0.16\theta - 12.63 + (4.82\theta - 367.58)Fi + (-0.01\theta + 0.88)T$$

## 4.5 The analysis of the quantitative model

### 4.5.1 Assessment of the quantitative model

In this study, the reflectance indices that are insensitive to LAI and Cab gained more attention. Based on the analysis, the indices R740/R630, R685/R850, and R750/R710 are selected, and a quantitative model is built in which canopy fluorescence is a function of the reflectance index, Fi, T, and θ. The fluorescence estimated from the quantitative model yields the good results ($R^2$ = 0.94, RMSE = 0.32 $Wm^{-2}\mu m^{-1}sr^{-1}$ for R685/R850 vs. L(F)761; $R^2$ =

0.95, RMSE = 0.30 $Wm^{-2}\mu m^{-1}sr^{-1}$ for R750/R710 vs. L(F)761; and $R^2$ = 0.95, RMSE = 0.29 $Wm^{-2}\mu m^{-1}sr^{-1}$ for R740/R630 vs. L(F)761) (Figure 4-9).

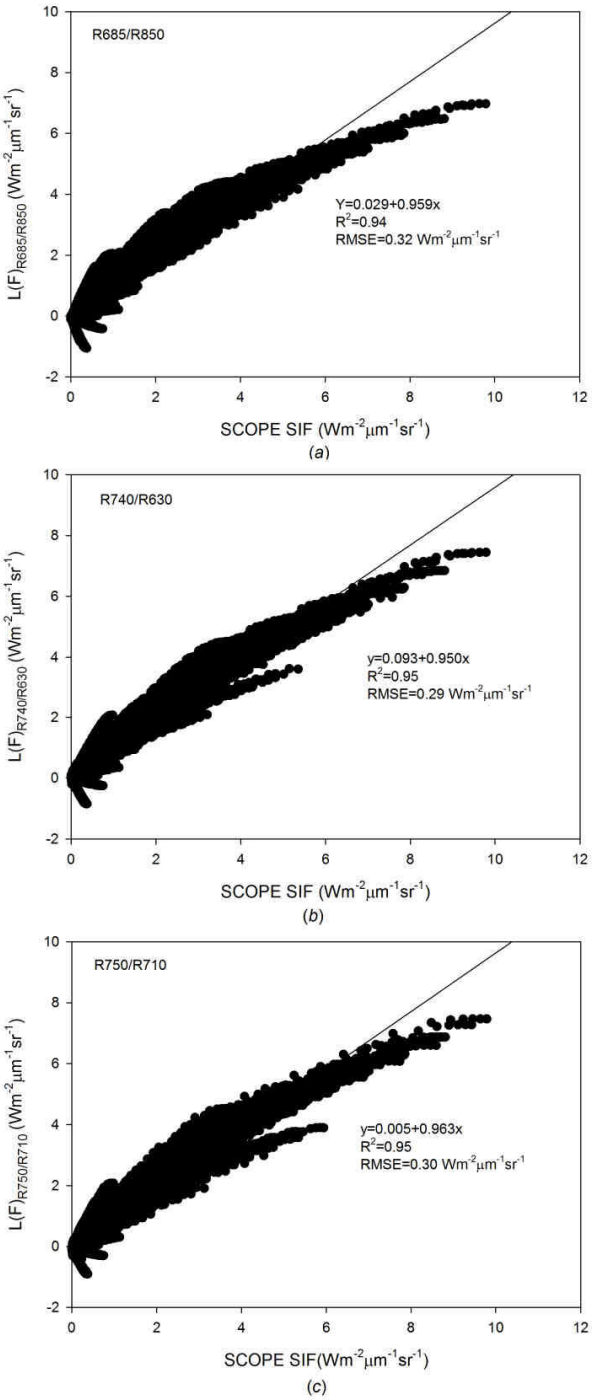


Figure 4-9 Comparison of L(F)761 with the fluorescence retrieved from the quantitative model using different reflectance indices: (a) R685/R850; (b) R740/R630; and (c) R750/R710.

### 4.5.2 Error analysis of the quantitative model

Figure 4-9 shows that under certain circumstances, the quantitative model may underestimate L(F)761. To identify the conditions under which the quantitative model can accurately estimate fluorescence, an error analysis is performed. The fluorescence computed using θ, Fi, T, and reflectance index is remarked as Findex, in which the 'index' is R740/R630 or R750/R710 or R685/R850. To understand the effect of the variation of the independent variable on the dependent variable of the function, the relationships between θ, Fi, T, and reflectance index with L(F)761-Findex are analysed (Figure 4-10).

Take Figures 4-10a, b, c and d as an example. When sun zenith angle is 60 deg, Fi ranges from 0.04 to 0.05, T is 15 $^{o}$C, and R685/R850 is 0.6-0.7, L(F)761-FR685/R850 is limited to the range of -0.7-0.7 $Wm^{-2}\mu m^{-1}sr^{-1}$.Variations in Fi and T lead to wide fluctuation in L(F)761-Findex. It should be noted that the fluorescence decreased with increasing θ. When sun zenith angle is 60 deg, the fluorescence is very low. Although a smaller θ leads to a large error between Findex and L(F)761, the small θ should be considered first.

In the models based on R740/R630 and R750/R710, θ varies from 30-40 deg, Fi range from 0.03-0.04, T ranges from 15-20 $^{o}$C, and the values of L(F)761-FR740/R630 and L(F)761-FR750/R710 are in the range of -0.8-0.8 $Wm^{-2}\mu m^{-1}sr^{-1}$. In addition, the variations in R740/R630 or R750/R710 lead to the only small changes in L(F)761-$F_{index}$.

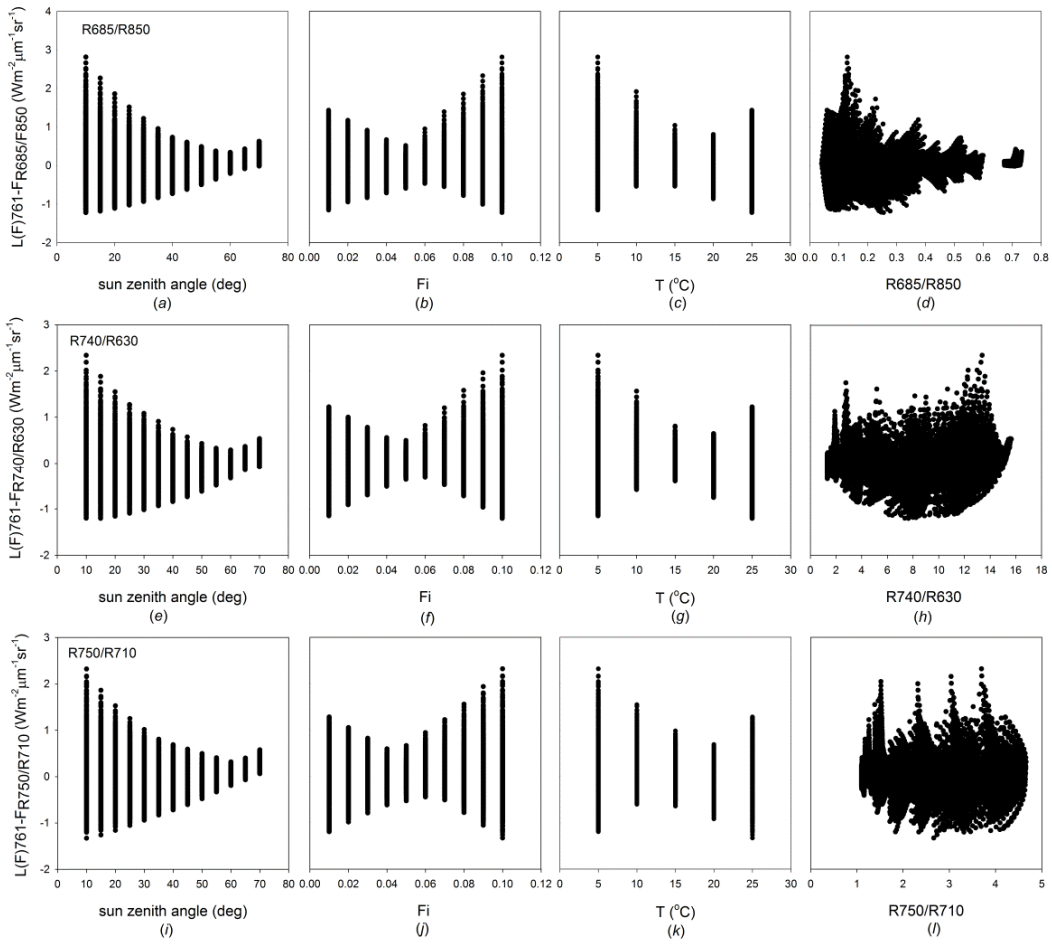


Figure 4-10 Error analysis of the quantitative model under the precondition: θ=10-70 deg, Fi = 0.01-0.1, T = 5-25 $^{o}$C, LAI = 0.1-8, and Cab = 10-90 μg cm$^{-2}$.

## 4.5.3 Comparison among the retrieval results, FLD and 3FLD

The radiance-based methods are thought to be good methods for the quantitative retrieval of fluorescence. The fluorescence retrieved using FLD and 3FLD are compared with the canopy fluorescence radiance L(F)761. The 3FLD method performs better than FLD ($R^2$ = 0.99 and RMSE = 0.29 Wm$^{-2}$μm$^{-1}$sr$^{-1}$ for 3FLD vs. L(F)761; $R^2$ = 0.98 and RMSE = 0.41 Wm$^{-2}$μm$^{-1}$sr$^{-1}$ for FLD vs. L(F)761; Figure 4-11).

Compared with FLD and 3FLD, the method in this study also yields good results. The correlation coefficients between the new methods derived from the reflectance indices R685/R850, R740/R630, and R750/R710 and L(F)761 are 0.94, 0.95 and 0.95, respectively, and the RMSE values are 0.32 Wm$^{-2}$μm$^{-1}$sr$^{-1}$, 0.29 Wm$^{-2}$μm$^{-1}$sr$^{-1}$, and 0.3 Wm$^{-2}$μm$^{-1}$sr$^{-1}$, respectively (Figure 4-11). The correlation coefficients between the retrieved fluorescence

using the new method and L(F)761 are smaller than those between FLD or 3FLD and L(F)761. The RMSE between the retrieved fluorescence using the new method and L(F)761 is larger than that between FLD and L(F)761 and similar to that between 3FLD and L(F)761. The RMSE represents the sample standard deviation of the differences between the predicted and observed values. In this study, the small RMSE illustrates that the retrieved fluorescence has a small deviation with L(F)761. Considering the correlation coefficient and RMSE, the developed quantitative models can be used to retrieve fluorescence.

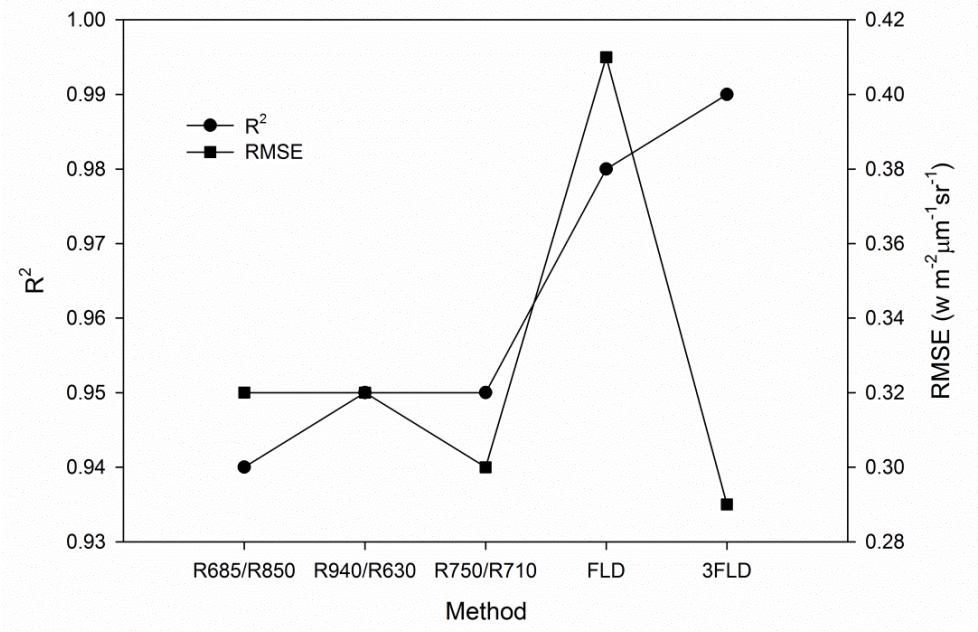


Figure 4-11 Comparison of $R^2$ and RMSE of the proposed method with FLD and 3FLD methods

## 4.6 Conclusions

This chapter shows that it is feasible to retrieval the SIF quantitatively using the reflectance index. The traditional reflectance-based methods only obtain the SIF relative value, and have the limitation in the application. The method presented in this paper exploited the existing reflectance indices along with other plant physiological parameters to estimate SIF near the ground. Because the simulated data is generated by FluorMOD which is designed to simulate the fluorescence under natural illumination and non-stress conditions, this method developed based on the simulated data can be used only under natural illumination condition.

In this study, the main conclusions are as follows:

(1) Using the FluorMOD model, we employ the reflectance indices (R685/R850, R740/R630, or R750/R710), the fluorescence quantum efficiency, and leaf temperature and sun zenith angle to build a quantitative model to estimate fluorescence radiation. Through comparing the method presented in this paper with FLD and 3FLD, it can be found that it also demonstrated that this method could be applied to quantitatively extract fluorescence.

(2) The reflectance-based methods with other parameters can retrieve the SIF quantitatively, and this method provides a new way to retrieve the fluorescence and paves the way to combine hyperspectral remote sensing and thermal infrared remote sensing to retrieve fluorescence.

# Chapter5. The atmospheric effects on the airborne/space-borne SIF retrieval

## 5.1 Background

When observing the SIF near the ground, we can consider that the SIF signal is the actual fluorescence because fluorescence is not affected by atmospheric absorption and scattering. Therefore, SIF is successful applied to the vegetation monitoring in the leaf scale and near the ground. The chapters 3 and 4 study the SIF detection at the leaf and near the ground separately. The SIF retrieving from the airborne/space-borne faces challenges. The SIF intensity is very small compared with the reflected energy, for example only account for 1-5% in the infrared region. Thus, retrieving the SIF in the airborne/space-borne should consider the atmospheric effects (Guanter et al., 2010; Frankenberg et al., 2011).Analyzing the effects of atmosphere on the SIF retrieval is a way to apprehend the idea of the SIF retrieval methods.

The SIF detection from the airborne/space-borne is an important research issue, and is considered as the core task of FLEX project. Until now, the study about the SIF detection has achieved some results, and previous literatures show that the SIF retrieved methods can be successful applied in GOSAT TANSO-FTS, GOME-2, SCIMACHY and OCO-2. Because the oxygen absorbed bands overlap with the peak of the fluorescence spectrum, the oxygen absorbed bands are thought to be best bands to retrieve the SIF. Combining with the atmospheric information, it is feasible to separate the fluorescence from the reflected energy.

The purpose of this chapter is to assess the atmospheric effect on the SIF retrieval in the O2-A band. Compared with Fraunhofer lines, oxygen absorption bands are used more extensively due to their width and depth. However, the atmospheric effects on oxygen absorption bands can result in an erroneous estimation of SIF (Damm et al., 2014). As the figure 5-1 shows, in this chapter, we use SCOPE and MODTRAN 4 to generate simulated top-of-atmosphere (TOA) data, and we evaluate the sensitivity of atmospheric parameters, including SZA, sensor height, elevation, VIS and water content, to the accuracy of SIF retrieval. In the last part, SIF is retrieved from the hyperspectral image acquired by the AISA sensor with atmospheric parameters to confirm the conclusions of the simulated analysis.

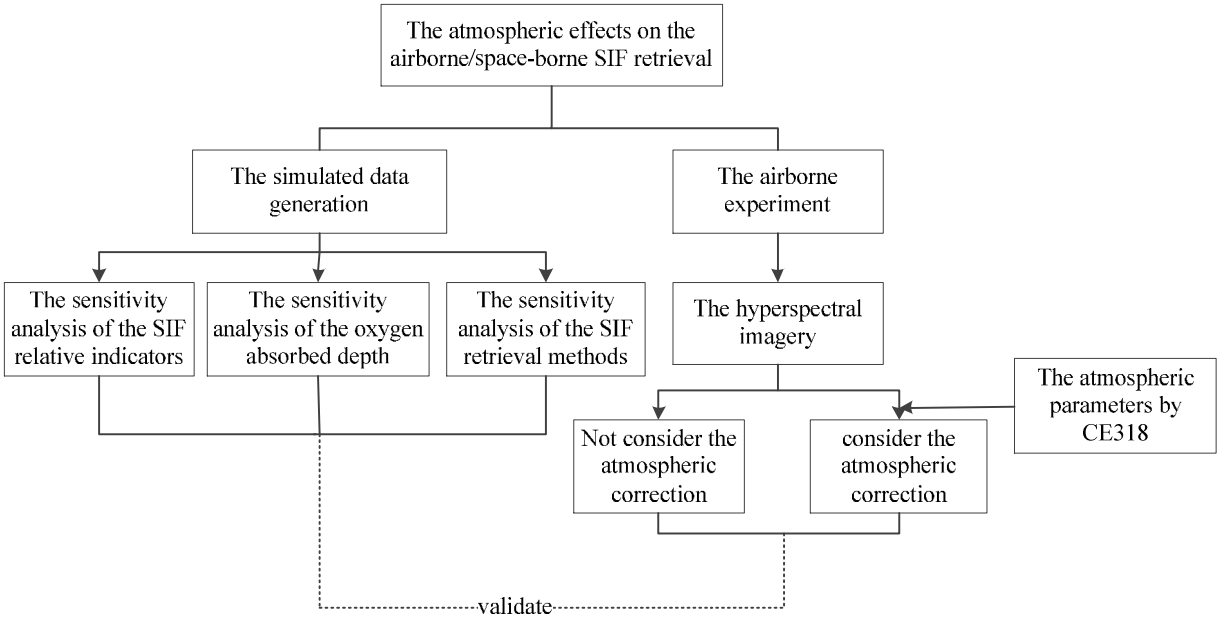


Figure 5-1 Flow chart

## 5.2 Generation of simulated data

In this chapter, the MODTRAN 4 and SCOPE models are used to simulate TOA radiation, including fluorescence radiation. Assuming that SIF and reflectance follow Lambert's law, the radiance at TOA, including SIF radiance, can be described as follows:

$$L_{TOA} = \frac{E_0 \cos(\theta)}{\pi} \rho_{so} + \frac{E_0 \cos(\theta)}{\pi} \frac{(\tau_{ss} + \tau_{sd}) R (\tau_{do} + \tau_{oo})}{1 - R \rho} + \frac{SIF (\tau_{do} + \tau_{oo})}{1 - R \rho} \quad (5\text{-}1)$$

On the right side of this equation, the first item is the atmospheric contribution to the TOA radiance signal, the second item is the surface-reflected radiance, and the last item is the fluorescence signal contribution to the TOA radiance. SIF and R come from the simulation of the SCOPE model, and the other parameters are computed by MODTRAN.

MODTRAN (MODerate resolution atmospheric TRANsmission) is a computer program designed to model atmospheric propagation of electromagnetic radiation for the 100-50000 $cm^{-1}$ (0.2 to 100 μm) spectral range. It covers the spectrum from middle ultraviolet to visible light to far infrared. The most recent version of the code, MODTRAN5, provides a spectral resolution of 0.2 $cm^{-1}$ using its 0.1 $cm^{-1}$ band model algorithm. Some aspects of MODTRAN are patented by Spectral Sciences Inc. and the US Air Force, who have shared development

responsibility for the code and related radiation transfer science collaboratively since 1987. The acronym MODTRAN was registered as trademark of the US Government, represented by the US Air Force, in 2008 (https://en.wikipedia.org/wiki/MODTRAN).

MODTRAN is a 'narrow band model' atmospheric radiative transfer code. The atmosphere is modeled as stratified (horizontally homogeneous), and its constituent profiles, both molecular and particulate, may be defined either using built-in models or by user-specified vertical profiles. MOTRAN solves the radiative transfer equation including the effects of molecular and particulate absorption/emission and scattering, surface reflections and emission, solar/lunar illumination, and spherical refraction. Users put the input parameters into the "*.tp5" according to a specific format, and run the Mod.exe, then get output files: ① *.tp6 contains the standard outputs, describing inputs used, path geometry, warnings, spectral data, and more; ② *.tp7 is the primary MODTRAN spectral output file containing transmittance, radiance and/or irradiance data; ③ *.7sc is a MODTRAN output file containing spectral transmittance, radiance and/or irradiance data that has been scanned using a user-specified filter function; ④ *.tp8 is an auxiliary MODTRAN spectral output file containing spectral data for each path segment along the observer (sensor) lines-of-sight; ⑤ *.plt is a MODTRAN spectral output file containing two columns of data, with a spectral grid in the first column and either transmittance, radiance or irradiance in the second column; ⑥ *.psc is a MODTRAN spectral output file containing two columns of data, with a spectral grid in the first column and either transmittance, radiance or irradiance in the second column. The second column of data has been scanned using a user-defined filter function (http://www.modtran5.com/faqs/index.html; Berk et al., 1999).

To generate the database, 1080 MODTRAN cases (Table 5-1), including four sun zenith angles, four sensor heights, three elevations, five surface meteorological ranges and three vertical water contents, are simulated(Damm et al., 2010 ; Daumard et al., 2015 ; Liu & Liu 2014 ; Joiner et al., 2013; Damm et al., 2014). Every case covers 10000-25000 $cm^{-1}$ at a $1cm^{-1}$ resolution. The atmospheric parameters, including $\rho_{so}$, $\rho$, $\tau_{ss}$, $\tau_{sd}$ and $\tau_{do}$ are computed from the simulated data.

Table 5-1 Input parameters of MODTRAN used in the generation of simulated data

| Parameter | Value | Unit | Description |
|---|---|---|---|
| SZA | 10, 30, 50,70 | Degree | Sun zenith angle |
| Sensor height | 0.5, 1.0, 10, 50, 100, 704 | km | Position of sensor |
| Elevation | 0.0, 0.05, 0.1 | km | Altitude of surface relative to sea level |
| VIS | 10, 20, 30, 40, 50 | km | Surface meteorological range |
| Water content | 0.5, 2.0, 3.5 | $gm/cm^2$ | Vertical water vapor column |

The SCOPE model can simulate fluorescence and reflectance on the canopy using the radiation transfer module and the leaf biochemical model. The input parameters of SCOPE are introduced in detail in the SCOPE documentation (Van der Tol 2013) and in a paper by Ni et al. (2015). In this study, based on the works of Damm et al.(2014), Liu et al. (2015) and Daumard et al.(2015), the chlorophyll $a+b$ content (Cab), fluorescence quantum yield efficiency (Fqe) and leaf area index (LAI) are set varied (Table 5-2). The other parameters are set to the default values. For each atmospheric condition, 48 SCOPE cases are simulated for the generation of reflectance and fluorescence on the canopy. In the final simulation, 43200 cases are generated.

Table 5-2 Input parameters of the SCOPE model

| Parameter | value | Unit | Description |
|---|---|---|---|
| Cab | 20, 40, 60, 80 | $ug/cm^2$ | Chlorophyll content |
| Fqe | 0.02, 0.04, 0.06 | -- | The fluorescence quantum field |
| LAI | 1, 2, 4, 6 | $m^2/m^2$ | Leaf area index |

Figure 5-2 shows the results of the simulated data generation process. Figures 5-2a, b and c show the canopy reflectance, fluorescence and soil spectra, respectively. The reflectance and fluorescence spectra are derived from the SCOPE model, and the soil spectrum is derived from the spectral library of ENVI. The reflectance, fluorescence and soil spectra are inputs into the radiative transfer equation to compute the TOA radiance. Figures 5-2e, f and g show the simulated results regarding the vegetation radiance, including the fluorescence radiance, soil radiance and sun irradiance. Because of the large number of simulated data points, only some data points are used to represent the results.

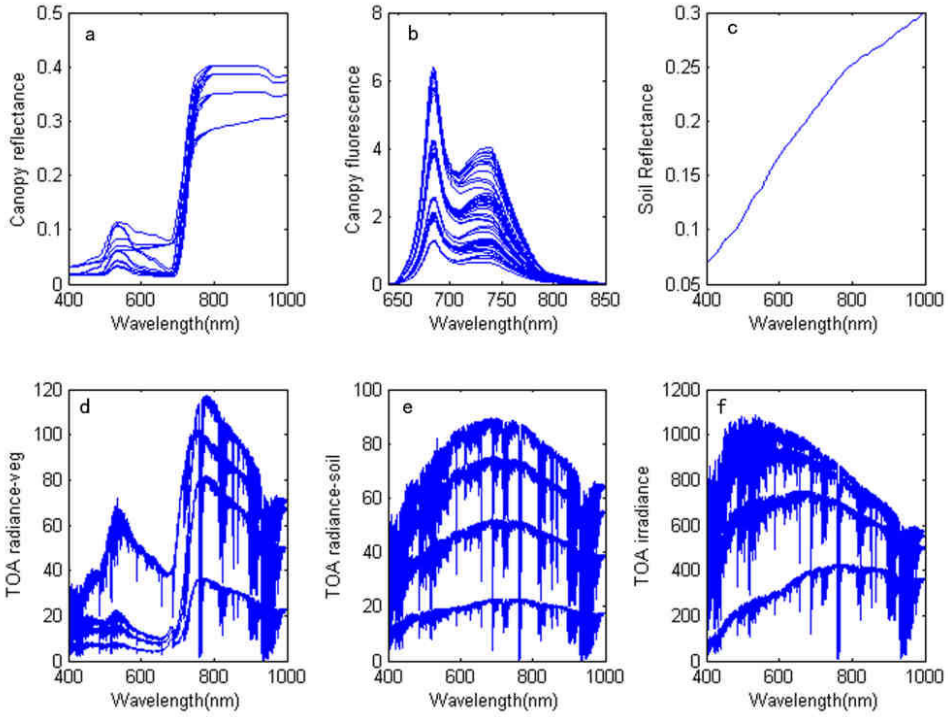


Figure 5-2 Input spectrum and the simulated results

a): Canopy reflectance spectrum from SCOPE; b): Canopy fluorescence spectrum from SCOPE ($W/m^2/\mu m/sr$); c): Soil reflectance spectrum from the library of ENVI; d): Simulated vegetation TOA radiance ($W/m^2/\mu m/sr$); e): Simulated soil TOA radiance ($W/m^2/\mu m/sr$); and f): Solar irradiance ($W/m^2$).

## 5.3 The effects of atmospheric parameters on the SIF retrieval

### 5.3.1 Sensitivity analysis

To illustrate the effects of the atmosphere on TOA radiance, sensitivity analysis is conducted using simulated data to illustrate which atmospheric parameters strongly affected the indicators of fluorescence (Figure 5-3). Gaussian Emulation Machine for Sensitivity Analysis (GEM-SA) software package is used for sensitivity analysis (Leng et al., 2014; Ni et al., 2005b). In sensitivity analysis, the indicator 'total effect' is applied to evaluate the effect of each input parameter on the output.

Figure 5-3a shows that the five atmospheric parameters had different effects on the depth of the oxygen absorption band (depth_oxygen_band). The absorption band depth is computed by dividing the value for one band outside of the absorption band by that for one band inside of the oxygen absorption band. It is expressed as the ratio a/b, in which a is the radiance

outside of the absorption band and b is the radiance inside of it (Daumard et al., 2007, 2015 ; Moya et al., 2004). In the $O_2$-A band, a is determined at 758 nm, and b is measured at 760 nm. In the $O_2$-B band, a is set to 685 nm and b is measured at 687 nm. For the $O_2$-A band, the absorption band depth is sensitive to variations in the SZA and sensor height; the effect of elevation can be ignored. The VIS and water content have minor effects on the absorption band depth. In the $O_2$-B band, the absorption band depth is the most sensitive to variations in sensor height, and the second most sensitive parameter is the SZA followed by the VIS and water content. The effect of elevation is even weaker and can be ignored.

In the Figure 5-3b, the absorption band depth difference is used to show the fluorescence. The absorption band depth difference is computed as the oxygen absorption depth derived from the radiance without the fluorescence minus that including the contribution of fluorescence, marked as depth_nofs-depth_withfs.The SZA has a significant effect on the absorption band depth difference in the oxygen absorption bands. The other parameters have a minor effect and are negligible.

Figure 5-3c shows the effects of variation of the atmospheric parameters on the radiance in the oxygen-absorption band. The radiance includes the fluorescence radiance in the $O_2$-A band. For the $O_2$-A and $O_2$-B bands, each parameter has a similar effect on the radiance, and the SZA, sensor height and VIS are much more sensitive than the other parameters.

In Figure 5-3d, the indicator SIF/radiance is selected for analysis. SIF/radiance (SIF radiance divided by the total radiance) is used to illustrate the contribution of fluorescence to the total radiance at-sensor in the oxygen absorption band. The SZA and sensor height still have strong influences on SIF/radiance.

The results of sensitivity analysis reveal that the SZA and sensor height are two important atmospheric parameters that affect fluorescence retrieval from space-borne data.

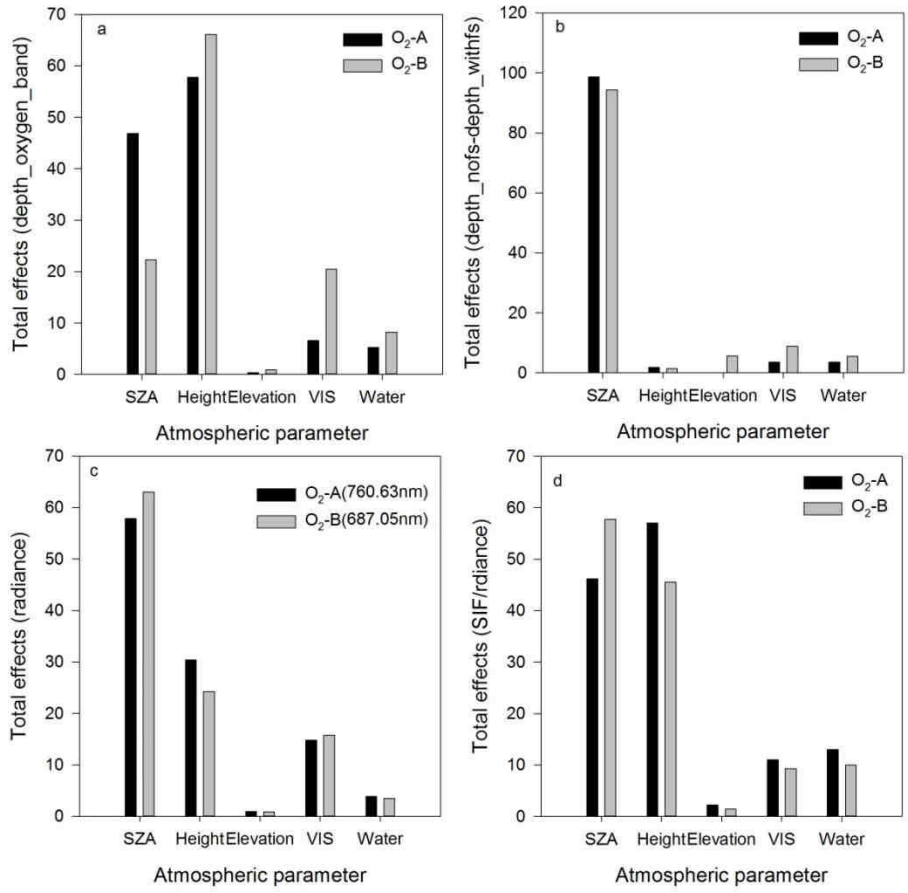


Figure5-3 The results of sensitivity analysis. Four indicators are selected: a): depth_oxygen_band; b): depth_nofs-depth_withfs; c): radiance; and d): SIF/radiance.

## 5.3.2 Effects of atmospheric parameters on the oxygen-absorption depth in the O2-A and O2-B bands

### 5.3.2.1 Solar zenith angle

The SZA causes a strong variation in the path length of solar irradiance. In MODTRAN, the SZA varies from 10° to 70°, with an increment of 20°. The absorption depth in the $O_2$-A band is much larger than that in the $O_2$-B band. With an increase in the SZA, the oxygen absorption depth increases gradually, but it does so more quickly in the $O_2$-A band than in the $O_2$-B band (Figure 5-4a). Because of the variation in the SZA, the observed maximum depth variations are 111.4% in the $O_2$-A band and 27.5% in the $O_2$-B band (Table 5-3). The SZA is an important parameter that affects the $O_2$-A band absorption depth.

#### 5.3.2.2 Sensor height

As shown in Figure 5-4b, with an increase in sensor height, the oxygen-absorption depth first rapidly increases and then slowly changes. The sensor height is set to vary from 0.5 km to 704 km, including 0.5, 1.0, 10, 50, 100 and 704 km. From 0.5 km to 10 km, the oxygen absorption depth changes quickly; and from 10 km to 704 km, the depths tend to be similar. These findings are consistent with Damm's conclusions (Damm et al., 2014). The observed maximum depth variations are 77.1% in the $O_2$-A band and 32.6% in the $O_2$-B band (Table 5-3).

#### 5.3.2.3 Elevation

Sensor height and elevation are two factors that determine the geometric air mass and $O_2$ absorption rates. Notably, the depth decreases as the elevation increases, particularly in the $O_2$-A band (Figure 5-4c). The variation in elevation from 0.0 to 0.1 km causes depth variations of 2.8% in the $O_2$-A band and 0.9% in the $O_2$-B band (Table 5-3).

#### 5.3.2.4 VIS

VIS is the vertical distribution of the aerosol concentration in MODTRAN, and it characterizes the surface meteorological range. VIS can be expressed as a function of AOD (Aerosol Optical Depth) at 550 nm. It varies from a minimum value of 10 km to a maximum value of 50 km, and the depth decreases as VIS increases (Figure 5-4d). The variation in VIS causes depth variations of 17.2% in the $O_2$-A band and 22.4% in the $O_2$-B band (Table 5-3).

#### 5.3.2.5 Water content

Figure 5-4e shows that variation in the water content results in a little change in the oxygen absorption depth, and that the maximum depth variations are only 0.63% in the $O_2$-A band and 0.01% in the $O_2$-B band (Table 5-3). Therefore, the water content is not a sensitive parameter for the depth of either oxygen absorption band. Damm et al. (2014) obtained the similar conclusions.

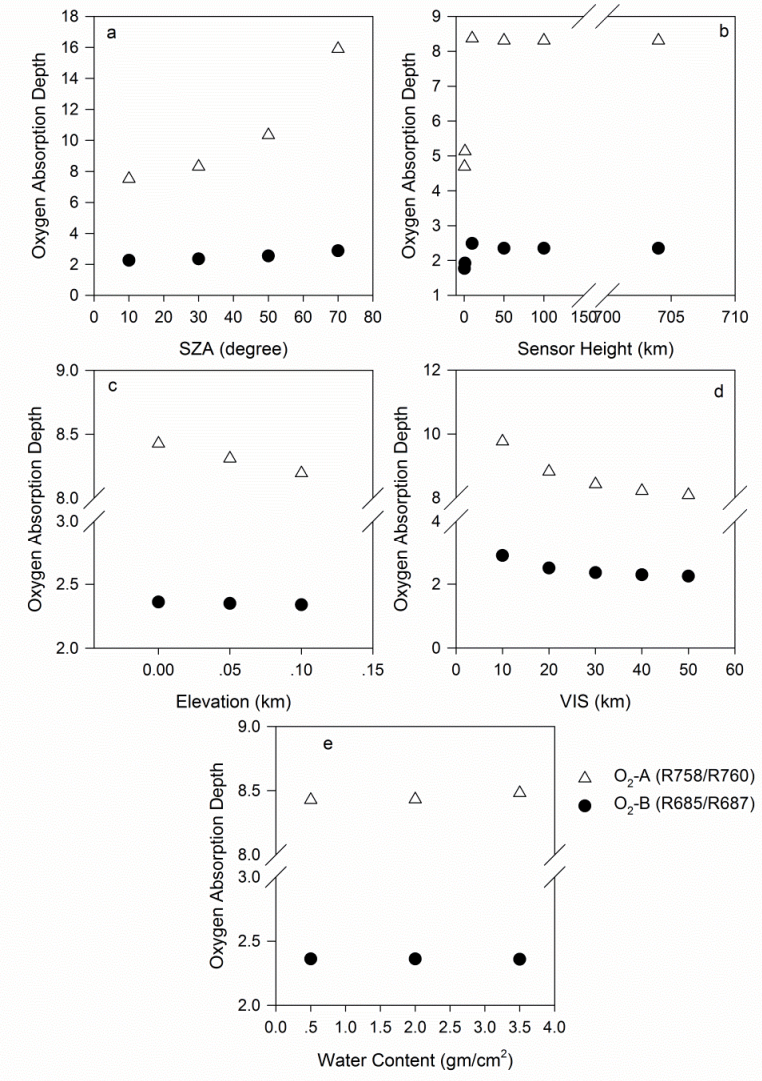


Figure 5-4 Atmospheric effects on the oxygen absorption band depth

Table 5-3 Sensitivity analysis

| Parameter | Variation range | Correlation with depth | Depth variation | |
|---|---|---|---|---|
| | | | $O_2$-A | $O_2$-B |
| SZA | 10-70 | + | 111.4% | 27.5% |
| Sensor height | 0.1-704 km | + | 77.1% | 32.6% |
| Elevation | 0.0-0.1 km | - | 2.80% | 0.90% |
| VIS | 10-50 km | - | 17.2% | 22.4% |
| Water content | 0.5-3.5 gm/cm$^2$ | + | 0.63% | 0.01% |

The depth variation is the maximum variation and is calculated as the variation value divided by the base value

## 5.3.3 The analysis of the SIF retrieval methods

### 5.3.3.1 The SIF retrieval methods

In the chapter 2, we introduce the airborne/space-borne SIF retrieval methods. In this chapter, we select the Damm method (Damm et al., 2010, 2014), DOAS (Khosravi 2012) and Braun method (Raychaudhuri Braun 2014) to retrieve SIF. These three methods exploit different strategies to retrieve fluorescence. FLD/3FLD requires accurate atmospheric parameters; DOAS is carried out based on the physical model; and the Braun method uses the no-vegetation region to remove the effects of the atmosphere.

The expressions of these three methods are introduced in the chapter 2.5. It should be noted that for Damm method, the inside the oxygen absorbed band is 760 nm, and the outside the oxygen absorbed bands are 753 nm and 771 nm separately; for DOAS method, the retrieval spectral window is 745-758 nm; for Braun method, the inside the oxygen absorbed band is 760.46 nm, and the outside the oxygen absorbed bands are 758.03 nm and 771.01 nm.

### 5.3.3.2 Comparison of the three methods of retrieving fluorescence

In the chapter 5.3.3.1, three methods of estimating fluorescence are introduced. Based on the simulated data, these three methods are employed to compute fluorescence. The results of these methods are compared with the fluorescence at 761 nm derived from SCOPE (SCOPE SIF), and two indicators are used to assess the performance of these two methods: the correlation parameter ($R^2$), and root mean square error (RMSE).

Table 5-4 shows that the fluorescence values computed using the Damm and DOAS methods in the $O_2$-A and $O_2$-B bands are strongly correlated with the SCOPE SIF values, whereas the values determined using the Braun method are negatively correlated with the SCOPE SIF values in the oxygen-absorption bands. These findings indicate that marked differences exists between the Braun method and SCOPE SIF. From the Table 5-4, it can be found that the RMSEs of the three methods are relatively small in the $O_2$-A band and are larger for the Damm and DOAS methods in the $O_2$-B band. The findings for these three indicators suggest that the Damm method has the best performance, particularly in the oxygen-A band. DOAS is also acceptable for determination of fluorescence, despite the large standard deviation in the oxygen-B band. In contrast, the Braun method cannot be used to

estimate fluorescence, as the accuracy and error of the estimated fluorescence may not satisfy our requirements.

Table 5-4 Comparison of Damm, Braun and DOAS methods

| | $O_2$-A band | | $O_2$-B band | |
|---|---|---|---|---|
| | $R^2$ | RMSE | $R^2$ | RMSE |
| Damm vs. SCOPE SIF | 0.99 | 0.13 | 0.88 | 0.84 |
| Braun vs. SCOPE SIF | -0.20 | 1.37 | -0.73 | 5.31 |
| DOAS vs. SCOPE SIF | 0.78 | 0.40 | 0.66 | 1.58 |

RMSE unit: W/m²/μm/sr

The comparisons among the fluorescence values derived from the three methods and SCOPE SIF indicate the Damm and DOAS methods have good retrieval accuracy. The effects of the atmospheric parameters on these two methods are analyzed in Table 5-5. In this study, the maximum variation is used in analysis and is calculated as the variation value divided by the base value. In the $O_2$-A band, the variation of SZA and sensor height cause -9.80% and 2.3% of the fluorescence estimated by the Damm method. The equivalent fluorescence variation values are -0.13 and 0.03 W/m2/μm/sr, and the effects of the elevation and water content can be neglected. In the $O_2$-B band, the results of sensitivity analysis of the atmospheric parameters are similar for the Damm method. For the DOAS method, VIS is the only sensitive parameter in the $O_2$-A band, and the variation in VIS causes a 61.8% fluorescence variation. The effects of SZA, sensor height and elevation are negligible. In the $O_2$-B band, elevation is the sensitive parameter, and it causes a variation of 113%. Notably, because of the characteristics of DOAS, in the process of data fitting, the initial value of the model must be given, and the selection of the initial value can result in the abnormal results using this method.

Table 5-5 Study of the sensitivities of different methods to atmospheric parameters.

| Indicator | Band | Method | SZA | Sensor height | Elevation | VIS | Water content |
|---|---|---|---|---|---|---|---|
| | | | 10°-70° | 0.5-704 km | 0.0-0.1 km | 10-50 km | 0.5-3.5 gm/cm² |
| Variation | $O_2$-A | Damm | -9.80% | 2.30% | 0.00% | -0.06% | 0 |
| | | DOAS | 0.00% | 0.00% | 0.00% | 61.80% | 0.44% |
| | $O_2$-B | Damm | 19.40% | 13.50% | 0.12% | 0.62% | 0.41% |
| | | DOAS | 0.03% | 0.12% | 113% | 0.66% | 0.01% |
| ΔF W/m²/μm /sr | $O_2$-A | Damm | -0.13 | 0.03 | 0.0004 | -0.0008 | 0 |
| | | DOAS | -0.0003 | -0.00018 | 0 | -0.74 | 0 |
| | $O_2$-B | Damm | -0.88 | 0.49 | 0.005 | 0.03 | -0.02 |
| | | DOAS | 0 | 0.004 | -3.9 | -0.002 | 0 |

The variation is the observed maximum fluorescence variation, and it is calculated as the variation value divided by the base value. ΔF is the max value of variation in fluorescence. The reference configuration is for SZA=30°, sensor_height=704 km, elevation=0.0 km, VIS=30 km and water content=0.5 gm/cm$^2$. To assess the performance of one parameter, the other parameters are set as a reference configuration.

## 5.4 The airborne experiment

The airborne experiment was conducted on September 1, 2013 in Baoding, Hebei Province, China (Figure 5-5). The study site is an agricultural area with maize and trees such as toon and elm, and the mean elevation is 16.8 m. In the experiment, the AisaEAGLE hyperspectral imaging system is set in the airship to obtain the hyperspectral image, and the PAM-2500 is used to measure the fluorescence on the ground, besides, the CE318 photometer is used to get the atmospheric information.


Figure 5-5 The research region

### 5.4.1 AisaEAGLE hyperspectral imaging system

An airborne hyperspectral imaging system designed by Specim Spectral Imaging Oy Ltd., Finland, is carried on the airship (Figure 5-6a) in this experiment, including an AisaEAGLE sensor, a data acquisition and power unit (DPU), a high-performance GPS/IMU positioning system (POS) and CaliGeoPRO software (Figure 5-6b). The AisaEAGLE sensor is a high-performance airborne visible and near infrared (VNIR) push-broom hyperspectral system in the 400-970 nm spectral range with 3.3-nm spectral resolutions. The sensor parameters are listed in Table 5-6. The POS uses RT3100 produced by Oxford Technical Solutions, England, with a positioning accuracy of 0.5 m. The original image is radiometrically and geometrically corrected using CaliGeoPRO software package. In this work, the reference white board (Figure 5-6c) is set in a blank area in the research area.

The hyperspectral data are acquired from 16:00 to 17:00 UTC+8 using an AisaEAGLE sensor at a 400-m altitude. At the same time, a high-performance field and laboratory chlorophyll fluorometer (PAM-2500) is used to measure the chlorophyll fluorescence parameter on the ground.

Table 5-6 The AisaEAGLE sensor parameters

| | |
|---|---|
| Spectral range | 400-970 nm |
| Spectral resolution | 3.3 nm |
| Spectral sampling interval | 0.67 nm |
| Focal length | 18.5 mm |
| FOV | 36.7 degrees |
| IFOV | 0.036 degrees |
| Swath width | 0.66 x altitude |
| Ground resolution @ 400-m altitude | 0.32 m |
| SNR | 1250:1 (maximum theoretical) |

### 5.4.2 CE318 photometer

A CE318 photometer (Figure 5-6d), designed by Cimel Electronique S.A.S in Paris, was used to measure the optical properties of the atmosphere. It provides quantification and physical-optical characterization of the aerosols. The SZA, VIS and water content are

extracted from the measured data for CE318 (Table 5-7), and these parameters are then entered into MODTRAN to obtain the atmospheric parameters.

Table 5-7 The retrieved parameters by CE318

| Parameter | Value | Unit |
|---|---|---|
| SZA | 30.10 | degree |
| Water content | 3.97 | gm/cm$^2$ |
| VIS | 44.48 | km |


Figure 5-6 Experimental setup

a): airship; b): AisaEAGLE airborne Hyperspectral Imaging System; c): reference white board; d): CE318

## 5.5 The analysis of the airborne experiment

The oxygen absorption band is the main window to retrieve the SIF. In this chapter, we analyze the effects of the atmospheric absorption and scattering on the oxygen absorption depth. The oxygen absorption depth is determined by the atmosphere and the filling of the SIF. Through the analysis of oxygen absorption depth, we can understand the effects of the atmosphere on the SIF retrieval directly.

### 5.5.1 Using the Damm method to retrieve fluorescence from airborne imagery

The analysis in chapter 5.3 highlights the importance of atmospheric effects, and it also demonstrates that these effects can be compensated for to obtain accurate SIF measurements using atmospheric absorption features. In this experiment, CE318 is used to measure the atmospheric parameters (Table 5-7), and through MODTRAN, the required atmospheric parameters are computed. The Damm method is used to retrieve fluorescence from AISA imagery. Figure 5-7 depicts the AISA imagery (true-color composite), and five types of vegetation are selected for analysis.

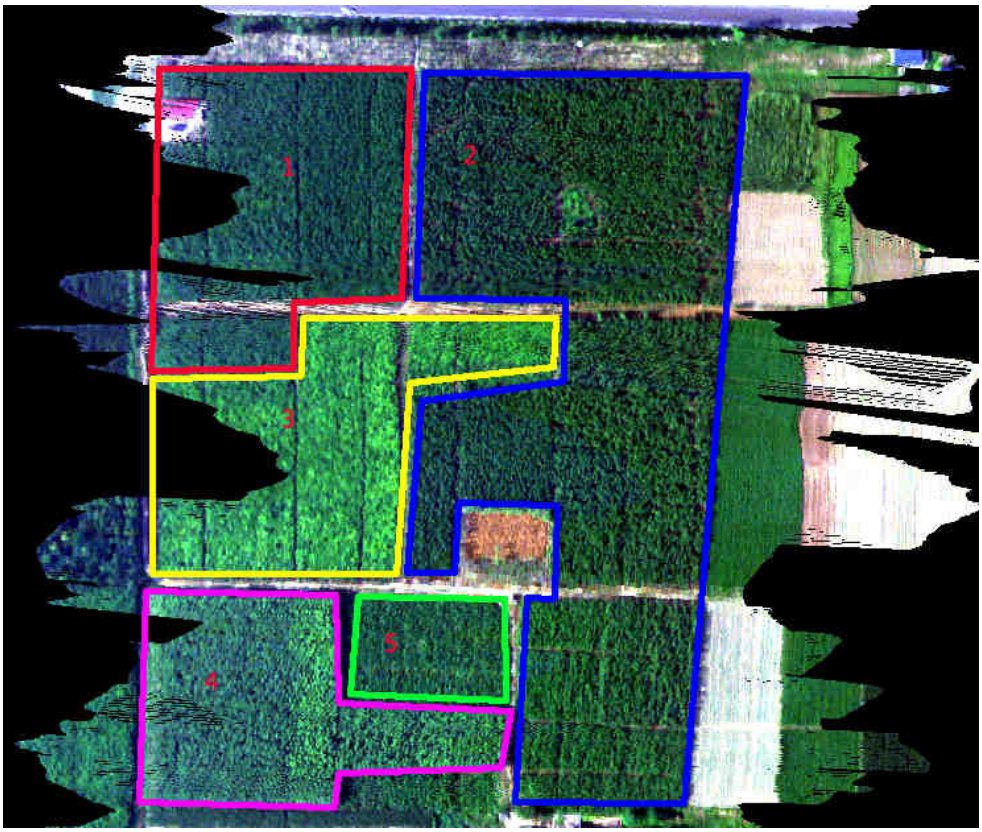


Figure 5-7 Airborne hyperspectral imagery acquired with an AISA sensor, shown as a true-color composite. Different plants are marked in the figure: 1: ailanthus; 2: elm; 3: mountain peach; 4: willow; and 5: Chinese ash

The 3FLD and Damm methods are introduced in section 2.4. In the formulas, L and Eg are the surface-reflected radiance and solar irradiance, respectively. When retrieving fluorescence, L is obtained directly from the hyperspectral image, and Eg is obtained from the reference white board. Figure 5-8 shows the results of fluorescence retrieval using the Damm method, and Figure 5-9 presents the fluorescence retrieved using the 3FLD method without considering the atmospheric information. Figure 5-8shows that the fluorescence values of elm

and Chinese ash are higher than those of the other three types of vegetation and that there are differences among these five types of vegetation. However, it is difficult to draw a clear dividing line between the adjacent vegetation. It is clear that the fluorescence retrieval results are affected by noise. The same conclusions can be made from Figure 5-9.

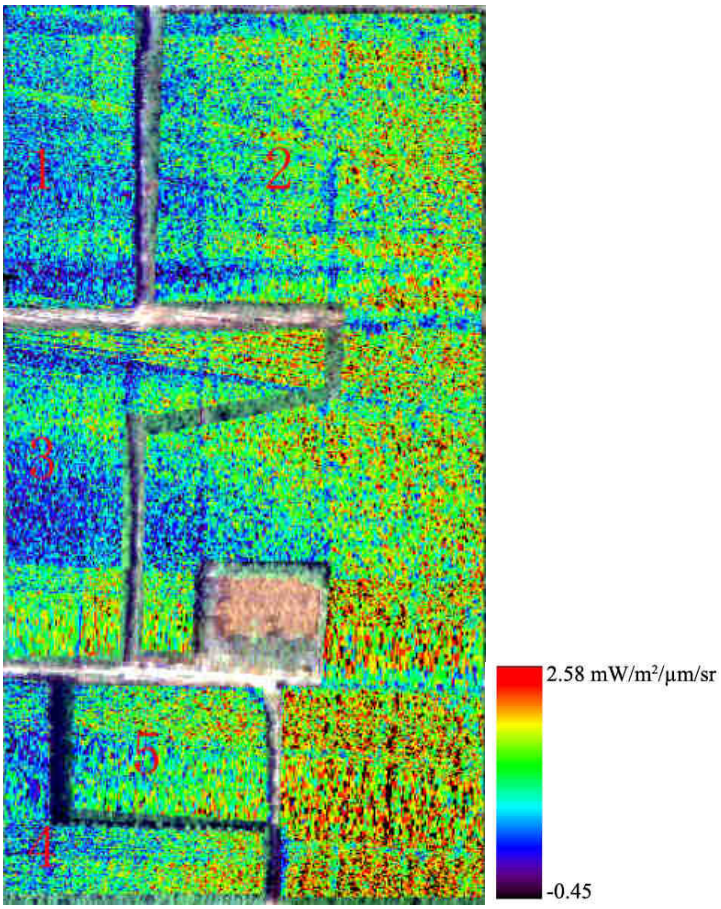


Figure 5-8 Retrieved fluorescence from AISA imagery using the Damm method with atmospheric information; 1: ailanthus; 2: elm; 3: mountain peach; 4: willow; and 5: Chinese ash.

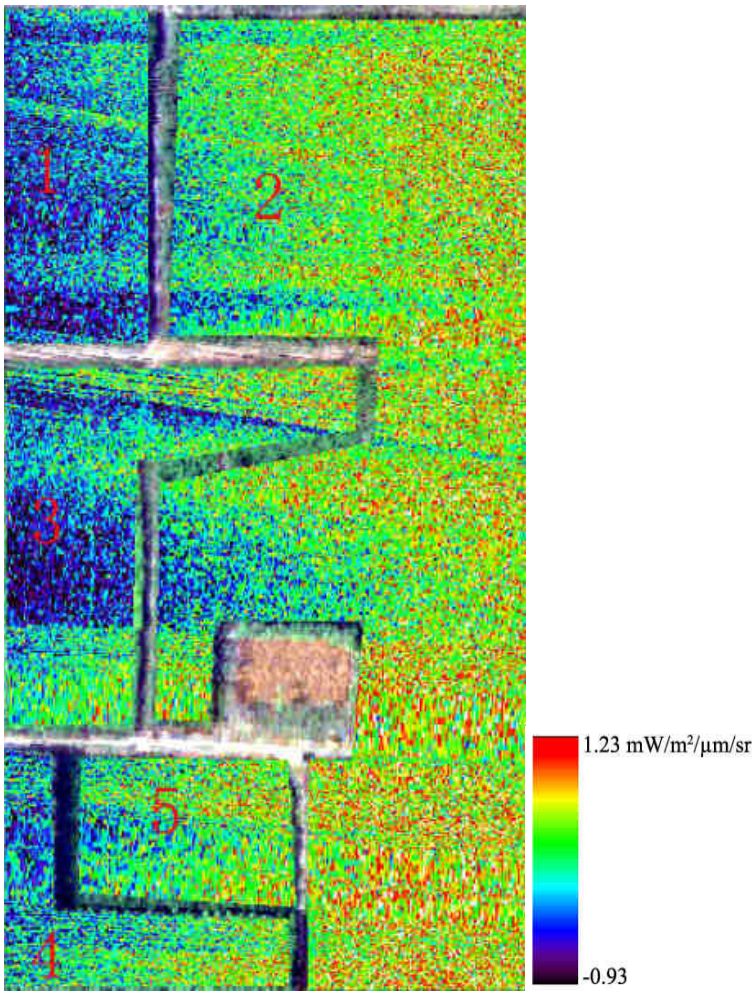


Figure 5-9 Retrieved fluorescence from AISA imagery using the 3FLD method; 1: ailanthus; 2: elm; 3: mountain peach; 4: willow; and 5: Chinese ash

## 5.5.2 The comparison between retrieved fluorescence and ground measurement

A comparison between Figures 5-8 and 5-9 reveals that accurate atmospheric information can improve retrieval accuracy. In the experiment, the PAM is used to measure the steady-state fluorescence of vegetation, whereas the sensor collects data. A comparison between the fluorescence derived from the airborne data and that from PAM-2500 is conducted. $R^2$ between the retrieved fluorescence using the Damm method and PAM-2500 is 0.91 (Figure 5-10a), whereas that between the retrieved fluorescence using the 3FLD method and PAM-2500 is 0.65 (Figure 5-10b). These results indicate that fluorescence derived from the airborne data is reliable and that results obtained using the Damm method are much closer to the PAM measurements than those obtained using the 3FLD method. Figure 5-10c shows that there are differences in fluorescence among the different types of vegetation. The mean fluorescence value for each type of vegetation is used herein to illustrate the trend in the variation of

vegetation. The results of the PAM measurements demonstrate that the fluorescence of Chinese ash is the highest among the five types of vegetation, followed by elm, mountain peach, willow and ailanthus. The results of the airborne measurement indicate that the fluorescence values of Chinese ash and elm are greater than those of the other vegetation. The trend of variation of the vegetation is consistent between the two measurement scales. These findings also indicate that it is possible to detect different types of vegetation using fluorescence.

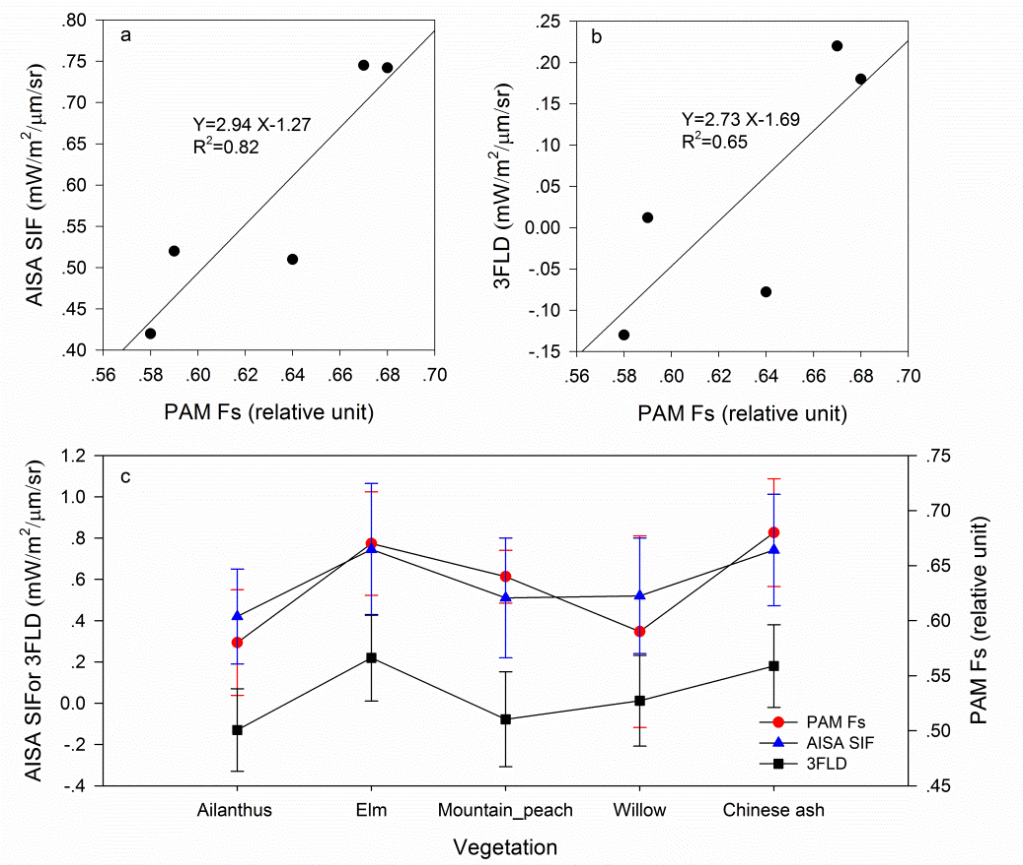


Figure 5-10 The Comparison between AISA SIF and PAM Fs:
a is the relationship between AISA SIF and PAM Fs; b is the relationship between 3FLD and PAM Fs; and c is the comparison of fluorescence among the five types of vegetation.

## 5.6 Conclusions

The effects of the atmosphere are not negligible in the method of retrieving fluorescence. Therefore, in this chapter, we firstly study the effects of the atmospheric parameters on fluorescence in oxygen-absorption bands using simulated data generated by MODTRAN and SCOPE. Under the different combinations of canopy (Cab, Fqe and LAI), atmospheric (VIS

and water content) and imaging geometric parameters (SZA, sensor height and elevation), the TOA radiance, including the contribution of fluorescence, is simulated by the radiation transfer equation. We test the sensitivities of five parameters (SZA, sensor height, elevation, VIS and water content) to the oxygen absorption depth and other indicators relative to fluorescence. Then, we examine the accuracies of the Damm, Braun and DOAS methods for fluorescence retrieval and the performances of these three methods under variation of the atmospheric parameters. Finally, we apply the Damm method to the AISA airborne image and compare airborne fluorescence with ground measurements.

The main conclusions are as follows:

(1) Sensitivity analysis shows that SZA, sensor height and VIS are the significant and sensitive parameters of these four indicators. We focus on the sensitivity of the atmospheric parameters on the oxygen absorption depth. The depth increases gradually with increases in SZA and sensor height. In contrast, it decreases with increases in VIS and elevation, and it changes little with variation in water content.

(2) Analysis of Damm method, Braun and DOAS shows that the accurate atmospheric parameters can improve the SIF retrieval accuracy. Besides, the Damm method is sensitive to variations in SZA and sensor height in the $O_2$-A and $O_2$-B bands. For the DOAS method, elevation and VIS are sensitive parameters in the $O_2$-A and $O_2$-B bands, respectively.

(3) We use the Damm and 3FLD methods to retrieve fluorescence from an AISA airborne image, and the results of these two methods have the close relationship with the PAM-2500 measurements and the performance of the Damm method is better than that of the 3FLD method. Analysis of five plants, *i.e.*, ailanthus, elm, mountain peach, willow and Chinese ash, revealed the presence of differences in fluorescence among the different types of vegetation. Among these five types of vegetation, the fluorescence values of Chinese ash and elm are greater than those of the other vegetation. The variation trends of the fluorescence using the active and passive fluorescence are consistent.

# Chapter6. Conclusions and perspectives

Chlorophyll fluorescence is a new way to monitor the vegetation state, and play an important role in the global carbon cycle, vegetation photosynthesis and so on. Based on the knowledge of the fluorescence remote sensing, we develop the SIF detection at the leaf-scale, near the ground and the airborne/space-borne. In this chapter, we summarize the main conclusions and the remained problems and propose perspectives.

## 6.1 Main conclusions

The main conclusions of this thesis are as follows:

**(1) Leaf chlorophyll fluorescence detection under the different water content**

SCOPE model is used to simulate the response of SIF and temperature to the different stress. When the plant is in stress condition, the SIF diminishes, and temperature augments. The daily variation of the SIF and temperature first increases and then decreases and the SIF difference under the different water content reaches to the maximum at noon.

The potted maize is the research object, and treated with the water control in the heading stage. In the heading stage, maize needs a large amount of water to keep the normal production. The water control experiment includes the gradient water and the filling water experiments. Through these two experiments, we analyze the variation of the chlorophyll fluorescence (active and passive fluorescence), the temperature and the soil water content. The gradient experiment illustrates that the chlorophyll fluorescence and the temperature can reflect the early water stress. In condition of water stress, the chlorophyll fluorescence is low, and the temperature is high.

After the filling water, all the potted maize is treated with the same amount of water. In the early water stress, the plant tissue is not destroyed owing to water deficit. Because the timely water can relieve the water stress, the vegetation can recover to the healthy state. Chlorophyll fluorescence recovers to the healthy state with the water stress relieving, but the temperature doesn’t recover to the healthy state. It fully illustrates that the chlorophyll fluorescence is more sensitive than the temperature to the early water stress, and that chlorophyll fluorescence combined with temperature observations can improve the remote sensing monitoring early water stress.

Through the comparison between active and passive fluorescence in the water control experiment, the result shows that the active measurement is consistency with the passive measurement, and that the active fluorescence can validate the passive measurement accuracy.

**(2) SIF retrieval method near the ground using the reflectance index**

The FluorMOD model is used to simulate the SIF without considering the stress condition. The results of the sensitive analysis of FluorMOD show that the flurescence@761nm is sensitive to the sun zenith angle θ, the fluorescence quantum yield Fi, the temperature T, the leaf area index LAI, the leaf distribution function LIDF and the chlorophyll content Cab. Assuming the LIDF to be a spherical distribution, a simulated database is generated including θ, Fi, T, LAI and L(F)761. From the existed reflectance index, we select three optimal reflectance indices: R685/R850, R740/R630 and R750/R710. These three reflectance index are not sensitive to the variation of LAI and Cab, and are only affected by θ, Fi and T. The quantitative relationships between L(F)761 and the reflectance indices are built to retrieve the SIF quantitatively. The results of this method are compared with the results of FLD and 3FLD methods, and the $R^2$ and RMSE show that it is feasible to use this method to retrieve the fluorescence quantitatively.

The traditional reflectance-based methods only estimate the SIF qualitatively, and do not allow reaching quantitative fluorescence value. The method developed using the reflectance index provides the new way for retrieving the SIF, and paves the way to combine hyperspectral and thermal infrared remote sensing to retrieve fluorescence.

**(3) The atmospheric effects on the airborne/space-borne SIF retrieval**

The study of the airborne/space-borne SIF detection is the current hot topic. In this thesis, with the combination of the different vegetation parameters (chlorophyll content, fluorescence quantum yield, leaf area index), atmospheric parameters (visibility and water vapor content) and imaging geometry parameters (solar zenith angle, satellite altitude and elevation), MODTRAN and SCOPE model are combined to generate the simulated radiance data including the fluorescence contribution. The four indicators associated with the chlorophyll fluorescence are selected: depth_oxygen_band, depth_nofs-depth_withfs, radiance and fs/radiance. Sensitivity analysis shows that the four indicators parameters are sensitive to the variation of sun zenith angle and satellite altitude. On this basis, we analyze the effect of atmospheric parameters on the oxygen absorption depth. The results show that the variations

of sun zenith angle and satellite altitude have a large impact on the oxygen absorption band in $O_2$-A and $O_2$-B band, especially in the $O_2$-A band.

The airborne/space-borne SIF extraction methods can be divided into two categories: the method based on the oxygen absorption band and the algorithm based on Fraunhofer lines. We choose three methods (Damm, DOAS and Braun methods) to obtain the SIF, and compare the SIF with SCOPE SIF. The correlation parameter and RMSE show that the Damm method yields the best results following by DOAS and Braun method. Therefore, Damm method is the prior selection among these three methods.

The analysis of Damm method, DOAS and Braun method show that accurate atmospheric parameters can improve SIF extraction accuracy. The airborne hyperspectral data in Baoding site are used to retrieve the SIF using the different methods. The first, one is Damm method which takes into account the atmospheric correction, and other is 3FLD method without atmospheric correction. The retrieved SIF is compared with the PAM measurements, and the results show that the correction parameter for Damm vs. PAM Fs is 0.91, and that for 3FLD vs. PAM Fs is 0.65. It can be found that the retrieval accuracy of Damm method is much higher than that of 3FLD method. It also reveals that accurate atmospheric correction can improve the retrieval accuracy. Besides, five types of vegetation are selected to show that the vegetation type can affect the fluorescence yield, and the comparison between active and passive fluorescence of five types of vegetation also illustrate the consistency of active and passive measurement.

## 6.2 Discussions and perspectives

Despite that the study of multi-scale SIF detection has made some achievements in this thesis, there are still problems to be solved.

(1) In the water control experiment, the soil water content is used to express the vegetation water state. However, the soil water content has a difference with the vegetation water content. In future experiment, it should be good to measure the leaf water potential directly to improve the experimental convincingness. Besides, the design of airborne experiments with different flying attitudes can further illustrate the role of atmospheric correction for the SIF retrieval.

(2) The fluorescence models used in this paper are FluorMOD and SCOPE. In the process of the simulated data generation, leaf distribution function is set to spherical in order to avoid overly complex analysis. Despite the spherical distribution is the common LIDF, it will be interesting to consider different kinds of LIDF to cover the comprehensive data.

(3) In the quantitative SIF retrieval method using the reflectance index, it is validated by the traditional methods (FLD and 3FLD). Through the comparison between this method and the traditional methods, it shows that SIF method is feasible to retrieve the SIF quantitatively. Besides, it still needs to be validated using the field data.

(4) When we investigate the effects of atmospheric absorption and scattering on the SIF retrieval, we consider the effects of the several atmospheric parameters. In future study, we should consider more parameters and widen the range of the selected parameter in order to increase the coverage. In addition, we can analyze the effects of the atmospheric parameters on more SIF retrieval methods. In this thesis, we only analyze three SIF retrieval methods. It is necessary to give the full analysis of all SIF retrieval methods and analyze carefully the advantages and disadvantages of the SIF retrieval methods.

SIF is thought to be a direct, effective and non-destruction probe to monitor the vegetation, and is paid much more attention by the researchers. The basic theory of chlorophyll fluorescence, the retrieval methods and its applications have gradually developed and improved. The problems, such as the global ecological balance, the contradiction between the crop production and the population increasing, make people to focus on the problem of vegetation. Because of the close relationship between the chlorophyll fluorescence and photosynthesis, the chlorophyll fluorescence attracts more and more people's attention. The FLEX project developed by ESA takes the SIF detection as the main task. Through the continually competition, the FLEX project was selected as the eighth earth explorer project on Nov. 2015, and the fluorescence satellite is planned to launch in 2022. FLEX project can provide more information about the land surface vegetation, and also provide the much better quality data source, and further promote the application of chlorophyll fluorescence.

# Reference

Acharya, P. K, Berk, A., Bernstein, L. S., Matthew, M. W., Adler-Golden, S. M., Robertson, D. C., Anderson, G. P., Chetwynd, J. H., Kneizys, F. X., & Shettle, E. P. 1998. "MODTRAN user's manual versions 3.7 and 4.0." *Air Force Research Laboratory, Space Vehicles Directorate, Hanscom Air Force Base, Mass*.

Agati, G., Mazzinghi, P., Fusi, F., & Ambrosini, I. 1995. "The F685/F730 Chlorophyll Fluorescence Ratio as a Tool in Plant Physiology: Response to Physiological and Environmental Factors*." *Journal of Plant Physiology* 145 (3):228-238.

Agati, G., Cerovic, Z. G. &Moya, I. 2000. "The effect of decreasing temperature up to chilling values on the in vivo F685/F735 chlorophyll fluorescence ratio in Phaseolus vulgaris and Pisum sativum: The role of the photosystem I contribution to the 735 nm fluorescence band." *Photochemistry and Photobiology* 72 (1):75-84.

Agati, G., Foschi, L., Grossi, N., Guglielminetti, L., Cerovic, Z.G., &Volterrani, M. 2013. Fluorescence-based versus reflectance proximal sensing of nitrogen content in Paspalum vaginatum and Zoysia matrella turfgrasses. *European journal of agronomy*, 45: 39-51.

Agati, G., Foschi, L., Grossi, N., &Volterrani, M. 2015. In field non-invasive sensing of the nitrogen status in hybrid bermudagrass (Cynodon dactylon× C. transvaalensis Burtt Davy) by a fluorescence-based method. *European Journal of Agronomy*, 63: 89-96.

Alonso, L., Gómez-Chova, L., Vila-Francés, J., Amorós-López, J., Guanter, L., Calpe, J., & Moreno, J. F. 2007. Sensitivity analysis of the fraunhofer line discrimination method for the measurement of chlorophyll fluorescence using a field spectroradiometer. Paper presented at the IGARSS, pp. 3756-3759.

Alonso, L., Gomez-Chova, L., Vila-Frances, J., Amoros-Lopez, J., Guanter, L., Calpe, J., & Moreno, J. F. 2008. "Improved Fraunhofer Line Discrimination method for vegetation fluorescence quantification." *Geoscience and Remote Sensing Letters, IEEE* 5 (4):620-624.

Alatayud, A., & Barreno, E. 2001. Chlorophyll a fluorescence, antioxidant enzymes and lipid peroxidation in tomato in response to ozone and benomyl. *Environmental Pollution*, 115(2), 283-289.

Amoros-Lopez, J., Gomez-Chova, L., Vila-Frances, J., Alonso, L., Calpe, J., Moreno, J., & del Valle-Tascon, S. 2008. "Evaluation of remote sensing of vegetation fluorescence by the analysis of diurnal cycles." *International Journal of Remote Sensing* 29 (17-18):5423-5436.

Bürling, K., Cerovic, Z. G., Cornic, G., Ducruet, J. M., Noga, G., & Hunsche, M. 2013. "Fluorescence-based sensing of drought-induced stress in the vegetative phase of four contrasting wheat genotypes." *Environmental and Experimental Botany* 89:51-59.

Baker, N. R. 2008. "Chlorophyll fluorescence: a probe of photosynthesis in vivo." *Annu. Rev. Plant Biol.* 59:89-113.

Bellvert, J., Marsal J., Girona J., and Zarco-Tejada P. J. 2015. "Seasonal evolution of crop water stress index in grapevine varieties determined with high-resolution remote sensing thermal imagery." *Irrigation Science* 33 (2):81-93.

Berk, A. G. P. A., Anderson, G. P., Acharya, P. K., Chetwynd, J.H., Bernstein, L. S., Shettle, E. P., Matthew ,M.W., & Adler-Golden, S.M. 1999. "MODTRAN4 user's manual." *Air Force Research Laboratory, Space Vehicles Directorate*:1-5.

Berni, J. A. J., Zarco-Tejada, P. J., Sepulcre-Cantó, G., Fereres, E., & Villalobos, F. 2009b. "Mapping canopy conductance and CWSI in olive orchards using high resolution thermal remote sensing imagery." *Remote Sensing of Environment* 113 (11):2380-2388.

Buddenbaum, H., Rock, G., Hill, J., &Werner, W. 2015. Measuring stress reactions of beech seedlings with PRI, fluorescence, temperatures and emissivity from VNIR and thermal field imaging spectroscopy. *European Journal of Remote Sensing*, 48, 263-282.

Bussotti, F., Desotgiu, R., Cascio, C., Pollastrini, M., Gravano, E., Gerosa, G., &Manes, F. 2011. Ozone stress in woody plants assessed with chlorophyll a fluorescence. A critical reassessment of existing data. *Environmental and Experimental Botany*, 73, 19-30.

Calatayud, A., &Barreno, E. 2001. Chlorophyll a fluorescence, antioxidant enzymes and lipid peroxidation in tomato in response to ozone and benomyl. *Environmental Pollution*, 115(2), 283-289.

Calatayud, A., Ramirez, J. W., Iglesias, D. J., &Barreno, E. 2002. Effects of ozone on photosynthetic $CO_2$ exchange, chlorophyll a fluorescence and antioxidant systems in lettuce leaves. *Physiologia Plantarum*, 116(3), 308-316.

Calatayud, A., &Barreno, E. 2004. Response to ozone in two lettuce varieties on chlorophyll a fluorescence, photosynthetic pigments and lipid peroxidation. *Plant Physiology and Biochemistry,* 42(6), 549-555.

Campbell, P. E., Middleton, E. M., Corp, L. A., & Kim, M.S. 2008. "Contribution of chlorophyll fluorescence to the apparent vegetation reflectance." *Science of the Total Environment* 404 (2):433-439.

Campbell, P. E., Middleton, E. M., McMurtrey, J. E., & Chappelle, E.W. 2007. "Assessment of vegetation stress using reflectance or fluorescence measurements." *Journal of environmental quality* 36 (3):832-845.

Carter, G.A., Jones, J.H., Mitchell, R.J., & Brewer, C.H. 1996. Detection of solar-excited chlorophyll a fluorescence and leaf photosynthetic capacity using a Fraunhofer line radiometer. *Remote Sensing of Environment*, 55(1):.89-92.

Chaerle, L., Leinonen, I., Jones, H. G., & Van Der Straeten, D. 2007. "Monitoring and screening plant populations with combined thermal and chlorophyll fluorescence imaging." *Journal of experimental botany* 58 (4):773-784.

Cheng, Y. B., Middleton, E. M., Zhang, Q., Huemmrich, K. F., Campbell, P. K. E., Cook, B. D., Kustas, W. P., & Daughtry, C. S. 2013. "Integrating Solar Induced Fluorescence and the Photochemical Reflectance Index for Estimating Gross Primary Production in a Cornfield." *Remote Sensing* 5 (12):6857-6879.

Corp, L. A., Middleton, E. M., Daughtry, C. S. T., & Campbell, P. K. E. 2006. Solar induced fluorescence and reflectance sensing techniques for monitoring nitrogen utilization in corn. Paper presented at the Geoscience and Remote Sensing Symposium, IGARSS. IEEE International Conference.

Corp, L. A., McMurtrey, J. E., Middleton, E. M., Mulchi, C. L., Chappelle, E. W., & Daughtry, C. S. T. 2003. "Fluorescence sensing systems: In vivo detection of biophysical variations in field corn due to nitrogen supply." *Remote Sensing of Environment* 86 (4):470-479.

Corp, L. A., Middleton, E. M., Campbell, P. K. E., Huemmrich, K. F., Cheng, Y.-B., &Daughtry, C. S. T. 2009. "Remote sensing techniques to monitor nitrogen-driven carbon dynamics in field corn." In Proc. of SPIE, 7454( 745403-1).

Ciompi, S., Gentili E., Guidi L. Soldatini G.F. 1996. The effect of nitrogen deficiency on leaf gas exchange and chlorophyll fluorescence parameters in sunflower. *Plant Science*, 118(2): 177-184.

Damm, A., Elbers, J. A. N., Erler, A., Gioli, B., Hamdi, K., Hutjes, R., Kosvancova, M., Meroni, M., Miglietta, F., & Moersch, A. 2010a. "Remote sensing of sun ‐ induced fluorescence to improve modeling of diurnal courses of gross primary production (GPP)." *Global Change Biology* 16 (1):171-186.

Damm, A., Schickling, A., Schläpfer, D., Schaepman, M., &Rascher, U. 2010b. Deriving sun-induced chlorophyll fluorescence from airborne based spectrometer data. Paper presented at the ESA Hyperspectral Workshop.

Damm, A., Guanter, L., Laurent, V. C. E., Schaepman, M. E., Schickling, A., & Rascher, U. 2014. "FLD-based retrieval of sun-induced chlorophyll fluorescence from medium spectral resolution airborne spectroscopy data." *Remote Sensing of Environment* 147:256-266.

Damm, A., Guanter L., Paul-Limoges E., van der Tol C., Hueni A., Buchmann N., Eugster W., Ammann C., &Schaepman M. E. 2015. "Far-red sun-induced chlorophyll fluorescence shows ecosystem-specific relationships to gross primary production: An assessment based on observational and modeling approaches." Remote Sensing of Environment 166 : 91-105.

Daumard, F., Goulas Y., Ounis A., Pedros R., & Moya I. 2007. Atmospheric correction of airborne passive measurements of fluorescence. Paper presented at the Proceedings of the 10th International Symposium on Physical Measurements and Signatures in Remote Sensing, ISPMSRS'07, Davos, Switzerland, 12–14 March 2007.

Daumard, F., Champagne, S., Fournier, A., Goulas, Y., Ounis, A., Hanocq, J. F., & Moya, I. 2010. "A field platform for continuous measurement of canopy fluorescence." *Geoscience and Remote Sensing, IEEE Transactions on* 48 (9):3358-3368.

Daumard, F., Goulas, Y., Ounis, A., Pedros, R., &Moya, I. 2015. "Measurement and Correction of Atmospheric Effects at Different Altitudes for Remote Sensing of Sun-Induced Fluorescence in Oxygen Absorption Bands." Geoscience and Remote Sensing, IEEE Transactions on 53(9): 5180-5196.

Dobrowski, S. Z., Pushnik, J. C., Zarco-Tejada, P. J., &Ustin, S. L. 2005. "Simple reflectance indices track heat and water stress-induced changes in steady-state chlorophyll fluorescence at the canopy scale." *Remote Sensing of Environment* 97 (3):403-414.

Evain, S., Flexas, J., &Moya, I. 2004. "A new instrument for passive remote sensing: 2. Measurement of leaf and canopy reflectance changes at 531 nm and their relationship with photosynthesis and chlorophyll fluorescence." *Remote Sensing of Environment* 91 (2):175-185.

Fedotov, Y., Bullo, O., Belov, M., &Gorodnichev, V. 2016. Experimental Research of Reliability of Plant Stress State Detection by Laser-Induced Fluorescence Method. *International Journal of Optics*, 2016:1-6.

Flexas, J., Briantais, J. M., Cerovic, Z., Medrano, H., &Moya, I. 2000. "Steady-state and maximum chlorophyll fluorescence responses to water stress in grapevine leaves: a new remote sensing system." *Remote Sensing of Environment* 73 (3):283-297.

Flexas, J., Escalona, J. M., Evain, S., Gulías, J., Moya, I., Osmond, C. B., &Medrano, H. 2002. "Steady-state chlorophyll fluorescence (Fs) measurements as a tool to follow variations of net $CO_2$ assimilation and stomatal conductance during water‐stress in C3 plants." *Physiologia Plantarum* 114 (2):231-240.

Flowers, M. D., Fiscus, E. L., Burkey, K. O., Booker, F. L., &Dubois, J. J. B. 2007. Photosynthesis, chlorophyll fluorescence, and yield of snap bean (Phaseolus vulgaris L.) genotypes differing in sensitivity to ozone. *Environmental and Experimental Botany*, 61(2), 190-198.

Frankenberg, C., Butz, A., &Toon, G. C. 2011a. "Disentangling chlorophyll fluorescence from atmospheric scattering effects in $O_2$ A-band spectra of reflected sun-light." *Geophysical Research Letters* 38 (3).

Frankenberg, C., Fisher, J. B., Worden, J., Badgley, G., Saatchi, S. S., Lee, J. E., Toon, G. C., Butz, A., Jung, M., &Kuze, A. 2011b. "New global observations of the terrestrial carbon cycle from GOSAT: Patterns of plant fluorescence with gross primary productivity." *Geophysical Research Letters* 38 (17).

Fuchs, M., &Tanner, C. B. 1966. "Infrared thermometry of vegetation." *Agronomy Journal* 58 (6):597-601.

Gao, B. C. 1996. "NDWI—a normalized difference water index for remote sensing of vegetation liquid water from space." *Remote Sensing of Environment* 58 (3):257-66.

Gao, B. C., Montes, M. J, Davis, C. O., &Goetz, A. F. H. 2009. "Atmospheric correction algorithms for hyperspectral remote sensing data of land and ocean." *Remote Sensing of Environment* 113:S17-S24.

Gao, L., Qin, Z.-h., Lu, L.-p. 2007. An overview on agricultural drought monitoring models based on vegetation index and surface temperature feature space. *Remote Sensing for Land & Resources* 9: 1-6.

Gameiro, C., Utkin, A. B., Cartaxana, P., da Silva, J. M., &Matos, A. R. 2016. "The use of laser induced chlorophyll fluorescence (LIF) as a fast and non‐destructive method to investigate water deficit in Arabidopsis." Agricultural Water Management 164 : 127-136.

Genty, B., Briantais, J. M., &Baker, N. R. 1989. "The relationship between the quantum yield of photosynthetic electron transport and quenching of chlorophyll fluorescence." *Biochimica et Biophysica Acta (BBA) - General Subjects* 990 (1):87-92.

Gerosa, G., Marzuoli, R., Rossini, M., Panigada, C., Meroni, M., Colombo, R., &Iriti, M. 2009. A flux-based assessment of the effects of ozone on foliar injury, photosynthesis, and yield of bean (Phaseolus vulgaris L. cv. Borlotto Nano Lingua di Fuoco) in open-top chambers. *Environmental Pollution*, 157(5), 1727-1736.

Gitelson, A. A., Gritz, Y., & Merzlyak, M. N. 2003. "Relationships between leaf chlorophyll content and spectral reflectance and algorithms for non-destructive chlorophyll assessment in higher plant leaves." *Journal of Plant Physiology* 160 (3):271-282.

Gomez-Chova, L., Alonso-Chorda, L., Amoros-Lopez, J., Vila-Frances, J., Del Valle-Tascon, S., Calpe, J., & Moreno, J. 2006. "Solar induced fluorescence measurements using a field spectroradiometer". In Earth Observation for Vegetation Monitoring and Water Management(AIP Conference Proceedings) 852: 274-281.

Guanter, L., Alonso, L., Gómez-Chova, L., Amorós-López, J., Vila, J., &Moreno, J. 2007. "Estimation of solar induced vegetation fluorescence from space measurements." *Geophysical Research Letters* 34 (8).

Guanter, L., Alonso, L., Gómez-chova, L., Meroni, M., Preusker, R., & Fischer, J. 2010. "Developments for vegetation fluorescence retrieval from spaceborne high resolution spectrometry in the $O_2$-A and $O_2$-B absorption bands." *Journal of Geophysical Research: Atmospheres (1984-2012)* 115 (D19).

Guanter, L., Frankenberg, C., Dudhia, A., Lewis, P. E., Góez-Dans, J., Kuze, A., Suto, H., & Grainger, R. G. 2012. "Retrieval and global assessment of terrestrial chlorophyll fluorescence from GOSAT space measurements." *Remote Sensing of Environment* 121:236-251.

Guanter, L., Rossini, M., Colombo, R., Meroni, M., Frankenberg, C., Lee, J. E., &Joiner, J. 2013. "Using field spectroscopy to assess the potential of statistical approaches for the retrieval of sun-induced chlorophyll fluorescence from ground and space." *Remote Sensing of Environment* 133:52-61.

Guanter, L., Zhang, Y., Jung, M., Joiner, J., Voigt, M., Berry, J. A., &Frankenberg, C. 2014. "Global and time-resolved monitoring of crop photosynthesis with chlorophyll fluorescence." *Proceedings of the National Academy of Sciences* 111 (14):E1327-E1333. doi: 10.1073/pnas.1320008111.

Guan, K., Berry, J.A., Zhang, Y., Joiner, J., Guanter, L., Badgley, G., &Lobell, D.B. 2016. Improving the monitoring of crop productivity using spaceborne solar-induced fluorescence. *Global change biology*, 22(2):716-726.

Guidi, L., Nali, C., Ciompi, S., Lorenzini, G., &Soldatini, G. F. 1997. The use of chlorophyll fluorescence and leaf gas exchange as methods for studying the different responses to ozone of two bean cultivars. *Journal of Experimental Botany*, 48(1), 173-179.

Heldt, H. W., & Piechulla, B. 2004. *Plant biochemistry*: Academic Press.

Hunt, E. R., & Rock, B. N. 1989. "Detection of changes in leaf water content using near-and middle-infrared reflectances." *Remote Sensing of Environment* 30 (1):43-54.

Jackson, R. D., Idso, S. B., Reginato, R. J., & Pinter, P. J. 1981. "Canopy temperature as a crop water stress indicator." *Water resources research* 17 (4):1133-1138.

Joiner, J., Guanter, L., Lindstrot, R., Voigt, M., Vasilkov, A. P., Middleton, E. M., Huemmrich, K. F., Yoshida, Y., &Frankenberg, C. 2013. "Global monitoring of terrestrial chlorophyll fluorescence from moderate-spectral-resolution near-infrared satellite measurements: methodology, simulations, and application to GOME-2." *Atmospheric Measurement Techniques* 6 (10):2803-2823.

Joiner, J., Yoshida, Y., Vasilkov, A. P., &Middleton, E. M. 2011. "First observations of global and seasonal terrestrial chlorophyll fluorescence from space." *Biogeosciences* 8 (3):637-651.

Joiner, J., Yoshida, Y., Vasilkov, A. P., Middleton, E. M., Campbell, P. K. E., &Kuze, A. 2012. "Filling-in of near-infrared solar lines by terrestrial fluorescence and other geophysical effects: Simulations and space-based observations from SCIAMACHY and GOSAT." *Atmospheric Measurement Techniques* 5 (4):809-929.

Kalaji, H.M., Oukarroum, A., Alexandrov, V., Kouzmanova, M., Brestic, M., Zivcak, M., Samborska, I.A., Cetner, M.D., Allakhverdiev, S.I., &Goltsev, V. 2014. Identification of nutrient deficiency in maize and tomato plants by in vivo chlorophyll a fluorescence measurements. *Plant Physiology and Biochemistry*, 81:16-25.

Köhler, P., Guanter, L., &Joiner, J. 2015a. "A linear method for the retrieval of sun-induced chlorophyll fluorescence from GOME-2 and SCIAMACHY data." *Atmospheric Measurement Techniques Discussions* 7 (12):12173-12217.

Köhler, P., Guanter, L., &Frankenberg, C. 2015b. "Simplified Physically Based Retrieval of Sun-Induced Chlorophyll Fluorescence From GOSAT Data." *Geoscience and Remote Sensing Letters, IEEE* 12 (7):1446-1450.

Kautsky, H., &Bruijn, H. D. 1931. "Die Aufklärung der Photoluminescenztilgung fluorescierender Systeme durch Sauerstoff: Die Bildung aktiver, diffusionsfähiger Sauerstoffmoleküle durch Sensibilisierung." *Naturwissenschaften* 19 (52):1043-1043.

Khosravi, N. 2012. "Terrestrial Plant Fluorescence as seen from Satellite Data." M. sc.-thesis, University of Bremen.

Kooten, O., &Snel, J. F. H. 1990. "The use of chlorophyll fluorescence nomenclature in plant stress physiology." *Photosynthesis Research* 25 (3):147-150.

Krause, G. H., &Weis, E. 1984. "Chlorophyll fluorescence as a tool in plant physiology." *Photosynthesis Research* 5 (2):139-157.

Larcher, W. 1994. "Photosynthesis as a tool for indicating temperature stress events." In *Ecophysiology of photosynthesis*, 261-277. Springer.

Lazár, D. 1999. Chlorophyll a fluorescence induction. Biochimica et Biophysica Acta (BBA)-Bioenergetics, 1412(1):1-28.

Lee, J. E., Frankenberg, C., van der Tol, C., Berry, J. A., Guanter, L., Boyce, C. K., &Fisher, J. B. 2013. "Forest productivity and water stress in Amazonia: observations from GOSAT chlorophyll fluorescence." *Proceedings of the Royal Society B: Biological Sciences* 280 (1761). doi: 10.1098/rspb.2013.0171.

Lee, J. E., Berry, J.A., Tol, C., Yang ,X., Guanter, L., Damm, A., Baker, I., &Frankenberg, C., 2015. Simulations of chlorophyll fluorescence incorporated into the Community Land Model version 4. *Global change biology*, 21(9):3469-3477.

Leng, P., Song, X., Li, Z.-L., Ma, J., Zhou, F., & Li, S. 2014. "Bare surface soil moisture retrieval from the synergistic use of optical and thermal infrared data." *International Journal of Remote Sensing* 35 (3):988-1003.

Lichtenthaler, H. K. 1988a. "In vivo chlorophyll fluorescence as a tool for stress detection in plants." In *Applications of Chlorophyll Fluorescene in Photosynthesis Research, Stress Physiology, Hydrobiology and Remote Sensing*, 129-142. Springer.

Lichtenthaler, H. K, & Miehe, J. A. 1997. "Fluorescence imaging as a diagnostic tool for plant stress." *Trends in Plant Science* 2 (8):316-320.

Lichtenthaler, H. K, & Buschmann, C. 1988b. "Reflectance and Chlorophyll Fluorescence Signatures of Leaves." In *Applications of Chlorophyll Fluorescene in Photosynthesis Research, Stress Physiology, Hydrobiology and Remote Sensing*, 325-332. Springer Netherlands.

Lichtenthaler, H. K. 1992. "The Kautsky effect: 60 years of chlorophyll fluorescence induction kinetics." *Photosynthetica* 27 (1-2):45-55.

Lichtenthaler, H. K, Lang, M., Sowinska, M., Heisel, F., &Miehe, J. A. 1996. "Detection of vegetation stress via a new high resolution fluorescence imaging system." *Journal of Plant Physiology* 148 (5):599-612.

Liu, L., Zhang, Y., Wang, J., & Zhao, C. 2006. "Detecting photosynthesis fluorescence under natural sunlight based on Fraunhofer line." *JOURNAL OF REMOTE SENSING-BEIJING*- 10 (1):130.

Liu, L., &Cheng, Z. 2011. "Mapping C3 and C4 plant functional types using separated solar-induced chlorophyll fluorescence from hyperspectral data." *International Journal of Remote Sensing* 32 (24):9171-9183.

Liu, L., & Cheng, Z. 2010. "Detection of vegetation light-use efficiency based on solar-induced chlorophyll fluorescence separated from canopy radiance spectrum." *Selected Topics in Applied Earth Observations and Remote Sensing, IEEE Journal of* 3 (3):306-312.

Liu, L., Zhang, Y., Jiao, Q., &Peng, D. 2013a. "Assessing photosynthetic light-use efficiency using a solar-induced chlorophyll fluorescence and photochemical reflectance index." *International Journal of Remote Sensing* 34 (12):4264-4280.

Liu, L., Zhang, Y., Wang, J., &Zhao, C. 2005. "Detecting solar-induced chlorophyll fluorescence from field radiance spectra based on the Fraunhofer line principle." *Geoscience and Remote Sensing, IEEE Transactions on* 43 (4):827-832.

Liu, L., Zhao, J., &Guan, L. 2013b. "Tracking photosynthetic injury of Paraquat-treated crop using chlorophyll fluorescence from hyperspectral data." *European Journal of Remote Sensing* 46:459-473.

Liu, X., &Liu, L. 2014. "Assessing Band Sensitivity to Atmospheric Radiation Transfer for Space-Based Retrieval of Solar-Induced Chlorophyll Fluorescence." *Remote Sensing* 6 (11):10656-10675.

Liu, X., &Liu, L. 2015. "Improving chlorophyll fluorescence retrieval using reflectance reconstruction based on principal components analysis." *Geoscience and Remote Sensing Letters, IEEE* 12 (8):1645-1649.

Liu, X., Liu, L, Zhang, S., &Zhou, X. 2015. "New Spectral Fitting Method for Full-Spectrum Solar-Induced Chlorophyll Fluorescence Retrieval Based on Principal Components Analysis." *Remote Sensing* 7 (8):10626-10645.

Louis, J., Ounis, A., Ducruet, J. M., Evain, S., Laurila, T., Thum, T., Aurela, M., Wingsle, G., Alonso, L., &Pedros, R. 2005. "Remote sensing of sunlight-induced chlorophyll fluorescence and reflectance of Scots pine in the boreal forest during spring recovery." *Remote Sensing of Environment* 96 (1):37-48.

Méthy, M., Olioso, A., &Trabaud, L. 1994. "Chlorophyll fluorescence as a tool for management of plant resources." *Remote Sensing of Environment* 47 (1):2-9.

Drusch, M. 2008. "ESA SP-1313/4 Candidate Earth Explorer Core Missions-Reports for Assessment: FLEX-Fluorescence EXplorer." *ESA Communication Production Office*.

Mathur, S., Jajoo, A., Mehta, P., &Bharti, S. 2011. Analysis of elevated temperature‐induced inhibition of photosystem II using chlorophyll a fluorescence induction kinetics in wheat leaves (Triticum aestivum). *Plant Biology*, 13(1):1-6.

Maier, S. W, Günther, K. P., &Stellmes, M. 2003. "Sun-induced fluorescence: A new tool for precision farming." *Digital imaging and spectral techniques: Applications to precision agriculture and crop physiology* (digitalimaginga):209-222.

Maier, S. W. 2001. "Method of deriving sunlight induced fluorescence from radiance measurements and devices for executing the method." In.: Google Patents.

Marcassa, J. C., Ferreira, J., Zucoloto, S., Silva Jr, O. D. C., Marcassa, L. G., &Bagnato, V. S. 2006. Detection of hepatocarcinoma in rats by integration of the fluorescence spectrum: experimental model. *Laser physics*, 16(5), 827-832.

Maxwell, K., &Johnson, G. N. 2000. "Chlorophyll fluorescence--- practical guide." *Journal of experimental botany* 51 (345):659-668.

Mazzoni, M., Agati, G., Bianco, S. D., Cecchi, G., &Mazzinghi, P. 2006. High resolution measurements of solar induced chlorophyll fluroescence in the fraunhofer Ha and in the atmospheric oxygen lines. Paper presented at the Proceedings of the 6th International Conference on Space Optics.

Mazzoni, M., Meroni, M., Fortunato, C., Colombo, R., &Verhoef, W. 2012. "Retrieval of maize canopy fluorescence and reflectance by spectral fitting in the O 2–A absorption band." *Remote Sensing of Environment* 124:72-82.

Mazzoni, M., Agati, G., Del Bianco, S., Cecchi, G., &Mazzinghi, P. 2007. "High resolution measurements of solar induced chlorophyll fluorescence in the Fraunhofer Ha and in the atmospheric oxygen lines." In *Proceedings of the 3rd International Workshop on Remote Sensing of Vegetation Fluorescences*. Florence, Italy.

Mazzoni, M., Falorni, P., &Verhoef, W. 2010. "High-resolution methods for fluorescence retrieval from space." *Optics express* 18 (15):15649-15663.

McFarlane, J. C., Watson, R. D., Theisen, A. F., Jackson, R. D., Ehrler, W. L., Pinter, P. J., Idso, S. B., &Reginato, R. J. 1980. "Plant stress detection by remote measurement of fluorescence." *Applied Optics* 19 (19):3287-3289.

Meroni, M., Busetto, L., Colombo, R., Guanter, L., Moreno, J., &Verhoef, W. 2010. "Performance of spectral fitting methods for vegetation fluorescence quantification." *Remote Sensing of Environment* 114 (2):363-374.

Meroni, M., & Colombo, R. 2006. "Leaf level detection of solar induced chlorophyll fluorescence by means of a subnanometer resolution spectroradiometer." *Remote Sensing of Environment* 103 (4):438-448.

Meroni, M., Rossini, M., Guanter, L., Alonso, L., Rascher, U., Colombo, R., &Moreno, J. 2009. "Remote sensing of solar-induced chlorophyll fluorescence: Review of methods and applications." *Remote Sensing of Environment* 113 (10):2037-2051.

Meroni, M., Panigada, C., Rossini, M., Picchi, V., Cogliati, S., &Colombo, R. 2009. "Using optical remote sensing techniques to track the development of ozone-induced stress." *Environmental pollution* 157 (5):1413-1420.

Meroni, M., Rossini, M., Picchi, V., Panigada, C., Cogliati, S., Nali, C., &Colombo, R. 2008a. "Assessing steady-state fluorescence and PRI from hyperspectral proximal sensing as early indicators of plant stress: The case of ozone exposure." *Sensors* 8 (3):1740-1754.

Meroni, M., Picchi, V., Rossini, M., Cogliati, S., Panigada, C., Nali, C., Lorenzini, G., &Colombo, R. 2008b. Leaf level early assessment of ozone injuries by passive fluorescence and photochemical reflectance index. *International Journal of Remote Sensing*, 29(17-18), 5409-5422.

Middleton, E. M., Cheng, Y. B., Corp, L., Campbell, P. K. E., Huemmrich, K. F., Zhang, Q., &Kustas, W. P. 2012. Canopy level Chlorophyll Fluorescence and the PRI in a cornfield. Paper presented at the Geoscience and Remote Sensing Symposium (IGARSS), IEEE International.

Middleton, E. M., Corp, L. A., &Campbell, P. K. E. 2008. "Comparison of measurements and FluorMOD simulations for solar induced chlorophyll fluorescence and reflectance of a corn crop under nitrogen treatments." *International Journal of Remote Sensing* 29 (17-18):5193-5213.

Middleton, E. M., McMurtrey, J. E., Campbell, P. K. E., & Butcher, L. M. 2006. "Fluorescence sensing techniques for vegetation assessment." *Applied Optics* 45 (5):1023-1033.

MMiller, J. R., Berger, M., Jacquemoud, S., Moreno, J., Mohammed, G., Moya, I., Pedros, R., Verhoef, W., Zarco-Tejada, P. J., &Alonso, L. 2004. Overview of FluorMOD: A project to develop an integrated leaf-canopy fluorescence simulation model. Paper presented at the 2nd International Workshop on Remote Sensing of Vegetation Fluorescence, 17-19 November, Montreal (Canada).

Misra, A. N., Misra, M., & Singh, R. 2012. *Chlorophyll fluorescence in plant biology*: INTECH Open Access Publisher.

Mistele, B., Elsayed, S., &Schmidhalter, U. 2012. Assessing water status in wheat under field conditions using laser-induced chlorophyll fluorescence and hyperspectral measurements. In 11th International Conference on Precision Agriculture'. International Society of Precision Agriculture: Indianapolis, IN USA.

Moreno, J. 2006. SEN2FLEX campaign overview. In Proceedings of the SEN2FLEX Workshop.

Moreno, J., Laurila T., and Moya I. 2002. Solar Induced Fluorescence Experiment (SIFLEX) Final Report. Finnish meteorological institute.

Monteith, J., & Szeicz G. 1962. Radiative temperature in the heat balance of natural surfaces. *Quarterly Journal of the Royal Meteorological Society* 88(378): 496-507.

Moya, I., Camenen, L., Evain, S., Goulas, Y., Cerovic, Z. G., Latouche, G., Flexas, J., &Ounis, A. 2004. "A new instrument for passive remote sensing: 1. Measurements of sunlight-induced chlorophyll fluorescence." *Remote Sensing of Environment* 91 (2):186-197.

Moya, I., Cartelat, A., Cerovic, Z. G., Ducruet, J. M., Evain, S., Flexas, J., Goulas, Y., Louis, J., Meyer, S., &Moise, N. 2003. Possible approaches to remote sensing of photosynthetic activity. Paper presented at the Geoscience and Remote Sensing Symposium, IGARSS'03. Proceedings.

Moya, I., Daumard, F., Moise, N., Ounis, A., &Goulas, Y. 2006. "First airborne multiwavelength passive chlorophyll fluorescence measurements over La Mancha (Spain) fields." *Second recent advances in quantitative remote sensing*:820-825.

Naumann, J. C., Bissett, S. N., Young, D. R., Edwards, J., &Anderson, J. E. 2010. Diurnal patterns of photosynthesis, chlorophyll fluorescence, and PRI to evaluate water stress in the invasive species, Elaeagnus umbellata Thunb. Trees, 24(2), 237-245.

Ni, Z., Liu, Z., Huo, H., Li, Z.-L., Nerry, F., Wang, Q., & Li, X. 2015a. "Early Water Stress Detection Using Leaf-Level Measurements of Chlorophyll Fluorescence and Temperature Data." *Remote Sensing* 7 (3):3232-3249.

Ni, Z., Liu, Z., Li, Z.-L., Nerry, F., Huo, H., &Li, X. 2015b. "Estimation of solar-induced fluorescence using the canopy reflectance index." *International Journal of Remote Sensing*, 36 (19-20):5239-5256.

Ni, Z., Liu, Z., Li, Z.-L., Nerry, F., Huo, H., Sun, R., Yang, P., &Zhang, W. 2016. Investigation of Atmospheric Effects on Retrieval of Sun-Induced Fluorescence Using Hyperspectral Imagery. *Sensors* , *16*:480.

O'Hagan, A. 2006. "Bayesian analysis of computer code outputs: a tutorial." *Reliability Engineering & System Safety* 91 (10):1290-1300.

Pérez-Priego, O., Zarco-Tejada, P. J., Miller, J. R., Sepulcre-Cantó, G., &Fereres, E. 2005. "Detection of water stress in orchard trees with a high-resolution spectrometer through chlorophyll fluorescence in-filling of the $O_2$-A band." *Geoscience and Remote Sensing, IEEE Transactions on* 43 (12):2860-2869.

Paloscia, S., &Pampaloni, P.. 1984. "Microwave remote sensing of plant water stress." *Remote Sensing of Environment* 16 (3):249-255.

Panigada, C., Rossini, M., Meroni, M., Cilia, C., Busetto, L., Amaducci, S., Boschetti, M., Cogliati, S., Picchi, V., &Pinto, F. 2014. "Fluorescence, PRI and canopy temperature for water stress detection in cereal crops." *International Journal of Applied Earth Observation and Geoinformation* 30:167-178.

Pedrós, R., Goulas, Y., Jacquemoud, S., Louis, J., &Moya, I. 2010. "FluorMODleaf: A new leaf fluorescence emission model based on the PROSPECT model." *Remote Sensing of Environment* 114 (1):155-167.

Peters, A. J., Walter-Shea, E. A., Ji, L., Vina, A., Hayes, M., &Svoboda, M. D. 2002. "Drought monitoring with NDVI-based standardized vegetation index." *Photogrammetric engineering and remote sensing* 68 (1):71-75.

Perez-Priego, O., Guan, J., Rossini, M., Fava, F., Wutzler, T., Moreno, G., Carvalhais, N., Carrara, A., Kolle, O., Julitta, T., &Schrumpf, M., 2015. Sun-induced Chlorophyll fluorescence and PRI improve remote sensing GPP estimates under varying nutrient availability in a typical Mediterranean savanna ecosystem. Biogeosciences Discussions, 12(14).

Plascyk, J. A. 1975a. "The MK II Fraunhofer line discriminator (FLD-II) for airborne and orbital remote sensing of solar-stimulated luminescence." *Optical Engineering* 14 (4):339-440.

Plascyk, J. A., & Gabriel, F. C. 1975b. "The Fraunhofer line discriminator MKII-an airborne instrument for precise and standardized ecological luminescence measurement." *Instrumentation and Measurement, IEEE Transactions on* 24 (4):306-313.

Porcar-Castell, A., Tyystjärvi, E., Atherton, J., van der Tol, C., Flexas, J., Pfündel, E. E., Moreno, J., Frankenberg, C., & Berry, J. A. 2014. "Linking chlorophyll a fluorescence to photosynthesis for remote sensing applications: mechanisms and challenges." *Journal of experimental botany*:eru191.

Rascher, U., Agati, G., Alonso, L., Cecchi, G., Champagne, S., Colombo, R., Damm, A., Daumard, F., Miguel, E. D., & Fernandez, G. 2009. "CEFLES2: the remote sensing component to quantify photosynthetic efficiency from the leaf to the region by measuring sun-induced fluorescence in the oxygen absorption bands." *Biogeosciences Discussions* 6 (1):2217.

Raychaudhuri, B. 2014. "Solar-induced fluorescence of terrestrial chlorophyll derived from the O2-A band of Hyperion hyperspectral images." *Remote Sensing Letters* 5 (11):941-950.

Razavi, F., Pollet, B., Steppe, K., &Van Labeke, M. C. 2008. "Chlorophyll fluorescence as a tool for evaluation of drought stress in strawberry." *Photosynthetica* 46 (4):631-633.

Rahimzadeh-Bajgiran, P., Munehiro, M., &Omasa, K. 2012. Relationships between the photochemical reflectance index (PRI) and chlorophyll fluorescence parameters and plant pigment indices at different leaf growth stages. *Photosynthesis research,* 113(1-3), 261-271.

Ranulfi, A.C., Cardinali, M.C., Kubota, T.M., Freitas-Astúa, J., Ferreira, E.J., Bellete, B.S., da Silva, M.F.G., Boas, P.R.V., Magalhães, A.B., &Milori, D.M. 2016. Laser-induced fluorescence spectroscopy applied to early diagnosis of citrus Huanglongbing. *Biosystems Engineering*, 144: 133-144.

Rosema, A., Snel, J. F. H., Zahn, H., Buurmeijer, W. F., &Van Hove, L. W. A. 1998. "The relation between laser-induced chlorophyll fluorescence and photosynthesis." *Remote Sensing of Environment* 65 (2):143-154.

Rodríguez-Moreno, L., Pineda, M., Soukupová, J., Macho, A.P., Beuzón, C.R., Nedbal, L., Barón, M., &Ramos, C., 2008. Chlorophyll Fluorescence Imaging for Detection of Bean Response to Pseudomonas syringae in Asymptomatic Leaf Areas. In Pseudomonas syringae Pathovars and Related Pathogens–Identification, Epidemiology and Genomics (pp. 37-44). Springer Netherlands.

Saltelli, A., Ratto, M., Andres, T., Campolongo, F., Cariboni, J., Gatelli, D., Saisana, M., &Tarantola, S. 2008. *Global sensitivity analysis: the primer*: Wiley.

Sandholt, I., Rasmussen, K., &Andersen, J. 2002. "A simple interpretation of the surface temperature/vegetation index space for assessment of surface moisture status." *Remote Sensing of Environment* 79 (2):213-224.

Schächtl, J., Huber, G., Maidl, F-X., Sticksel, E., Schulz, J., &Haschberger, P. 2005. "Laser-induced chlorophyll fluorescence measurements for detecting the nitrogen status of wheat (Triticum aestivum L.) canopies." *Precision Agriculture*, 6( 2): 143-156.

Schreiber, U., Vidaver, W., Runeckles, V. C., & Rosen, P. 1978. Chlorophyll fluorescence assay for ozone injury in intact plants. Plant Physiology, 61(1), 80-84.

Schreiber, U., Bilger, W., & Neubauer, C.. 1994. "Chlorophyll fluorescence as a nonintrusive indicator for rapid assessment of in vivo photosynthesis." In *Ecophysiology of photosynthesis*, 49-70. Springer.

Sobrino, J. A., Franch, B., Jimenez-Muñoz, J. C., Hidalgo, V., Soria, G., Julien, Y., Oltra-Carrio, R., Mattar, C., Ruescas, A., &Daumard, F. 2011. "Fluorescence estimation in the framework of the CEFLES2 campaign." *International Journal of Remote Sensing* 32 (20):5875-5889.

Subhash, N., & Mohanan, C. N. 1997. "Curve-fit analysis of chlorophyll fluorescence spectra: Application to nutrient stress detection in sunflower." *Remote Sensing of Environment* 60 (3):347-356.

Suárez, L., Zarco-Tejada P. J., Berno J. A. J., Gonzalez-dugo V., Fereres, E. 2009. Modelling PRI for water stress detection using radiative transfer models. *Remote Sensing of Environment* 113(4): 730-744.

Tanner, C. B. 1963. "Plant temperatures." *Agronomy Journal* 55 (2):210-211.

Theisen, A. F. 2000. "A Passive Method for Detecting Vegetation Stress from Orbit: Chlorophyll Fluorescence Spectra from Fraunhofer Lines."

Thwe, A. A., Vercambre, G., Gautier, H., Gay, F., Phattaralerphong, J., &Kasemsap, P. 2014. Response of photosynthesis and chlorophyll fluorescence to acute ozone stress in tomato (Solanum lycopersicum Mill.). *Photosynthetica*, 52(1), 105-116.

Timmermans, J. 2011. "Coupling optical and thermal directional radiative transfer to biophysical processes in vegetated canopies." *Enschede, University of Twente Faculty of Geo-Information and Earth Observation (ITC), ITC Dissertation* 193.

Van der Tol, C., Verhoef, W., Timmermans, J., Verhoef, A., &Su, Z. 2009b. "An integrated model of soil-canopy spectral radiance observations, photosynthesis, fluorescence, temperature and energy balance." *Biogeosciences Discussions* 6:6025-6075.

Van der Tol, C. 2013. SCOPE Version 1.51 User Manual.

Vereecken, H., Weihermüller, L., Jonard, F., &Montzka, C. 2012. "Characterization of crop canopies and water stress related phenomena using microwave remote sensing methods: A review." *Vadose zone journal* 11 (2).

Verhoef, W., 2004. Extension of SAIL to model solar-induced canopy fluorescence spectra. In Proceedings of 2nd International Workshop on Remote Sensing of Vegetation Fluorescence, Saint-Hubert, Canada (pp. 17-19).

Verhoef, W. 2011. Modeling vegetation fluorescence observations. Paper presented at the Proceedings of the EARSel 7th SIG-Imaging Spectroscopy Workshop, Edinburgh, UK.

Verrelst, J., Rivera, J.P., van der Tol, C., Magnani, F., Mohammed, G., &Moreno, J. 2015. Global sensitivity analysis of the SCOPE model: What drives simulated canopy-leaving sun-induced fluorescence?. *Remote Sensing of Environment*, 166:8-21.

Verrelst, J., van der Tol, C., Magnani, F., Sabater, N., Rivera, J.P., Mohammed, G., &Moreno, J. 2016. Evaluating the predictive power of sun-induced chlorophyll fluorescence to estimate net photosynthesis of vegetation canopies: A SCOPE modeling study. *Remote Sensing of Environment*, 176:139-151.

Vountas, M, Rozanov, V. V., &Burrows, J. P. 1998. "Ring effect: Impact of rotational Raman scattering on radiative transfer in Earth's atmosphere." *Journal of Quantitative Spectroscopy and Radiative Transfer* 60 (6):943-961.

Walker, J. P. 1999. "Estimating soil moisture profile dynamics from near-surface soil moisture measurements and standard meteorological data." the University of Newcastle.

Wang, L., &Qu, J. J. 2009. "Satellite remote sensing applications for surface soil moisture monitoring: A review." *Frontiers of Earth Science in China* 3 (2):237-247.

Wang, S., Huang, C., Zhang, L., Lin, Y., Cen, Y., &Wu, T. 2016. Monitoring and assessing the 2012 drought in the great plains: Analyzing satellite-retrieved solar-induced chlorophyll fluorescence, drought indices, and gross primary production. Remote Sensing, 8(2), p.61.

Winkel, T., Méthy, M., &Thénot, F. 2002. Radiation use efficiency, chlorophyll fluorescence, and reflectance indices associated with ontogenic changes in water-limited Chenopodium quinoa leaves. *Photosynthetica*,40(2), 227-232.

White, A.J., &Critchley, C. 1999. Rapid light curves: a new fluorescence method to assess the state of the photosynthetic apparatus. *Photosynthesis research*, 59(1):63-72.

Yang, P., & Liu, Z. 2013. Remote sensing of solar-induced chlorophyll fluorescence from an unmanned airship platform. In Geoscience and Remote Sensing Symposium (IGARSS), IEEE International.

Zadoks, J. C., Chang, T. T, &Konzak, C. F. 1974. "A decimal code for the growth stages of cereals." *Weed research* 14 (6):415-421.

Zarco-Tejada, P. J. 2000a. "Hyperspectral remote sensing of closed forest canopies: Estimation of chlorophyll fluorescence and pigment content." York University Toronto.

Zarco-Tejada, P. J, Miller, J. R., Mohammed, G. H., &Noland, T. L. 2000b. "Chlorophyll fluorescence effects on vegetation apparent reflectance: I. Leaf-level measurements and model simulation." *Remote Sensing of Environment* 74 (3):582-595.

Zarco-Tejada, P. J, Miller, J. R., Mohammed, G. H., Noland, T. L., &Sampson, P. H. 2000c. "Chlorophyll fluorescence effects on vegetation apparent reflectance: II. Laboratory and airborne canopy-level measurements with hyperspectral data." *Remote Sensing of Environment* 74 (3):596-608.

Zarco-Tejada, P. J, Miller, J. R., Mohammed, G. H., Noland, T. L., &Sampson, P. H. 2001. "Estimation of chlorophyll fluorescence under natural illumination from hyperspectral data." *International Journal of Applied Earth Observation and Geoinformation* 3 (4):321-327.

Zarco-Tejada, P. J, Pushnik, J. C., Dobrowski, S., &Ustin, S. L. 2003. "Steady-state chlorophyll *a* fluorescence detection from canopy derivative reflectance and *double-peak* red-edge effects." *Remote Sensing of Environment* 84 (2):283-294.

Zarco-Tejada, P.J., Pérez-Priego, O., Sepulcre-Cantó, G., Miller, J.R., &Fereres, C. E. 2004. Chlorophyll Fluorescence Detection with a High-Spectral Resolution Spectrometer through in-filling of the $O_2$-A band as function of Water Stress in Olive Trees.

Zarco-Tejada, P.J., Miller, J.R., Pedrós, R., Verhoef, W., &Berger, M. 2006. FluorMODgui V3. 0: A graphic user interface for the spectral simulation of leaf and canopy chlorophyll fluorescence. *Computers & Geosciences*, 32(5):577-591.

Zarco-Tejada, P. J., Berni, J. A. J., Suárez, L., Sepulcre-Cantó, G., Morales, F., &Miller, J. R. 2009. "Imaging chlorophyll fluorescence with an airborne narrow-band multispectral camera for vegetation stress detection." *Remote Sensing of Environment* 113 (6):1262-1275.

Zarco-Tejada, P. J., González-Dugo, V., &Berni, J. A. J. 2012. "Fluorescence, temperature and narrow-band indices acquired from a UAV platform for water stress detection using a micro-hyperspectral imager and a thermal camera." *Remote Sensing of Environment* 117:322-337.

Zarco-Tejada, P. J., Catalina, A., González, M. R., &Martín, P. 2013a. "Relationships between net photosynthesis and steady-state chlorophyll fluorescence retrieved from airborne hyperspectral imagery." *Remote Sensing of Environment* 136:247-258.

Zarco-Tejada, P. J., Morales, A., Testi, L., &Villalobos, F. J. 2013b. "Spatio-temporal patterns of chlorophyll fluorescence and physiological and structural indices acquired from hyperspectral imagery as compared with carbon fluxes measured with eddy covariance." *Remote Sensing of Environment* 133:102-115.

Zarco-Tejada, P.J., González-Dugo, M.V., & Fereres, E. 2016. Seasonal stability of chlorophyll fluorescence quantified from airborne hyperspectral imagery as an indicator of net photosynthesis in the context of precision agriculture. *Remote Sensing of Environment*, 179:89-103.

Zhang, Y., Guanter, L., Berry, J. A., Joiner, J., Tol, C., Huete, A., Gitelson, A., Voigt, M., &Köhler, P. 2014. "Estimation of vegetation photosynthetic capacity from space‐based measurements of chlorophyll fluorescence for terrestrial biosphere models." *Global Change Biology* 20 (12):3727-3742.

Zhang, Y., Wagle, P., Guanter, L., Jin, C., &Xiao, X. 2015. Phenology and gross primary production of maize croplands from chlorophyll light absorption, solar-induced chlorophyll fluorescence and CO2 flux tower approaches. In EGU General Assembly Conference Abstracts, 2015 April (Vol. 17, p. 7810).

Zhao, F., Guo, Y., Verhoef, W., Gu, X., Liu, L., &Yang, G. 2014. A method to reconstruct the solar-induced canopy fluorescence spectrum from hyperspectral measurements. *Remote Sensing*, 6(10):10171-10192.

Zhao, F., Guo, Y., Huang, Y., Verhoef, W., Tol, C. V. D., Dai, B., &Liu, G. 2015. Quantitative Estimation of Fluorescence Parameters for Crop Leaves with Bayesian Inversion. *Remote Sensing*, 7(10), 14179-14199.

Zhuoya NI

# Méthode pour L'estimation de la fluorescence de la chlorophylle et son application pour la détection précoce du stress hydrique


## Résumé

La fluorescence chlorophyllienne induite par le soleil est une nouvelle façon de suivre l'évolution de la végétation et le cycle global du carbone. Grâce au modèle simulé et aux expériences sur le terrain et aéroportée, la recherche multi-échelles de méthode de détection de la fluorescence de la chlorophylle induite par le soleil est développé dans cette thèse.

Les principales conclusions et innovations sont les suivantes :

1. Les expériences de contrôle en eau du maïs montrent que la fluorescence passive peut être utilisée pour détecter le stress hydrique des culture. L'analyse de la réponse de la fluorescence et de la température montre que la fluorescence est très sensible au stress hydrique précoce.
2. Après avoir analysé les effets de la température, de l'angle zénithal solaire et du rendement quantique de la fluorescence sur la détermination de la fluorescence, nous proposons une méthode d'obtention de la fluorescence qualitative basée sur l'indice de réflectance.
3. L'analyse des effets de la détermination de la fluorescence aéroportée nous a permis de montrer que l'angle zénithal solaire et la hauteur du capteur aéroporté sont les facteurs importants qui influent sur la détermination de la fluorescence induite par le soleil.


Mots clés: Télédétection de la végétation, fluorescence induite par le soleil, multi-échelles, méthode de détermination de la fluorescence, effets atmosphériques, correction atmosphérique.


## Résumé en anglais

Sun-induced chlorophyll fluorescence is a new way to monitor the vegetation change and global carbon cycle. Through the model simulated analysis, the pot experiment and the airborne flying experiment, the research on detecting the multi-scale sun-induced chlorophyll fluorescence is developed in this dissertation.

The main conclusions and innovations are as follows:

1. The maize water control experiments demonstrate that the passive fluorescence can be used to detect the crop water stress, and the analysis of the different responses of the fluorescence and temperature illustrates that the fluorescence is much sensitive to the early water stress.
2. Analyze the effects of temperature, sun zenith angle and fluorescence quantum efficiency on the qualitative fluorescence retrieval, and propose a qualitative fluorescence retrieval method based on the reflectance index.
3. Analyze the effects of airborne fluorescence retrieval, and obtain that sun zenith angle and airborne sensor height are the important factors to affect the sun-induced fluorescence retrieval from the simulated analysis and airborne flying experiment.


Key words: Vegetable remote sensing, sun-induced fluorescence, multi-scale, fluorescence retrieval method, atmospheric effects, atmospheric correction.